

**The impact of starch- and fat-rich diets on intestinal
microbiota, metabolism, and immunity in differentially
immune-biased C57BL/6 and BALB/c mice**

By

Raktim Mukherjee

LIFE11201704004

National Institute of Science Education and Research (NISER), Bhubaneswar

A thesis submitted to the Board of studies in Life Sciences

In partial fulfilment of requirements for the Degree of

DOCTOR OF PHILOSOPHY

Of

HOMI BHABHA NATIONAL INSTITUTE

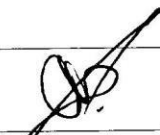


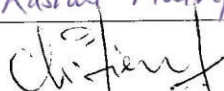
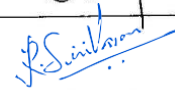
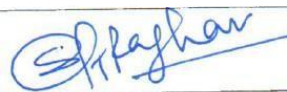


December, 2021

Homi Bhabha National Institute¹

Recommendations of the Viva Voce Committee

As members of the Viva Voce Committee, we certify that we have read the dissertation prepared by Mr. Raktim Mukherjee entitled "The impact of starch- and fat-rich diets on intestinal microbiota, metabolism, and immunity in differentially immune-biased C57BL/6 and BALB/c mice" and recommend that it may be accepted as fulfilling the thesis requirement for the award of Degree of Doctor of Philosophy.


Chairman – Dr. Asima Bhattacharyya		Date: 10.12.21
Guide / Convener - Dr. Palok Aich		Date: Dec 09/21
Co-guide – N/A		
Examiner – Prof. Kasturi Mukhopadhyay		Date: 10/12/21
Member 1- Dr. Tirumala Kumar Chowdary		Date: Dec 09/21.
Member 2- Dr. Ramanujam Srinivasan		Date: 10/12/21
Member 3- Dr. Sunil K. Raghav		Date: Dec 09/21

Final approval and acceptance of this thesis is contingent upon the candidate's submission of the final copies of the thesis to HBNI.

I/We hereby certify that I/we have read this thesis prepared under my/our direction and recommend that it may be accepted as fulfilling the thesis requirement.

Date: Dec 09/21

Place: NISER, Jatni


Dr. Palok Aich (Thesis supervisor)

¹ This page is to be included only for final submission after successful completion of viva voce

Statement by author

This dissertation has been submitted in partial fulfilment of requirements for an advanced degree at Homi Bhabha National Institute (HBNI) and is deposited in the library to be made available to borrowers under the rules of the HBNI.

Brief quotations from this dissertation are allowable without any special permission, provided that accurate acknowledgment of the source is made. Requests for permission for extended quotation from or reproduction of this manuscript in whole or in part may be granted by the competent authority of HBNI when in his or her judgment the proposed use of the material is in the interests of the scholarship. In all other instances, however, permission must be obtained from the author.

Name of the student: Raktim Mukherjee

Raktim Mukherjee

Signature of the student

Dated: 12/12/2021

Declaration

I, hereby declare that the investigation presented in the thesis has been carried out by me. The work is original and has not been submitted earlier as a whole or in part for a degree / diploma at this or any other Institution / University.

Name of the student: Raktim Mukherjee

Raktim Mukherjee

Signature of the student

Dated: 12/12/2021

List of publications arising from the thesis

Journal papers related to the thesis

1. ¹Guha, D., ¹Mukherjee, R., & ²Aich, P. (2020). Macrophage plays important role in cortisol and serotonin induced adipogenesis in vitro. *In Vitro Cellular & Developmental Biology – Animal*, 56, 511–521. <https://doi.org/10.1007/s11626-020-00482-1>
2. ¹Guha, D., ¹Mukherjee, R., & ²Aich, P. (2021). Effects of two potential probiotic *Lactobacillus* bacteria on adipogenesis in vitro. *Life Sciences*, 278. <https://doi.org/10.1016/j.lfs.2021.119538>
3. Mukherjee, R., & ²Aich, P. (2021). The starch-rich diet causes lipidemia while the fat-rich diet induces visceral adiposity, meta-inflammation, and insulin resistance differentially in immune biased mouse strains. *Food Bioscience*, 42. <https://doi.org/10.1016/j.fbio.2021.101136>
4. Mukherjee, R., Pandey, S., Ghosh, A., & ²Aich, P. (2021). Effects of starch-rich or fat-rich diets on metabolism, adiposity, and glycemia in immune-biased, C57BL/6 and BALB/c mice. *Journal of Nutritional Biochemistry*, JNB-D-21-00788. (communicated).

5. Mukherjee, R., & ²Aich, P. Temporal impact of starch and fat-rich diet perturbed intestinal microbes on lipidaemia and visceral adiposity of C57BL/6 and BALB/c mice (under preparation)

(¹ Contributed equally)

Other co-authored journal papers

1. Naik, A. K., Pandey, U., Mukherjee, R., Mukhopadhyay, S., Chakraborty, S., Ghosh, A., & ²Aich, P. (2019). *Lactobacillus rhamnosus* GG reverses mortality of neonatal mice against *Salmonella* challenge. *Toxicology Research*, 8(3), 361–372. <https://doi.org/10.1039/C9TX00006B>

2. Guha, D., Banerjee, A., Mukherjee, R., Pradhan, B., Peneva, M., Aleksandrov, G., Suklabaidya, S., Senapati, S., & ²Aich, P. (2019). A probiotic formulation containing *Lactobacillus bulgaricus* DWT1 inhibits tumor growth by activating pro-inflammatory responses in macrophages. *Journal of Functional Foods*, 56, 232–245. <https://doi.org/10.1016/j.jff.2019.03.030>

List of Conferences/symposiums participated

1. Understanding the Relationship between Diet-Induced Alteration in Gut Microbiota and Host Physiology Using Mouse as a Model Organism. ¹Raktim Mukherjee and ²Palok Aich. India, EMBO Symposium on “Human microbiome: Resistance and disease.” 09 – 12 November 2019, NIBMG, Kalyani, India

2. Anti-adipogenic effects of two Lactobacillus probiotics: A combined in vivo and in vitro study. ¹Raktim Mukherjee and ²Palok Aich. A virtual conference on “INFECTIOUS DISEASE, MICROBIOME and PUBLIC HEALTH IN THE CURRENT SCENARIO.” 10th - 11th August 2020. NISER, India.

3. Understanding the temporal changes in visceral adiposity caused by diet-induced cecal microbiota dysbiosis using mouse model. ¹Raktim Mukherjee and ²Palok Aich. A virtual conference on “5th Biennial Conference of PAI and International Symposium”. 19th-20th November 2020. NDRI, Karnal, India.

4. Understanding the role of macrophages in regulating stress hormone-induced adipogenesis using in vitro murine model. ¹Raktim Mukherjee and ²Palok Aich. A virtual conference on “Integrating Metabolism and Immunity”. 25th-28th January 2021. Keystone, Canada.

¹ Presenting author

² Corresponding author

Name of the student: Raktim Mukherjee

Raktim Mukherjee

Signature of the student

Dated: 12/12/2021

Dedication

I dedicate this thesis to my family members, friends and teachers who helped me throughout my journey.

Acknowledgement

I would like to express my deep gratitude towards my Ph.D. supervisor, Dr. Palok Aich, for his unconditional support, throughout my journey and for granting me profound freedom regarding the work. My sincere gratitude towards my doctoral committee members Dr. Asima Bhattacharyya, Dr. Tirumala Kumar Chowdary, Dr. Ramanujam Srinivasan and Dr. Sunil K. Raghav for helping me to improve my work with their insightful advice. I would also like to give special thanks to all the members of Dr. Aich's current research group, for their constructive opinion regarding the project and for creating an ambient working environment in the lab. Specially, I would like to thank Dr. Dipanjan Guha, Dr. Biswaranjan Pradhan, Dr. Pratikshya Ray, Mr. Aman Kumar Naik, Ms. Sohini Mukhopadhyay, Mr. Uday Pandey, Mr. Dhyanendra Singh Chauhan and, Ms. Swati Sagarika Panda for their technical, intellectual and moral support. Also, I would thank Dr. Arindam Ghosh and Ms. Shalini Pandey for their assistance in NMR related experiments.

I would express my deep respect and appreciation towards Prof. Sudhakar Panda, director, National Institute of Science Education and Research (NISER) and all the competent authority for providing me the opportunity to pursue Ph. D. Also, I would like to thank the authority of Homi Bhabha National Institute (HBNI) and Department of Atomic Energy (DAE) for providing administrative and financial support throughout my tenure. Since the major portion of my work concerns animal experimentation, I cannot but thank the staff members of the animal experimentation, breeding and housing facility of NISER.

I would like to acknowledge my batchmates and friends Mr. Debashish Chakraborty, Mr. Prakash Haloi, Mr. Tushar Kanti Acharya, Mr. Nishant Kumar Dubey and Mr.

Chandan Mahish for their moral support, throughout my Ph. D. journey and for making the difficult times, easier for me. I shall also thank the fellow students, respected faculty members and staffs of NISER for their support.

Finally, I would express my gratitude towards my family members and friends for keeping their faith on me.

Contents

Summary

Diet is an indispensable part of an organism's physiological requirements. Mammalian physiology, largely depends upon the balance between energy intake, its utilization and metabolism, also known as energy homeostasis. The energy homeostasis is affected largely by various systemic needs of the animal. The immunological processes, required for the sustenance of normalcy, takes a huge share from the energy that has been extracted by the organism. The bidirectional switching between an aggressive, hyperactive immune status to a more tolerogenic immune response, thus governs the connection between the immune and metabolic system. On top of the regular physiological processes, the mammalian intestinal microbes influence the host metabolism in various ways and regulates the host metabolism and immunity. Presently we have investigated the interplay between metabolism, immunity and intestinal microbes by perturbing the physiological normalcy by means of dietary alteration. Using immune biased C57BL/6 and BALB/c mice, we have demonstrated how diets rich in either starch (SRD) or fat (unsaturated and saturated, USFD and SFD) can influence the adiposity, glycemia and meta-inflammation in comparison to untreated controls. Along with this, we have also evaluated the influence of intestinal microbes in the diet mediated physiological changes. We found that with time, SRD mostly enhances lipidemia while ameliorating glycemia and meta-inflammation. Such enhancement and reduction in the said parameters could be associated with the abundance of microbes from the phylum Proteobacteria and Verrucomicrobia, respectively. While, USFD had mostly ameliorative effects, SFD augmented the adipogenic, glycemia and meta-inflammation related parameters. Such effects of SFD

could be linked with the enhanced levels of the phyla Firmicutes, Proteobacteria and Epsilonbacteraeota.

From our *in vivo* study, it appeared, that the metabolic abnormalities associated with enhancement in visceral adiposity were frequently accompanied by enhancement in meta-inflammation. We further evaluated the immune-metabolic interactions of murine system, *in vitro* by adapting a co-culture system of adipocytes and macrophages. As an inducer of adiposity, we used the chronic psychological stress model for influencing murine lipid metabolism. We found, adiposity to have an augmenting effect on inflammation, while the later also could enhance adiposity, under a condition of chronic psychological stress. As we observed the promoting effects of select diets and stress condition on adiposity, we further tried to understand if the intestinal microbes could further govern the regulations of murine physiology, given our observations related to the association of the intestinal microbes with host physiological processes. For this, we used select strains of lactic acid producing probiotic bacteria, to test their ameliorative effects on murine adiposity, *in vitro*. The probiotic bacteria *Lactobacillus acidophilus* and the cocktail of *Lactobacillus delbrueckii* sp. *bulgaricus* and *Streptococcus thermophilus*, catalytically reduced cellular adiposity and the adipogenic potential of murine adipocytes. Together, we identified the interplay, occurring between murine metabolism, the immune system and intestinal microbes by perturbing the energy homeostasis, by means of altered diets, chronic stress and probiotic bacteria.

Table of contents

Chapter description, details of sections and sub-sections with page numbers

Key words	31
Abbreviations used in the thesis	31
Chapter 1	33
Introductory understanding of the importance of diet in maintaining physiological energy homeostasis and the contribution of the intestinal microbes in sustaining the process	33
1.1. Importance of energy homeostasis, different contributing factors, and its impact on various physiological parameters.....	35
1.2. Different <i>in vivo</i> and <i>in vitro</i> systems for studying energy homeostasis and its physiological effects	38
1.3. Mouse as a model system for studying metabolism and associated pathophysiology.....	40
1.4. Different nutrient-rich diets as possible regulators of energy homeostasis.....	41
1.5. Chronic psychological stress as a regulator of energy homeostasis	45
1.6. Contribution of intestinal microbes in the regulation of host energy homeostasis.....	48
1.7. Altered diet as a perturbing agent of intestinal microbes	49
1.8. Probiotics, prebiotics, and postbiotics: impact on mammalian gut microbiota composition and subsequent effects on host physiology.....	53
Materials and Methods.....	57

2.1.	Diet formulation, preparation, and treatment conditions	57
2.2.	Housing and maintenance of experimental animals	59
2.3.	Animal autopsy, sample collection, and preservation	60
2.4.	Measurement of calorie intake, assessment of body weight and visceral fat.	61
2.5.	Assessment of serum hormones and lipid profiling.....	61
2.5.1.	<i>Protocol for the assessing total serum protein using Bradford assay.</i>	62
2.5.2.	<i>Protocol for the assessment of serum leptin/adiponectin/insulin level by sandwich ELISA</i>	63
2.5.3.	<i>Protocol for the assessment of serum ghrelin level by competitive ELISA.</i>	64
2.5.4.	<i>Protocol for the assessment of serum triglyceride level by spectrophotometry</i>	65
2.5.5.	<i>Protocol for the assessment of serum free fatty acid level by spectrophotometry</i>	66
2.6.	Oral glucose tolerance test (OGTT) and insulin resistance (IR) measurements	67
2.6.1.	<i>Performing OGTT and generation glucose response curve (GRC)....</i>	67
2.6.2.	<i>Assessment of insulin resistance by HOMA-IR model.....</i>	68
2.7.	Isolation of serum metabolites and sample preparation for metabolomic studies.....	68
2.8.	Assessment of serum metabolomics by ¹ H NMR	69
2.9.	Analysis of NMR data for metabolome-based segregation and quantification	

of the effects of dietary alterations	69
2.10. Measurement of visceral white adipose tissue (vWAT) morphology by hematoxylin and eosin (H & E) staining of paraffin-embedded tissue sections	71
2.10.1. <i>Paraffin embedding and sectioning of vWAT</i>	72
2.10.2. <i>Hematoxylin and eosin staining of vWAT tissue sections</i>	73
2.11. Measurement of vWAT lipid content by BODIPY staining of tissue whole mounts	74
2.12. Assessment of macrophage infiltration inside vWAT by direct immune fluorescence of vWAT whole mount	75
2.13. Image analysis by ImageJ software	76
2.14. RNA isolation and cDNA preparation from vWAT	76
2.14.1. <i>RNA isolation from vWAT</i>	76
2.14.2. <i>Determination of concentration and integrity of RNA by spectrophotometry and agarose gel electrophoresis</i>	78
2.14.3. <i>Preparation of cDNA from total RNA</i>	78
2.15. Relative mRNA expression analysis of select metabolic genes from vWAT	79
2.16. Isolation of genomic DNA (gDNA) from cecal content of mice	82
2.17. Assessment of cecal microbial diversity by 16S rRNA-based next-generation sequencing of cecal content gDNA.....	83
2.18. Assessment of cecal microbial diversity by Shannon diversity index	85
2.19. Clustering of different diet treated mice based on cecal microbial diversity, using LDA	85

2.20. Assessment of serum SCFA levels from serum metabolomic data.....	86
2.21. Mammalian cell lines and cell culture conditions	86
2.22. Probiotic bacteria culture and growth conditions	86
2.23. Differentiation of pre-adipocyte cell line into terminally differentiated adipocytes	87
2.24. Co-culturing of adipocyte and macrophage cell lines	87
2.25. Stress hormone treatment of co-cultured adipocyte and macrophage cells.	88
2.26. Treatment of differentiated adipocyte cell line with select strains of lactic acid bacteria.....	89
2.27. Oil Red O (ORO) staining of adipocytes	89
2.28. Quantification of cellular lipid content by extraction of intracellular ORO and measurement of its absorbance.....	90
2.29. RNA isolation, cDNA preparation, and qRT-PCR analysis of select genes from differentiated adipocyte and macrophage cell lines.....	90
2.30. Assessment of probiotic bacteria association/uptake inside differentiated 3T3-L1 cells.....	92
2.30.1. <i>Labeling of probiotic bacteria with CFDA/SE stain.</i>	92
2.30.2. <i>Flow cytometry analysis of select surface markers on macrophage cell line and probiotic association/uptake on differentiated 3T3-L1 cells</i>	93
2.30.3. <i>Fluorescent imaging of differentiated adipocytes, pre-treated with probiotic bacteria for measuring bacterial association/uptake</i>	94

2.30.4. <i>Bacterial association/uptake assay for measuring attached or internalized probiotic bacteria inside differentiated adipocytes</i>	94
2.31. Graphs and statistical analysis.....	95
Chapter 2.....	97
Evaluating the effects of starch or fat-rich diets on visceral adiposity, lipidemia, glycemia, and serum lipid profile of immune biased mice	97
3.1. Introduction.....	99
3.2. Effects of starch and fat-rich diets on calorie intake and body composition	100
3.3. Starch and fat-rich diets differentially affect physiological energy homeostasis by regulating metabolic hormones	103
3.4. Starch and fat-rich diets regulate visceral adiposity and lipidemia differently to maintain energy homeostasis	105
3.5. Glycemia is differentially affected by starch and fat-rich diets	113
3.6. Immune-biased mice are differentially impacted by the starch and fat-rich diets, leading to changes in their systemic metabolic profile	118
3.7. Altered metabolites reveal several pathways leading to the observed physiological changes	121
3.8. Discussion and conclusion.....	128
Chapter 3.....	134
Impact of diets on visceral adipose tissue meta-inflammation and elucidation of the immune-metabolic interactions occurring in the adipose tissue microenvironment	134

4.1.	Introduction	136
4.2.	Effect of starch and fat-rich diets on adipose tissue immune cell infiltration in immune-biased mice	137
4.3.	Chronic psychological stress as an effector of murine metabolic processes.....	142
4.3.1.	<i>Differentiation of murine pre-adipocyte cell line 3T3-L1 to terminally differentiated adipocytes.....</i>	142
4.3.2.	<i>Dose and timepoint standardization for cortisol and serotonin treatment</i>	144
4.3.3.	<i>Induction of lipid buildup in differentiated 3T3-L1 cells following cortisol and serotonin treatment</i>	146
4.3.4.	<i>Co-culturing differentiated 3T3-L1 cells with RAW264.7 cells further enhanced lipid accumulation under the influence of cortisol and serotonin...</i>	147
4.3.5.	<i>Immune metabolic interaction in simulated adipose tissue microenvironment in vitro.....</i>	149
4.4.	Discussion and conclusion	153
Chapter 4.....		158
Effects of diets on cecal microbial composition and understanding the impact of select microbes on regulating host metabolism		158
5.1.	Introduction	160
5.2.	Characterization of cecal microbial diversity following starch and fat-rich diet consumption.....	161
5.2.1.	<i>Diversity of major microbial phylum following dietary alterations for</i>	

<i>four and eight weeks</i>	162
5.2.2. <i>Clustering of control and treatment diet fed mice based on cecal microbiota abundance</i>	168
5.2.3. <i>Major SCFA producing microbial genera, affected by dietary alterations and their relationship with host physiology</i>	170
5.3. <i>Effect of select strains of Lactobacillus acidophilus and Lactobacillus delbrueckii sp. bulgaricus on adiposity, when co-cultured with murine adipocytes</i>	175
5.3.1. <i>LA and LDB-ST were associated/up taken by differentiated 3T3-L1 cells following exposure at optimum MOIs</i>	178
5.3.2. <i>Both LA and LDB-ST effectively reduced cellular lipid content and adipogenic gene expressions of differentiated 3T3-L1 cells</i>	180
5.4. <i>Discussion and conclusion</i>	182
References	188

List of figures and tables with page numbers

List of figures

Figure 1. Hormonal regulation of energy homeostasis in mice.....	44
Figure 2. Physiological impacts of stress and stress hormones on glycemic and adipogenic indices	47
Figure 3. Effects of different nutrients on the mammalian gut microbiota.....	52
Figure 4. Cumulative beneficial effects of probiotics, prebiotics, and postbiotics....	55
Figure 5. Comparative overview of calorie intake and resultant body composition changes in control and treatment (SRD, USFD, and SFD) diet-fed C57BL/6 and BALB/c mice.....	102
Figure 6. Comparative overview of the levels of metabolic hormones from control and treatment (SRD, USFD, and SFD) diet-fed C57BL/6 and BALB/c mice	104
Figure 7. Comparative overview of serum lipid profile levels from control and treatment (SRD, USFD, and SFD) diet-fed C57BL/6 and BALB/c mice	106
Figure 8. Micrographs representing vWAT histology from control and treatment (SRD, USFD, and SFD) diet-fed C57BL/6 and BALB/c mice.....	107
Figure 9. Comparative overview of vWAT lipid content from control and treatment (SRD, USFD, and SFD) diet-fed C57BL/6 and BALB/c mice.....	109
Figure 10. Comparative overview of relative mRNA expressions (fold change relative to control mice) of select metabolic genes from vWAT of control and treatment (SRD, USFD, and SFD) diet-fed C57BL/6 and BALB/c mice	112
Figure 11. Comparative overview of glycemia levels from control and treatment (SRD, USFD, and SFD) diet-fed C57BL/6 and BALB/c mice.....	115

Figure 12. Comparative overview of blood and serum glycemic indices from control and treatment (SRD, USFD, and SFD) diet-fed C57BL/6 and BALB/c mice	117
Figure 13. Effect of diets on serum metabolomic changes of C57BL/6 and BALB/c mice, subjected to dietary alteration for a period of four and eight weeks	120
Figure 14. Pathways predicted to affect primary metabolic functions following dietary alterations in C57BL/6 and BALB/c mice, subjected to dietary alteration for four and eight weeks	122
Figure 15. Schematic representation of the significant metabolic changes impacting adiposity and glycemia of immune-biased C57BL/6 and BALB/c mice following intervention with control, SRD, USFD, and SFD for four and eight weeks, respectively	132
Figure 16. Comparative overview of macrophage infiltration levels from control and treatment (SRD, USFD, and SFD) diet-fed C57BL/6 and BALB/c mice	138
Figure 17. Comparative overview of relative mRNA expressions (fold change to control mice) of select immune genes from vWAT of control and treatment (SRD, USFD, and SFD) diet-fed C57BL/6 and BALB/c mice	141
Figure 18. Time course of 3T3-L1 differentiation	143
Figure 19. Dose and time titration for selecting an optimum dose for treating cortisol and serotonin on differentiated 3T3-L1 cells	145
Figure 20. Effects of cortisol and serotonin treatment, alone and in combination on differentiated 3T3-L1 cells	146
Figure 21. The effects of cortisol and serotonin treatment, combined with differentiated 3T3-L1 cells, co-cultured with RAW264.7 cells	148
Figure 22. Effects of co-culturing RAW264.7 cells, with differentiated 3T3-L1 cells, pre-treated with cortisol and serotonin, alone and in combination	150

Figure 23. Flow cytometric evaluation of pro and anti-inflammatory properties of RAW264.7 cells, co-cultured with cortisol and serotonin treated, differentiated 3T3-L1 cells.....	151
Figure 24. Scatter plots showing the population of RAW264.7 cells expressing select cell surface marker.....	152
Figure 25. Scatter plots showing the population of RAW264.7 cells expressing select cell surface marker.....	153
Figure 26. Schematic representation of diet and chronic psychological stress-induced meta-inflammation, <i>in vivo</i> and <i>in vitro</i>	156
Figure 27. Comparative overview of the significant intestinal microbial phyla and their diversity in control and treatment (SRD, USFD, and SFD) diet-fed C57BL/6 and BALB/c mice	164
Figure 28. Clustering of different diet-fed C57BL/6 and BALB/c mice based on intestinal microbial phyla diversity using a linear discriminant analysis (LDA) plot.	169
Figure 29. Comparative overview of short-chain fatty acid (SCFA) levels in serum from control and treatment (SRD, USFD, and SFD) diet-fed groups of C57BL/6 and BALB/c mice	171
Figure 30. Survival kinetics of differentiated 3T3-L1 cells treated with either Lactobacillus acidophilus MTCC10307 (LA) or a cocktail Lactobacillus delbrueckii sp. bulgaricus strain DWT1; CCM 7992 (LDB) and Streptococcus thermophilus strain DWT4; CCM 7992 (ST).....	177
Figure 31. Uptake of LA or LDB-ST in differentiated 3T3-L1 cells following treatment	179

Figure 32. Effects of treatment with LA or LDB-ST on differentiated 3T3-L1 cells.	181
Figure 33. Schematical representation of the diet-induced changes in intestinal microbes and their relation with host physiology.....	185

List of tables

Table 1: List of intestinal microbes and the meta-metabolites produced by them	50
Table 2: Diet composition.....	57
Table 3: List of primers used in <i>in vivo</i> experiments.....	80
Table 4: List of primers used in <i>in vitro</i> experiments.....	90
Table 5: Major metabolites and pathways impacting the physiology of control and treatment (SRD, USFD, SFD) diet treated C57BL/6 and BALB/c mice.....	123
Table 6: Possible associations between the major microbial phylum and the induced physiological changes following dietary alterations.....	165
Table 7. Percent abundance of Major SCFA producing microbial genera	172

Key words

Diet; nutrition; energy homeostasis; immune biased mice; adiposity; lipidemia; insulin resistance (IR); meta-inflammation; metabolomics; chronic psychological stress; cortisol; serotonin; co-culture; differentiated adipocyte; gut microbiota; probiotic bacteria; lipolysis.

Abbreviations used in the thesis

VM: Ventromedial nucleus; ARC: Arcuate nucleus; CRH: Corticotropin releasing hormone; ACTH: Adrenocorticotrophic hormone; SRD: Starch-rich diet; USFD: Unsaturated fat-rich diet; SFD: Saturated fat-rich diet; vWAT: visceral white adipose tissue; TG: Triglyceride; FFA: Free fatty acids; *Fabp4*: Fatty acid binding acid 4; *Acaca*: Acetyl-CoA Carboxylase Alpha; *Pparg*: peroxisome proliferator-activated receptor gamma; OGTT: Oral glucose tolerance test; AUC: Area under the curve; FBS: Fasting blood glucose; HOMA-IR: Homeostatic model assessment of insulin resistance; ATM: Adipose tissue macrophage; LDA: Linear discriminant analysis; *Il6*: Interleukin 6; *Tnfa*: Tumor necrosis factor alpha; Arg-1: Arginase-1; Tgf- β : Transforming growth factor beta; *Htr2a/5a*: 5-Hydroxytryptamine receptor 2a/5a; *Sert*: Serotonin transporter; *Il1b*: Interleukin 1b; *IL12*: Interleukin 12; *Nos2*: Nitric oxide synthase 2; *Tgfbr1*: Transforming growth factor beta 1 receptor; CD11c, 206, 163, 36: Cluster of differentiation 11c, 206, 163, 36; OD: Optical density; MOI: Multiplicity of infection; LA: *Lactobacillus acidophilus*; LDB-ST: *Lactobacillus delbrueckii* sp. *bulgaricus* and *Streptococcus thermophilus*; ST': *Salmonella typhimurium*.

Chapter 1

**Introductory understanding of the
importance of diet in maintaining
physiological energy homeostasis and the
contribution of the intestinal microbes in
sustaining the process**

1.1.Importance of energy homeostasis, different contributing factors, and its impact on various physiological parameters

The major objective of this chapter is to gain knowledge about current understandings of mammalian metabolism and immunity, and how these parameters are related to the mammalian intestinal microbes. We will also learn how the intestinal microbes can be modulated by diets and give rise to pathophysiological changes resulting in imbalance of energy homeostasis. Energy homeostasis sustains the immediate physiological needs of an organism by maintaining a balance between energy intake and utilization. On the one hand, it directs energy towards various biochemical, genetic, and molecular processes while also storing excess energy as multiple storage molecules (1). An imbalance in energy homeostasis may disrupt many physiological processes by either suppressing necessary functions or enhancing pathophysiological outcomes of over storage (2). The Pathophysiology of excess energy storage may include enhanced visceral adiposity, chronic inflammation, and reduced insulin sensitivity (3). To sustain energy homeostasis, a balanced intake and utilization of various nutrients is an absolute necessity. Generally, for organisms such as higher mammals, a diet consisting of appropriate amounts of carbohydrates, proteins, and fats is necessary for sustaining energy homeostasis. The organism's metabolic rate, habitat, and activity predict the required carbohydrate, protein, and fat. Herbivores skew their diet towards carbohydrates, mainly in the form of plant fibers. Complex carbohydrates like starch and polysaccharides can otherwise be exhausting to metabolize. Certain anatomical features such as an elongated gastrointestinal tract (GI tract) and an assemblage of intestinal microbiota capable of digesting the complex carbohydrates enable herbivores to sustain themselves with their food habits (4–6).

On the other hand, Carnivores support themselves with a protein and fat-rich diet of animal origin. Modified kidney structures and digestive mechanisms enable carnivores to maintain the physiological functions. A more intricate balance between the carbohydrate, protein, and fat is necessary for sustaining various physiological functions that are salient features of omnivore organisms such as humans (7–9). Carbohydrates and fats mainly fuel the body for performing physiological processes. Maintaining a balance of the carbohydrate and fat in diets is thus essential for humans. Irrespective of the form in which one consumes carbohydrates, if they are non-resistant, they ultimately form simple glucose molecules and get readily utilized in the body via several biochemical processes (10). Excess carbohydrates either enhance glycemia or get converted into glycogen in the liver. Prolonged glycemia can increase the chances of type-II diabetes. Increased glycogen storage however, can cause “glycogen storage diseases” such as von Gierke disease, Pompe’s disease, etc. (11). Nevertheless, resistant starches escape the mammalian digestive processes due to their complex chemical structure and form roughage. The resistant starches (RS) have beneficial properties. Certain intestinal bacteria can break down RS to produce beneficial meta-metabolites (12). Fats act mainly as storage molecules. They get transported to the adipose tissue via circulation and get stored for future use. The transportation of fats occurs via lipoproteins in the circulation and various binding proteins in the adipose tissue. In conditions like starvation, extreme cold exposure, and carbohydrate deprivation, fat gets used to produce energy-rich molecules for physiological sustenance and heat production (13). Excess storage of fats can also cause metabolic abnormalities such as visceral adiposity, lipidemia, NAFLD (Non Alcoholic Fatty Liver Disease), type-II diabetes, and cardiovascular disorders (14,

15). The saturation levels of the consumed fat molecules can also dictate the level of lethality or benefits they may cause.

Other factors such as irregular feeding and resting habits, improper lifestyle, psychological state, physical exercise, and genetic background can also influence homeostasis (16). Studies concerning the outcome of irregular meal consumption at an adolescent stage revealed that it might result in metabolic syndrome at a later stage of life (17). Also, high-calorie intake following fasting may result in acidosis (18). Hence, maintaining an appropriate feeding and fasting regime is an absolute necessity for sustaining proper metabolism. While the timing of feeding can dictate the metabolic processes, the activity pattern of the body is also essential for metabolic sustenance. Deprivation or fragmentation of sleep may lead to metabolic abnormalities such as imbalanced appetite, disrupted glucose metabolism, and cardiovascular anomalies (19–21). Nowadays, people frequently follow the irregular feeding and resting patterns of the “western lifestyle (WL).”

The so-called western lifestyle (WL) often causes many metabolic diseases (22). Activities like lack of physical exercise and sedentary routines are associated with the WL, leading to metabolic abnormalities (23). WL therefore is frequently associated with many types of psychological disturbances (24). Improper nutrition and resting, coupled with immense work pressure and an ambiance of high competitiveness, further enhances the chances of becoming psychologically vulnerable, leading to chronic stress (25, 26). Stress can lead to several metabolic abnormalities. Human studies have shown that psychological stress may be associated with several metabolic disorders (27), such as obesity, hypertension, insulin resistance, and cardiac disorders (28). The genetic background of an individual can be an independent risk factor for contracting several metabolic problems. Genome-wide association studies (GWAS)

conducted with different populations have identified mutations in several genes as independent risk factors for metabolic disorders. Lipid transport, packaging, adipogenesis, insulin sensitivity, and energy homeostasis-related genes are examples of metabolic disorder associated genes (29–31).

Together, the association between lifestyle, stress, food habit, and metabolism is essential for understanding the energy homeostasis of mammals. In subsequent sections, I will review how mechanistic understanding of the metabolic processes can be achieved, using different model systems.

1.2. Different *in vivo* and *in vitro* systems for studying energy homeostasis and its physiological effects

Different conventional and genetically modified animal models can help understanding how diet, lifestyle, genetics, and stress affect energy homeostasis. These models are valuable as they can recapitulate several aspects of the human system. Hence, pre-clinical studies conducted using animal models are beneficial for understanding critical questions related to energy homeostasis (32). Rodent models, including but not restricted to mice, rats, guinea pigs, and rabbits, are the most frequently used animal models for studying molecular mechanisms related to physiological energy homeostasis (33). The conventional Sprague-Dawley, Zucker rats, their genetic variants like Zucker fatty (ZF) and Zucker diabetic fatty (ZDF) rats are commonly used rat models for understanding many aspects of physiological energy homeostasis. Both ZF and ZDF rats have mutations in their leptin receptor genes, rendering them insensitive to the calorie-restrictive actions of leptin (34). Besides ZF and ZDF, other rat models include DahlS.Z-Leprfa/Leprfa (DS/obese).

DS/obese rats also have leptin receptor mutations and is very suitable for metabolic syndrome and diabetes-related studies (35). The Spontaneous hypertensive rat and Obese spontaneous hypertensive rat models are ideal for studies related to cardiovascular disorders and hypertension (36, 37).

The conventional C57BL/6 or BALB/c mice and their genetic variants, such as the leptin-deficient *ob/ob* mice, the leptin receptor-deficient *db/db* mice, are most common for studying molecular mechanisms associated with energy homeostasis (34, 38). Also, mutant mouse models like the agouti lethal yellow mice, melanocortin 4 receptor null (MC4-R^{-/-}), LDLR^{-/-} and apoE^{-/-} mice are very useful for studying different aspects of systemic and visceral adiposity (39). The mutant mouse models help understand the impact of varying nutrient-rich diets on metabolic abnormalities. However, other conventional models are also available for studying inter-system interactions occurring during metabolic disease conditions. Conventionally immune-biased mice such as the C57BL/6 and BALB/c, which are T_h1 and T_h2 biased, respectively (40) can be valuable tools for understanding the interaction between immune and metabolic systems. The intrinsic allelic variation of the inflammasome-forming *Nlrp1b* genes in the immune-biased mice makes them differentially susceptible to certain features of metabolic disorders such as adiposity and insulin resistance (41). Other than the immunological differences, BALB/c show less susceptibility towards lipid storage and metabolism. The reduced susceptibility of BALB/c mice is mediated by conventional triglyceride rich diets, compared to C57BL/6 mice. Interestingly, the differential adiposity of the immune biased mice was not related to mitochondrial metabolism (42). Also, substantial difference exists in baseline metabolism of the two mouse strains, for several organs (43). Also the two

strains have difference in dopaminergic neuronal system, leading to difference in cognitive skills, motor activity and circadian rhythmicity (44, 45).

Other than these *in vivo* systems, different *in vitro* systems can also recapitulate several features of metabolic abnormalities and energy homeostasis. Different 2D and 3D model systems utilize the interactions between cells residing in metabolically active tissues. Cell types such as adipocytes, macrophages, lymphocytes, and hepatocytes, of murine and human origin, are often used alone or in combinations (co-culturing) in this context. Studies in the *in vitro* systems are essential, particularly in the context of understanding the exact contribution of a particular cell type in a metabolic process, which is otherwise inaccessible in the *in vivo* systems. On top of these, the simultaneous culturing or co-culturing of multiple cell types can disclose additional information regarding the response of certain metabolically essential cell types in the proximity of other such cells. Thus, the co-culture systems can help dissect many aspects of metabolic disorders (46–48). The following section explains how the mouse model appears to be most suitable for metabolism related studies and how different contributing factors, especially nutrient-rich diets and psychological stress, conditions the murine energy homeostasis.

1.3. Mouse as a model system for studying metabolism and associated pathophysiology

Since mouse appears to be a suitable model system for studying various aspects of metabolism, the utility of studies conducted on mice for understanding metabolic processes is important to know. In spite of substantial cellular and anatomical differences (49), aging skews the lean and fat mass ratio of the body towards the later

in both mice and human. Increase in fat mass mostly occurs during 12-24 months in mice which is equivalent to 70-80 years in humans (50). Aging causes glyceimic changes in mice leading to a correlation in weight gain and glucose intolerance, which is not found in young mice (51). In humans above the age of 40, enhanced β -cell malfunction is observed, leading to increase in glycemia and IR (52). Hence in both mice and humans, aging enhances the risk of metabolic abnormality which shows the suitability of using mouse model. The etiological similarity in terms of genes involved in causing metabolic diseases further enhances the utility of mouse as a model for studying metabolic disorders. Genes, such as *Lep*, *Lepr*, *Ldlr*, *ApoE*, *Ap2* and *C/ebp* act as risk factors for metabolic disorders in both human and mice (39). In the next section, we will be discussing about the perturbing agents of energy homeostasis, for studies related to metabolic disorders.

1.4. Different nutrient-rich diets as possible regulators of energy homeostasis.

The models for studying physiological energy homeostasis can predict the amount of information, extractable from a particular investigation. The tools for perturbing the process of energy homeostasis however, can further the mechanistic understanding. Diets composed with biases towards certain nutrients are among the well-known tools for perturbing the equilibrium of energy homeostasis. Conventionally, diets consisting of either high fat, high sugar, or in combination (HFHS, high fat high sugar diet) are used to perturb the body's energy homeostasis (53). The general tendency of the HFHS diet is the induction of metabolic abnormalities, which consists of enhanced visceral adiposity (54), insulin resistance (55), and cardiovascular abnormalities in conventional model systems (56). These features frequently recapitulate aspects of human metabolic abnormalities (57, 58) arising out of unhealthy food habits. Also,

using genetically modified model systems discussed in the above section and other non-conventional, condition, and organ-specific mutant models gives additional insight into metabolic disorders' mechanisms (59). The conventional HFHS diets are frequently composed of animal triglyceride as a fat source, while sucrose is commonly used as a source of sugars. Recent studies have established that based on the source (animal or plant) and chemical nature of the constituent fatty acids (saturated/unsaturated/trans/omega), the HF diets can exert different physiological outcomes (60). For example, fats originating from plant sources are less harmful than animal sources (61). Again, the degree of saturation of the fatty acids determines how beneficial or detrimental the used fat can be (62). Similar facts are true for carbohydrate and sugar molecules also. Depending on whether the carbohydrate is resistant or non-resistant starch, the digestibility and metabolic outcomes can differ. Also, complexity of the sugar molecules in the polysaccharides can determine the health outcome of consuming a carbohydrate (63). Complex polysaccharides are otherwise indigestible by most higher mammals. Certain intestinal microbes possess various enzymes which can break down the polysaccharides of their mammalian hosts. The breakdown of the polysaccharides by the intestinal microbes produces an array of microbial metabolites or meta-metabolites, which frequently act as important signal transducer molecules, providing health benefits to the host system. The beneficial molecules include short-chain fatty acids (SCFAs) such as acetate, propionate, butyrate, etc. (64, 65). The SCFAs act as a substrate for cell signaling molecules and induce various signaling cascades. SCFAs can also confer additional energies to the host cells. Lastly, SCFAs can help generating anti-microbial peptides in host to combat pathogens and polarize immune cells. (66, 67).

Besides the above-discussed diets, protein-rich diets of specific compositions, supplemented with certain amino acids, also have various health outcomes. The branched-chain and sulfur-containing amino acids have been frequently associated with an enhanced risk for developing metabolic disorders. In contrast, amino acids such as glycine and taurine were associated with an ameliorated metabolic outcome (68). Irrespective of the composition, diets in turn, influence physiological energy homeostasis by maintaining a balance between energy intake and utilization. Consumption of calorie-rich food such as high fat diets, enhance the absorption of fatty acids increases in the gut. The fatty acids get incorporated into the low-density lipoproteins (LDL) and get carried to the white adipose tissue, to be stored in the form of triglycerides (TG) (69). Excess TG storage in the adipocytes induces the secretion of adipokines such as leptin, which regulates energy homeostasis by reducing calorie intake and enhancing lipid breakdown in the adipose tissue (70). The hormone leptin is secreted in circulation and travels to the brain's arcuate nucleus (ARC). In ARC, leptin interacting with the leptin receptors. interaction between leptin and its receptor enhances the number of synapses of the proopiomelanocortin (POMC) producing neuron while reducing the synapses in the neuropeptide Y (NPY) producing neurons. Leptin depolarizes the POMC-producing neurons and enables excess secretion of POMC, which generates α -MSH (melanocyte-stimulating hormone) to assist in bodyweight reduction by suppressing hunger (71, 72). The decrease in calorie intake is sensed by peripheral neurons, which stimulates ghrelin secretion from enteroendocrine cells in the gastrointestinal tract (GI tract). Then ghrelin travels to the brain, where it interacts with its receptor in the ARC, stimulating the release of NPY. The NPY, in turn, stimulates the appetite, enabling calorie intake to sustain the body's energy needs (73, 74). Besides leptin and ghrelin, an adipokine known as adiponectin

plays a significant role in enhancing lipolysis and reduce adiposity. Also, adiponectin can stimulate insulin secretion, which regulates blood glucose and ultimately Insulin sensitivity (75, 76) by promoting glucose uptake in the body cells. Together, the metabolic hormones influence the process of energy homeostasis in an integrated way, which has been described in Figure 1. Different nutrients can impact the secretion of the metabolic hormones differently, leading to differential regulation in energy homeostasis. Hence, nutrients can act as a potent manipulator of metabolic processes which will be discussed in the upcoming sections.

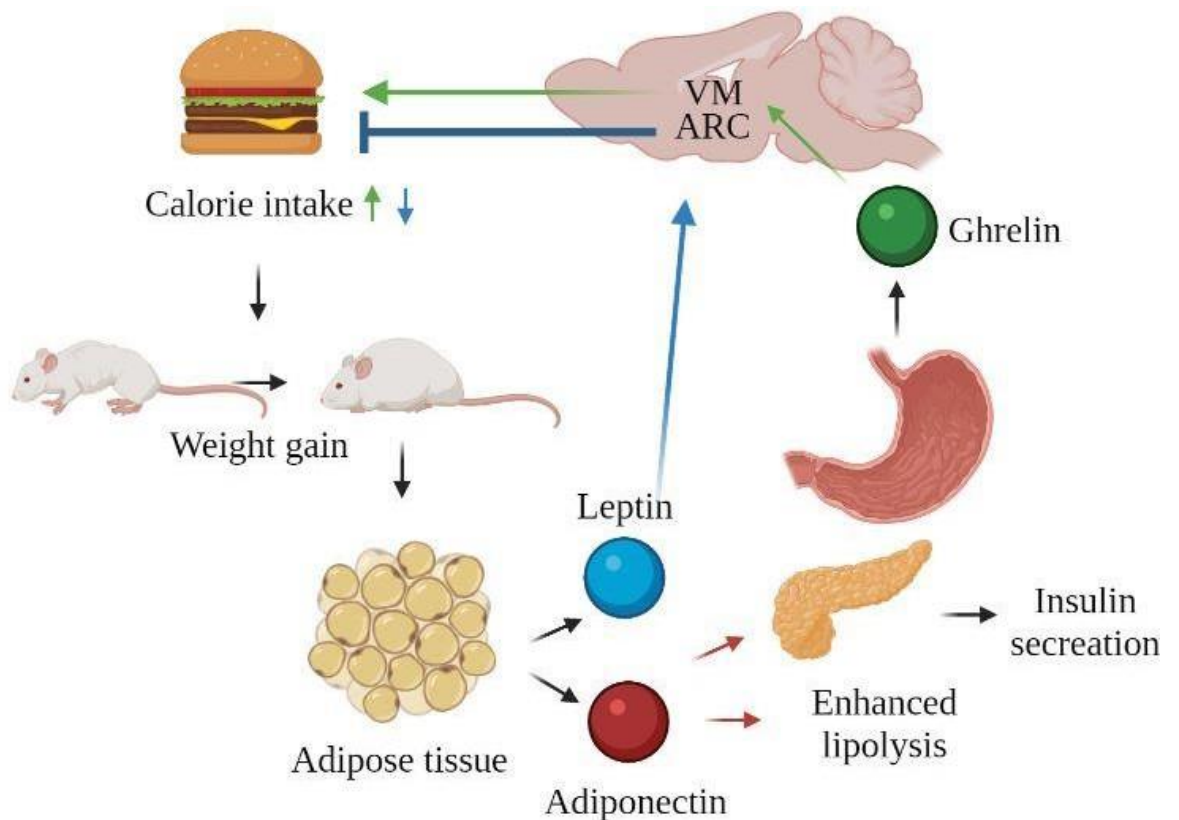


Figure 1. Hormonal regulation of energy homeostasis in mice.

Several hormones strictly regulate the dynamic process of energy homeostasis. Leptin; Excess calorie intake potentiates body weight gain, which fuels the adipose tissue to secrete the anorexigenic adipokine leptin. Leptin exerts its effects on the hypothalamic arcuate nucleus (ARC) and ventromedial nucleus (VM), where a cascade of molecular and cellular interactions hinders the urge of food intake. Adiponectin; Also, a metabolic adipokine, potentiates lipolysis and stimulates insulin release to regulate adiposity and insulin resistance. Ghrelin; A potent orexigenic metabolic hormone secreted by the enteroendocrine cells of the digestive tract, significantly stimulates appetite in a condition of energy starvation. The action center lies in the ARC region of the hypothalamus. The interaction between leptin, ghrelin, adiponectin, and insulin thus plays a critical role in regulating physiological energy homeostasis. (Figure made using <https://biorender.com/>)

1.5. Chronic psychological stress as a regulator of energy homeostasis.

Other than dietary manipulations, the psychological status of an individual can also act as a potent regulator of metabolism and energy homeostasis. Various conditions giving rise to acute and chronic psychological and physiological stress can alter metabolism. Stressor conditions may include irregular lifestyle, disrupted circadian clock, occupational hazards, etc. (77). Irrespective of the nature of the stressor, the outcome of stress may have certain standard features. Stress augments energy utilization which fuels various metabolic processes in the body. Sometimes stress can activate the immune system to combat multiple pathological circumstances arising collaterally with the stress condition. These systemic phenomena are often initiated and regulated by stress hormones such as corticosteroids and corticosteroid regulatory hormones (78). The response of the nervous system towards stress related

physiological abnormalities can stimulate the serotonergic and dopaminergic systems. Together, the corticotropic hormones, serotonin and dopamine control the pathophysiological outcomes of stress conditions (79). The stress hormones, alone or in combination, may regulate processes such as adipogenesis, glycemia, and thermogenesis for which the visceral adiposity and IR levels may change (26). To sustain the stress-associated systemic hyper-activity, the metabolic processes get augmented, affecting energy homeostasis. The altered metabolism can result in phenotypic changes such as enhanced or reduced body weight, aided by alteration in adipose tissue volumes (Figure 2). Enhanced adiposity often is associated with the secretion of chemokines that attracts the immune cells into the adipose tissue from the circulation. Immune cell infiltration in adipose tissue, leads to a persistent metabolism-associated pro-inflammatory condition, also known as meta-inflammation (80). The meta-inflammatory condition involves enhanced macrophage infiltration generating the pool of adipose tissue macrophage or ATM. The ATM may become pro-inflammatory, leading to the secretion of inflammatory cytokines that sustains the chronic systemic inflammatory condition (81). The various contributing factors in regulating energy homeostasis can also influence the intestinal microbiota composition of mammals. The alteration in gut microbiota composition again gives rise to multiple physiological changes, which are discussed in the subsequent sections.

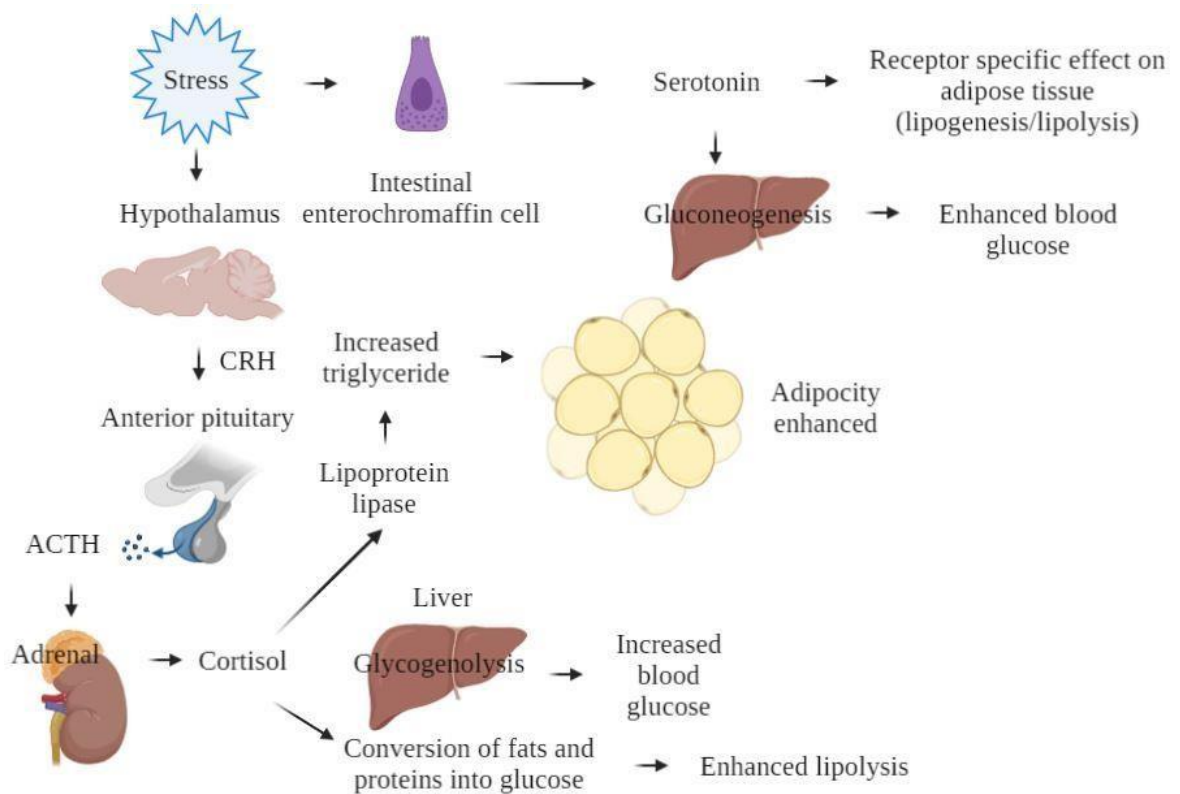


Figure 2. Physiological impacts of stress and stress hormones on glycemic and adipogenic indices.

Chronic psychological stress potentiates the release of primordial stress hormones to combat the physiological energy need. Hypothalamic corticotropin-releasing hormone (CRH), released as a response to stress, stimulates the secretion of adrenocorticotropic hormone (ACTH). The ACTH, in turn, stimulates the release of cortisol, a predominant glucocorticoid from the zona fasciculata of the adrenal cortex. Cortisol may stimulate triglyceride synthesis but may also facilitate the conversion of fat into glucose to aid in the body's excess energy need, which is otherwise taken care of by augmenting glycogenolysis in the liver. Stress may also induce the release of 5-hydroxytryptamine (5-HT), a derivative of tryptophan, and released from the intestinal enterochromaffin cells. 5-HT has similar effects to cortisol and stimulates glycogenolysis while also regulates lipid biosynthesis and metabolism. Both

hormones have a potent regulatory mode of action on the regulation of physiological energy homeostasis, for which they affect body metabolism. (Figure made using <https://biorender.com/>)

1.6. Contribution of intestinal microbes in the regulation of host energy homeostasis.

Intestinal microbes are an assemblage of microscopic organisms which are dominated by bacteria. Other than the bacteria, gut resident virus, fungi and protozoa contribute to the total gut-microbial pool. The gut bacteria live in all the parts of the GI tract, but their number and diversity vary with the organ's chemical environment, such as the level of pH and nutritional availability (82). For humans, initially, it was thought that the number of intestinal microbial cells was ten times of human cells (83) but currently, the numbers are estimated to be almost equal (84). Intestinal microbes contribute to the energy homeostasis processes of their host in several ways. Intestinal microbes can potentiate the breakdown of otherwise undigestible host nutrients. Microbes often harbor several protein-coding genes that generate enzymes to break down the undigested nutrients consumed by the host (65). The undigestible nutrients include resistant starch and other complex polysaccharides that form various meta-metabolites upon digestion by the microbes. Among the meta-metabolites, SCFAs are involved in an array of physiological effects. They often serve as an energy source for the colonocytes and act as cell signaling molecules that interact with G protein-coupled receptors (GPCR) (85). These interactions with the microbial and host cells result in several outcomes, such as cellular proliferation, survival, immunological actions, etc. (86). Hence, depending upon the composition of the intestinal microbes, the host energy homeostasis can be regulated. Perturbation of the intestinal microbes

by any means can indeed lead to a shift in various physiological processes. In this context, we will discuss how diet can act as a potent regulator of intestinal microbes and thus influence the process of energy homeostasis.

1.7. Altered diet as a perturbing agent of intestinal microbes.

The assemblage of intestinal microbes can be altered, by various means. Chemical substances, such as medicines, antibiotics, and other toxic macromolecules, can frequently act as a gut microbial perturbing agent (87, 88). Pathogenic microorganisms often compete with the native gut microbes for nutrients and habitat. The pathogenic microbes can act as a perturbing and disease-causing agent in several ways (89, 90). Ultimately, diets composed of several types of nutrients at various proportions can also influence the composition of intestinal microbes. Since different nutrients can selectively stimulate the growth of certain types of microbes, the nutrient balance in diet can act as a regulator of gut microbial diversity (91). In general, diets enriched with proteins and fibers from plant sources can enhance the microbes belonging to the genus *Bifidobacterium* and *Lactobacillus*. In contrast, the genera *Bacteroides* and *Clostridium* can be reduced. The proteins and fats extracted from animal sources, on the other hand, can show somewhat the opposite effect. The outcome, in turn, leads to a shift in the proportions of the microbial metabolites (Table 1) (92, 93). The change in microbial metabolites influences the physiological processes of the host, such as general metabolism, immune-modulation, adiposity, and glycemia (94). Thus, the pathophysiological conditions of the host depend partially on the intestinal microbes they harbor and the metabolites they produce (Figure 3, Table 1).

Table 1: List of intestinal microbes and the meta-metabolites produced by them

Microbial genera	Major microbial metabolites	Physiological functions
<i>Bacteroides</i> spp., <i>Bifidobacterium</i> spp., <i>Clostridium</i> spp., <i>Ruminococci</i> spp., <i>Akkermensia</i> spp., <i>Blautia</i> spp.	Acetate (95)	Reduces adiposity, enhances insulin sensitivity, and protects from enteropathogenic infection (96, 97).
<i>Clostridium</i> spp., <i>Eubacteria</i> spp., <i>Ruminococci</i> spp., <i>Fusobacteria</i> spp., <i>Coprococcus</i> spp.	Butyrate (95)	Provides intestinal protection, reduces adiposity, enhances insulin sensitivity and neurogenesis (98).
<i>Bacteroides</i> spp., <i>Clostridium</i> spp., <i>Propionibacteria</i> spp., <i>Veilonella</i> spp.	Propionate (95)	Reduces energy intake, body weight, and adiposity (99).
<i>Acidaminococcus</i> spp., <i>Acidaminobacter</i> spp., <i>Campylobacter</i> spp., <i>Clostridia</i> spp., <i>Eubacterium</i> spp.,	Short and branched-chain fatty acid (isobutyrate, 2-methyl-butyrate, and isovalerate) (100–103).	Enhances lipolysis, glucose transport, and immune-boosting (104).

<i>Fusobacterium</i> spp., <i>Peptostreptococcus</i> spp		
<i>Lactobacillus</i> spp., <i>Pseudomonas</i> spp.	Kynurenines (105, 106).	Augments gut-brain interactions (107).
<i>Achromobacter liquefaciens</i> , <i>Bacteroides ovatus</i> , <i>Bacteroides thetaiotamicron</i> ,	Indole (105, 108).	Increases gut integrity and reduces intestinal inflammation (109).
<i>Clostridium</i> spp., <i>Turicibacter</i> spp.	Serotonin (110, 111).	Enhances gut motility, strengthens gut-brain interactions (112).
<i>Escherichia coli</i> , <i>Morganella morganii</i> , <i>Lactobacillus vaginalis</i> .	Histamine (113).	It has profound immunomodulatory effects, regulates gastric inflammation, cardiovascular functions, and cell survival (114, 115).
<i>Enterococcus</i> spp., <i>Lactobacillus brevis</i> .	Dopamine (116, 117).	Acts as a potent neurotransmitter. Regulates cognitive functions, pain, and autoimmune responses (118).

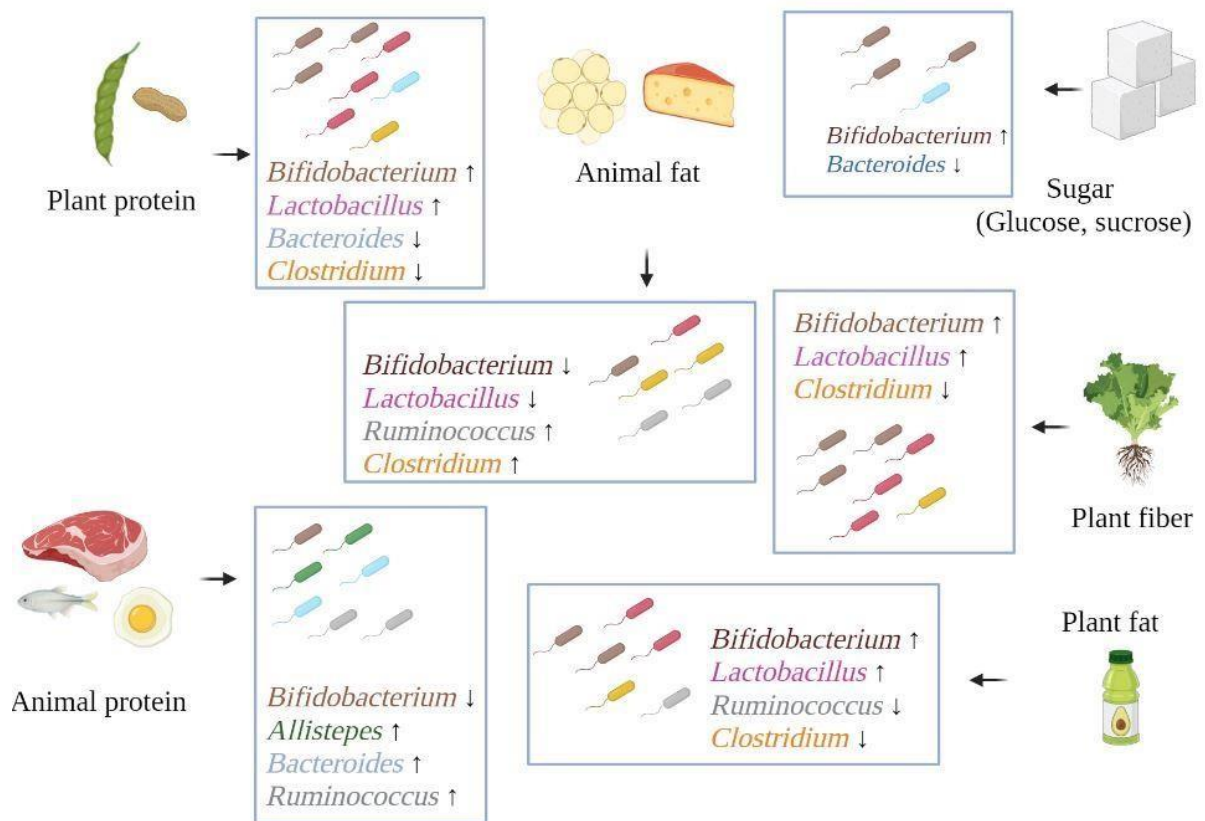


Figure 3. Effects of different nutrients on the mammalian gut microbiota.

A compilation of the consortia of critical short-chain fatty acid (SCFA) produced and gut bacteria enhanced/ reduced by consuming different nutrients such as proteins and fats derived from plant or animal sources, additional sugar, and complex polysaccharides. (Figure made using <https://biorender.com/>)

1.8. Probiotics, prebiotics, and postbiotics: impact on mammalian gut microbiota composition and subsequent effects on host physiology.

Isolating and utilizing beneficial intestinal microbes has been an age-old practice as they provide their host with various beneficial outcomes. The isolation and culturing of probiotic microbes is a highly challenging process. Most of the intestinal microbes are anaerobic (119, 120), and will perish upon an encounter with the aerobic environment. Being particular about the identity of the microbe and identifying its utility was initially done mostly by biochemical methods, which involved mainly the metabolic products of the microbes. Current use of advanced sequencing processes has provided additional strength for identifying the microbes and their beneficial effects. The methods either include marker gene-based or whole genome-based sequencing (121, 122).

Additionally, techniques related to proteome and metabolome characterization of the microbes, such as mass spectrometry (liquid and gas chromatography-based), have helped validate the microbes' functionality (123, 124). Following identification, the culturing and production of the microbes at an industrial scale has been an additional challenge due to the complex growth conditions. Several microbes have been found with the ability to tolerate an aerobic environment, to some extent. These facultative anaerobes have a unique growth requirement and can hence be cultured and utilized more effectively. Besides the isolation and culture, additional features are needed to retain the *in vivo* effects of the microbes. The microbes must survive the environment within their host, receiving them. On top of it, the microbes should colonize, multiply and continue their normal physiological processes. The microbes that confer their host health benefits are called “probiotics” and often involve live microorganisms alone or in combination (125, 126). Often the probiotics can be commercialized. The

probiotics provide their hosts with effects such as modulation of the gut microbiota population, combating pathogen, immune-boosting, and metabolic benefits. To further augment the results of the probiotics, most of the time, substrate components are added to them. These substrates, otherwise known as “prebiotics,” often are composed of complex carbohydrates and resistant starches upon which the microbes can generate their beneficial meta-metabolites (127). Together the probiotics and prebiotics give additional health benefits to their hosts and are called “synbiotics” (128). In various cases, probiotics cannot exert the desired effects on their hosts *in vivo* due to the incompatibility of the host environment. In other cases, the expected magnitude of effects requires excessive amounts of probiotics that are not physiologically possible to achieve. In the said cases, supplementing the hosts with only the beneficial meta-metabolites gives the desired physiological benefits. The microbes' meta-metabolites and other components (cell wall components and other organelles) are cumulatively called “postbiotics.” The postbiotics have been known for exerting equally beneficial effects as probiotics (129). We have provided a summary of the beneficial effects of the pro, pre and, postbiotics in Figure 4.

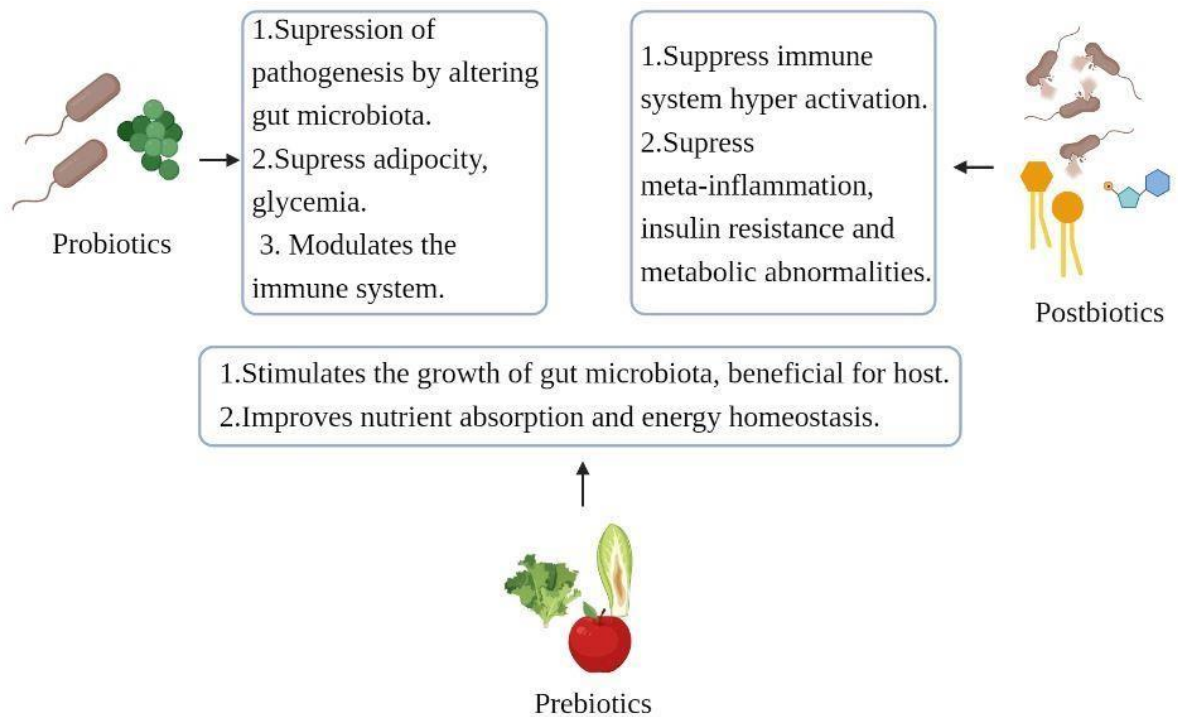


Figure 4. Cumulative beneficial effects of probiotics, prebiotics, and postbiotics.

Probiotics; living microorganisms, chiefly bacteria capable of colonizing and modulating the intestinal environment. These microbes release various types of beneficial metabolites, also called meta-metabolites having health benefits such as protection from pathogens and immune modulation. Prebiotics; The substrates on which probiotics and many intestinal microbes can thrive consist mainly of fibers and indigestible polysaccharides. They also have effects on the host, such as metabolic and immune benefits. Together the probiotics and prebiotics are known as synbiotics. Postbiotics; Composed mostly of meta-metabolites and microbial cell components such as SCFAs, exopolysaccharides and bacterial enzymes. Induces physiological benefits to the host. (Figure made using <https://biorender.com/>)

Materials and Methods:

This section provides details of the protocols and the used reagents for conducting the experiments, described in this thesis.

2.1. Diet formulation, preparation, and treatment conditions.

We used four types of diets for the study described previously (130). Diets consisted of either control, non-resistant starch-rich (for simplicity referred to as starch-rich, SRD), unsaturated fat-rich- (consists of sunflower oil containing 13% saturated fat, 36% polyunsaturated fat, 46% monounsaturated fat, and 5% trans-fat, USFD) or saturated fat-rich- (consists of coconut oil containing 88.2% saturated fat, 9.2% monounsaturated fat, 1.2% polyunsaturated fat, and 1.4% trans-fat, SFD) diet. We formulated and sterilized the diets following the previously mentioned procedure (131). The process involved autoclaving (OATG 52, Osworld Scientific Equipments) the prepared diets at 121°C and 10–15 Psi pressure for 20 min. We have enlisted nutrient details of the formulated diets in Table 2.

Table 2: Diet composition (We have provided the quantity of individual nutrients used to compose the diet in gram and Kcal unit)

Nutrients	Control diet		SRD		USFD		SFD	
	Amount in gram	Amount in Kcal	Amount in gram	Amount in Kcal	Amount in gram	Amount in Kcal	Amount in gram	Amount in Kcal

Corn starch (Himedia, India)	0	0	42.73	39.5	31.12	20.75	31.12	20.75
Wheat starch (Urban platter, India)	57.06	52.75	14.33	13.25	10.32	6.88	10.32	6.88
Sucrose (Himedia, India)	3.96	3.65	3.96	3.65	4.64	3.09	4.64	3.09
Casein (SRL, India)	32.02	29.6	32.02	29.6	13.23	8.82	13.23	8.82
Methionine (Himedia, India)	0.44	0.4	0.44	0.4	0.69	0.46	0.69	0.46
Sunflower oil (Nature land organics, India)	3.26	6.8	3.26	6.8	40	60	40	0

Coconut oil (Indic wisdom, India)	3.26	6.8	3.26	6.8	0	0	0	60
Total	100	100	100	100	100	100	100	100

Note: We provided the vitamin mixture (GrowelNeoxyvita Forte, India; 0.3% of the total weight of diet) and mineral mixture (Growel chelated growmin forte, India; 0.3% of the total weight of diet) in the same quantity for all the diets.

2.2. Housing and maintenance of experimental animals.

We procured all animals from the Animal Research and Experimentation Facility, School of Biological Sciences, NISER, Bhubaneswar, India. Following housing, we experimented with the animals in the said facility under sterile conditions. We collected samples from the animals after euthanizing them by cervical dislocation without the usage of any type of anesthetic. We used six-week old male C57BL/6 and BALB/c mice for all the experiments. We co-housed the animals for an initial period of one week. Following co-housing, we divided equal number of animals into either control or the treatment diet groups (SRD, USFD, SFD). We kept animals from each group in individually ventilated cages (IVC, Citizen, Gujrat, India) made of Polyphenylsulfone, bedded with sterilized corn cobs. The cages had *ad libitum* access to the respective type of food and sterile water. We maintained the rooms at 12 h light/12 h dark cycle, 23°C temperature, and 60% humidity. The Institutional Animal

Ethics Committee approved the protocols for animal usage (IAEC, Reg. No-1634/GO/ReBi/S/12/CPCSEA, protocol number NISER/SBS/IAEC/AH-181).

2.3. Animal autopsy, sample collection, and preservation.

We sacrificed the control and treatment diet fed C57BL/6 and BALB/c mice after a period of four and eight weeks of dietary alterations. We collected tissue, serum, and cecal samples from the mice. We handled the animals subjected to functional assay such as oral glucose tolerance test (OGTT) separately, described in subsequent sections. We collected the vWAT after sacrificing the animals by cervical dislocation at the end of four and eight weeks. We stored the vWAT from respective groups of animals in Allprotect Tissue Reagent (QIAGEN, USA, MD) and kept the tissues at -80°C freezer (CryoCube F570, Eppendorf, Germany, Hamburg) until processing for RNA isolation. Alternatively, we stored the tissues in 4% paraformaldehyde at room temperature for histological studies. We snap-froze the tissues by submerging them in liquid nitrogen and then kept them at -80°C for fluorescent imaging (by BODIPY) of whole-mount tissues. We used fresh vWAT for imaging macrophage cell surface proteins (F4/80 staining of adipose tissue macrophages).

After four and eight weeks, we isolated the blood from the animals by cardiac puncture following sacrificing by cervical dislocation. We allowed the blood to clot for 30 min at room temperature, after which the blood was centrifuged (Centrifuge 5430R, Eppendorf) at 1600×g for 15 min at 4°C, followed which we collected the serum.

We collected the caecae from respective groups of animals after sacrificing them at the end of four and eight weeks. After collection, we washed the cecum with sterile 1XPBS and then squeezed the tissue using forceps to extract the contents. We stored the cecal

contents in sterile 1.5 ml MCT and immediately snap-frozen them. We kept the cecal matter at -80°C until further usage. The processes of animal euthanasia, blood, tissue, and cecal matter collection for all experiments described in this thesis are consistent with the details of this section if not otherwise mentioned. We have provided details of all the experimental processes in subsequent sections.

2.4. Measurement of calorie intake, assessment of body weight and visceral fat.

We assessed the animals' calorie intake and body weight from week zero till the end of the experimental period (week 8). We measured body weight using a weighing balance (QUINTIX 224, Sartorius, Germany, Göttingen). We evaluated the changes in body weight relative to week zero to understand the assimilative effects of the diets on the mice. To assess caloric intake, we measured the daily food intake of the animals using a weighing balance (QUINTIX 224, Sartorius, Germany, Göttingen). We then multiplied the food weight by the calorie content of each diet. Further, we measured the visceral adipose tissue weight (vWAT weight) after four and eight weeks of dietary alterations and calculated a vWAT index. We used the following formula for calculating the vWAT index

$$\text{vWAT index} = \text{vWAT weight} / \text{mouse body weight}$$

2.5. Assessment of serum hormones and lipid profiling.

We used the isolated serum from each control and diet-treated mice to assess metabolic hormones and the lipid profile. Among the metabolic hormones, we evaluated the concentrations of leptin, adiponectin, ghrelin, and insulin. We also

determined the serum triglyceride and free fatty acid levels as a marker of the serum lipid profile. We performed all the assays spectrophotometrically (MultiscanGO, Thermo Scientific, USA, MA) using commercially available kits (RayBiotech, USA, GA for the hormones and Sigma, USA, MO for the lipid profiles). We are providing a brief description of all the protocols that we used for performing these assays.

2.5.1. Protocol for the assessing total serum protein using Bradford assay.

- A.** We performed the assay with a total reagent volume of 210 μl (Bio-Rad, USA), using the manufacturer's instructions (132).
- B.** Using a 1 mg/ml stock solution, we produced a 50-1000 $\mu\text{g/ml}$ BSA standard.
- C.** We added 10 μl of each sample and background (ddH₂O) in the appropriate reaction wells to make the total reaction volume 250 μl , using the diluted Bradford reagent (1 part stock reagent, 4 parts ddH₂O). Proper dilution for the samples was determined using an array of samples dilution in a pilot experiment.
- D.** After sample addition, we mixed and pipetted the samples in the wells, and incubated the plate for 10 minutes at room temperature (RT).
- E.** We recorded the absorbance of the samples from each well at 595 nm.
- F.** After subtracting from the background, we prepared the standard curve and determined the protein concentration of each sample. For the ELISA, we diluted the samples according to their respective protein concentrations.

2.5.2. Protocol for the assessment of serum leptin/adiponectin/insulin level by sandwich ELISA

- A.** We prepared the standards, positive, negative controls, and samples for all the assays separately, following the manufacturer's instructions (133–135). For the samples, we determined the appropriate dilutions following a pilot experiment. The following steps are identical for all the assays.
- B.** We brought all the kit's reagents to RT and added 100 μ l of each control, standard, and sample to the designated, capture antibody pre-coated wells. Next, we covered the wells and incubated them for 2.5 h at RT with gentle shaking.
- C.** After 2.5 h we discarded the well contents by inverting and blotted the wells dry with tissue paper. Next, we washed the wells with 300 μ l of 1Xwash buffer (provided), four times, after which wells were inverted and dried.
- D.** Next, we added 100 μ l of 1Xbiotinylated detection antibody to each well and incubated them for 1 h at RT with gentle shaking.
- E.** After 1 h, we discarded the solution from the wells and repeated step 'C'.
- F.** Next, we added 100 μ l of prepared streptavidin solution to each well and incubated the wells for 45 minutes at RT with gentle shaking.
- G.** After 45 minutes, we discarded the solution from the wells and repeated step 'C'.

- H.** Next, we added 100 μ l of TMB one-step substrate reagent to each well. We incubated after adding TMB for 30 minutes at RT in the dark with gentle shaking.
- I.** Finally, we added 50 μ l of stop solution to each well and took the readings of the wells at 450 nm immediately.
- J.** We used the standard well's readings to prepare a standard curve and determined the concentrations of the samples from their respective readings using this standard curve.

2.5.3. Protocol for the assessment of serum ghrelin level by competitive ELISA.

- A.** We prepared the plates, standards, positive, negative controls, and samples following the manufacturer's instructions (136). For the samples, we determined the appropriate dilutions following a pilot experiment.
- B.** We then added 100 μ l of anti-ghrelin antibody to the designated wells and incubated for 1.5 h at RT with gentle shaking.
- C.** After 1.5 h we discarded the well contents by inverting and blotted the wells dry with tissue paper. Next, we washed the wells with 300 μ l of 1Xwash buffer (provided), four times, after which wells were inverted and dried.
- D.** Then, we added 100 μ l of each standard, control, and sample to the designated wells, covered them, incubated for 2.5 h at RT with gentle shaking.
- E.** We then discarded the solution in the wells and repeated step 'C'.

- F.** Then we added 100 μ l of HRP-streptavidin solution to each well, incubated the wells for 45 minutes at RT with gentle shaking.
- G.** We then discarded the solution in the wells and repeated step 'C'.
- H.** Afterward, we added 100 μ l of TMB-one step substrate reagent to each well, incubated at RT for 30 minutes in the dark with gentle shaking.
- I.** Finally, we added 50 μ l of stop solution to each well and took the readings of the wells at 450 nm immediately.
- J.** We used the standard well's readings to prepare a standard curve and determined the concentrations of the samples from their respective readings using this standard curve.

2.5.4. Protocol for the assessment of serum triglyceride level by spectrophotometry

- A.** According to the manufacturer's instruction, we initially prepared the free glycerol and triglyceride reagents (provided) (137).
- B.** In the cuvettes designated for the background, standard, control, and treatment, we pipetted 0.8 ml of free glycerol reagent.
- C.** We next added 10 μ l of water, standard solutions, and serum from the control and treatment mice in the designated cuvettes, mixed by gentle inversion and incubated at 37°C for 5 minutes.
- D.** We then acquired the absorbance of each cuvette at a 540 nm wavelength. This absorbance value was named initial absorbance (*IA*).
- E.** We then added 0.2 ml of triglyceride reagent to each cuvette, mixed and incubated at 37°C for 5 minutes.
- F.** We then recorded the final absorbance (*FA*) at 540 nm wavelength.

G. We then calculated the serum glycerol and triglyceride concentrations using the following formulae.

H. Serum triglyceride concentration = $\frac{[FA_{Sa} - (IA_{Sa} \times 0.8)]}{[FA_{St} - (IA_{Ba} \times 0.8)]}$ X Concentration of standard

Where, IA_{Sa} = Initial absorbance of samples, IA_{Ba} = Initial absorbance of background FA_{Sa} = Final absorbance of sample, FA_{St} = Final absorbance of standard, 0.8 is the dilution factor of the free glycerol reagent to the total reaction volume.

2.5.5. Protocol for the assessment of serum free fatty acid level by spectrophotometry

- A.** We prepared the standards according to the manufacturer's protocol (138).
- B.** In a pilot experiment, we determined the appropriate dilution (with fatty acid assay buffer provided) for the serum samples.
- C.** We added the serum samples directly to the designated wells of a 96 well plate. Then we added a master solution containing 2 μ l of each fatty acid probe, enzyme mix, enhancer, and 44 μ l of fatty acid assay buffer (provided) to the wells.
- D.** We mixed the well contents by pipetting and incubated the reaction for 30 minutes at 37°C.
- E.** We measured the absorbance of each well at 570 nm.
- F.** The fatty acid concentration was determined using the following formula

Serum-free fatty acid concentration = $\frac{F_a}{S_v}$ Where F_a = amount of fatty acid in an unknown sample, S_v = Sample volume added to the wells.

2.6. Oral glucose tolerance test (OGTT) and insulin resistance (IR) measurements.

We performed OGTT to evaluate the glucose metabolism rate associated with each of the diets. We are providing below the details of the two processes.

2.6.1. Performing OGTT and generation glucose response curve (GRC)

- A.** We performed the OGTT after four and eight weeks of dietary intervention.
- B.** Before initiation, we deprived the mice of all the groups of food and water for six hours at night.
- C.** After six hours, we orally gavaged (20-gauge gavage needle, Sigma, USA) the mice with glucose (Himedia, India) at 2g/kg body weight.
- D.** After this, we collected blood from the mice by tail vein sampling and subjected them to blood glucose assessment by using a commercial glucometer (*Accu-CHEKO Instant S* Glucometer, Roche, Switzerland, Basel). We collected blood during fasting and 15, 30, 60, 90 minutes after administration of glucose.
- E.** From the values of blood glucose levels estimated at the mentioned time points, we generated a GRC.
- F.** We subsequently determined the area under the curve (AUC) for each condition using the trapezoid area determination method. We

performed area measurements to compare the cumulative blood glucose levels among treatment groups.

2.6.2. Assessment of insulin resistance by HOMA-IR model

- A. We determined the insulin resistance (IR) levels of the mice by using the Homeostatic model assessment of insulin resistance (HOMA-IR) method (139).
- B. We used the fasting blood glucose (FBS) and fasting serum insulin (FSI) levels to determine the IR levels, using the following formula.

$$\text{HOMA-IR} = (\text{FBS} \times \text{FSI}) / 22.5$$

2.7. Isolation of serum metabolites and sample preparation for metabolomic studies.

We used freshly isolated serum samples for this study. First, we processed the serum samples following the previously described protocol (89). Briefly, we first removed abundant serum proteins by passing the serum through pre-washed (7 times, Milli-Q water, SUREPRO PREFILTRATION SYSTEM, Millipore, India) Amicon Ultra-2ml 3000 MWCO (Merck Millipore, USA) column via centrifugation at 4°C and 12,000Xg. Then, we took a total of 700 µL solution to perform individual NMR experiments. The sample contained serum from individual mice belonging to each treatment group, deuterium oxide (Aldrich, USA, St Louis), pH maintenance buffer containing the internal standard Sodium 3-(Trimethylsilyl)-1-propane sulfonate (TCI, Japan, Tokyo) into 5 mm Wilmad NMR tubes (Sigma, USA, NJ).

2.8. Assessment of serum metabolomics by ¹H NMR.

We performed all NMR experiments at 298K on a Bruker 9.4T (400 MHz) Avance-III Nanobay solution-state NMR spectrometer equipped with a 5 mm broadband probe. For water suppression, we used excitation sculpting using gradients of duration 1 ms and strength 14.9 G/cm (31% of 48.15 G/cm peak power). We performed offset optimization using real-time 'gs' mode for each sample. In addition, we employed a Sinc-shaped pulse of 2 ms for selective excitation of the water resonance. We recorded 64 transients for each set of experiments with an average recycle delay of 1s. We recorded and processed the acquired spectra by Topspin 2.1. We used Chenomx NMR Suite7.6 (ChenomxInc., Edmonton, Canada) to identify (targeted) and quantify metabolite signals from NMR spectra. In addition, we performed pathway analysis by using Metaboanalyst 5.0 (a public software at <https://www.metaboanalyst.ca>).

2.9. Analysis of NMR data for metabolome-based segregation and quantification of the effects of dietary alterations

We classified the untreated (control) mice and those treated with different diets using the serum metabolites' linear discriminant analysis (LDA). LDA is a method of dimension reduction to find the distribution of the variables (metabolite abundance) for each mouse based on the mean and variance of the data. Each mouse is expressed as a linear combination of variables to determine how closely mice in a treatment group cluster together based on functional variances of components (metabolites in the current study) in two dimensions termed Function 1 and Function 2. Function 1 denotes the principal component with the highest variance, followed by Function 2. We classified the groups using the statistiXL 2.0 software to add to the MS-office version of the Excel spreadsheet in Windows OS. The multi-variate LDA analysis was

done on an untargeted list of metabolites. From the same list, we identified the differentially expressed significant metabolites in each experimental condition. We designated the metabolites to be differentially expressed if their concentrations were significantly different (2-way ANOVA, Bonferroni post-test) between the mice strains treated with a particular type of diet.

Following the LDA classification of the mice per treatment conditions, we wanted to quantify the differences exhibited as a result of various treatment conditions, including the control group. We introduced a newer methodology of calculating projections and contributions of each treatment cluster of mice on a vector space. We calculated the total vector displacement of the centroid of each treatment group (including control) from the origin of the vector space. For example, let's consider three treatment groups and know the distance between any two groups. We defined the resultant vector displacement between remaining groups of interest as the sum of vector distances between the centroids of the groups under consideration by using the formula.

$$r = \sqrt{(a + b \cos \theta)^2 + (b \sin \theta)^2}$$

Where r is the resultant distance to be determined between centroids of two remaining groups in consideration, \vec{a} and \vec{b} are the known vector distances and θ is the angle between \vec{a} and \vec{b} .

The respective vector displacements (Pearson correlation) correlated with the number and concentration differences of the significantly altered metabolites from individual treatment conditions to understand whether the metabolomic diversity or abundance was the most significant factor contributing to the physiological changes. We

calculated the serum metabolomic index for each control and treatment group using the following formula.

$$\text{Metabolomic index (Met I)} = -\sum M_i \ln M_i$$

Where M_i is the ratio of respective metabolite concentration divided by the total concentrations of metabolites in that group. $\ln M_i$ is the natural logarithm of M_i with a base of natural exponent (e) and $-\sum$ stands for the negative of the sum of $M_i \ln M_i$ for a mouse in a particular treatment condition.

Finally, we used the list of significantly altered metabolites to predict biological pathways using the MetPA function of the MetaboAnalyst 5.0 software. Briefly, we manually entered the compound lists into the pathway analysis module along with the necessary metadata. The metabolite lists generated an overview plot of the predicted pathways, with log-transformed p values of the pathway enrichment analysis in the Y-axis and pathway impact from the pathway topology analysis on the X-axis. From the list of predicted pathways, we chose the ones with high impact scores to be altered due to dietary interventions, giving rise to the altered physiological responses in the immune-biased mouse strains following the treatment periods.

2.10. Measurement of visceral white adipose tissue (vWAT) morphology by hematoxylin and eosin (H & E) staining of paraffin-embedded tissue sections.

We collected vWAT from each C57BL/6 and BALB/c mouse group at the end of four and eight weeks. We processed the tissues following the previously mentioned protocol (140). Below, we are providing a brief description of the process.

2.10.1. Paraffin embedding and sectioning of vWAT

- A.** After sacrificing the animals, we collected the vWAT from the mouse and immediately preserved the tissues in 4% paraformaldehyde (PFA, Himedia, India).
- B.** After overnight fixation, we washed the tissue in 1XPBS and cut them into small pieces.
- C.** Next, we placed the tissue pieces in pre-labeled histological cassettes (Himedia, India).
- D.** Following this, we incubated the tissue containing cassettes in a series of chemicals as described below
 - a.** 75% ethanol (Millipore, Germany) for 30 minutes.
 - b.** Twice, 95% ethanol for 75 minutes.
 - c.** Thrice, 100% ethanol for 60 minutes.
 - d.** Twice, 100% xylene (Himedia, India) for 60 minutes.
 - e.** Melted paraffin-1 (Surgipath paraplast high melt, Leica, Germany), 60 minutes at 60°C.
 - f.** It melted paraffin-2 overnight at 60°C.
 - g.** Melted paraffin-3, 60 minutes at 60°C.
- E.** Now, we placed several embedding molds (Leica, Germany) on a hot plate (Eppendorf, Germany), pre-set at 60°C. We poured melted paraffin into the molds.
- F.** We gently took out the embedding cassettes from melted paraffin-3 and took out the tissues from the cassettes. Then we placed the tissues on the molds.

- G.** Immediately, we took the molds and placed them at 4°C to get solidified.
- H.** After solidification, we tapped the molds and took out the paraffin blocks from them. The blocks were marked and cut to appropriate pieces for tissue sectioning.
- I.** We then set the molds on a microtome (HistoCore MULTICUT, Leica, Germany), cut 6 µm thick tissue sections, and placed them on poly-lysine coated slides.
- J.** We then stained the tissues attached to the slides using Hematoxylin and eosin.

2.10.2. *Hematoxylin and eosin staining of vWAT tissue sections*

- A.** To deparaffinized, rehydrate and stain the tissue pieces, we incubated the tissue containing slides in the following chemicals
 - a.** Twice, 100% xylene (Himedia, India) for 5 minutes.
 - b.** Twice, 100% ethanol for 5 minutes.
 - c.** 90% ethanol for 2 minutes.
 - d.** 80% ethanol for 2 minutes.
 - e.** 70% ethanol for 2 minutes.
 - f.** ddH₂O for 5 minutes.
 - g.** Mayer's Hematoxylin (Himedia, India) for 15 minutes.
 - h.** ddH₂O for 5 minutes.
 - i.** Scott's solution (Himedia, India) for 3 minutes.
 - j.** ddH₂O for 5 minutes.
 - k.** Eosin Y (Himedia, India) for 2 minutes.

- l.** 70% ethanol for 2 dips.
 - m.** 95% ethanol for 2 dips.
 - n.** Twice, 100% ethanol for 5 minutes.
 - o.** Twice, 100% xylene for 5 minutes.
 - p.** Mounted in DPX (Himedia, India).
- B.** We then observed and took brightfield images of the slides in the CKX53 microscope (OLYMPUS, Japan, Tokyo). We took the images in 40X magnification. We measured the frequency distribution of the adipocyte areas as a measure of vWAT histological changes.

2.11. Measurement of vWAT lipid content by BODIPY staining of tissue whole mounts.

We used snap-frozen vWAT for the assessment of the cellular lipid content. We stained the intracellular lipid droplets, using the fluorescent dye Difluoro{2-[1-(3, 5-dimethyl-2*H*-pyrrol-2-ylidene-*N*)phenylmethyl-3,5-dimethyl-1*H*-pyrroloato-*N*]boron (BODIPY 493/503, Sigma, USA), following previous protocol (140, 141). Briefly, we cut the tissues into small pieces and then washed them with 1XPBS thrice. We then incubated the pieces with the BODIPY stain (1:100 dilution) for 30 minutes. The pieces were then washed with 1XPBS thrice and mounted on slides using Fluoromount-G (ThermoFisher, USA). We imaged the whole mounts using an SP8 LIGHTNING confocal microscope (Leica, Germany) at 20X magnification. We measured the fluorescence intensity of the adipocytes, and from this, we measured the visceral adiposity levels by multiplying the average cellular fluorescence intensities with the vWAT index.

2.12. Assessment of macrophage infiltration inside vWAT by direct immune fluorescence of vWAT whole mount.

We identified the rate of macrophage infiltration of vWAT by performing direct immunofluorescence of the F4/80 +Ve cells. We counter-stained the tissues with DAPI to label the nuclei in the tissue. We used the following protocol for staining.

- A.** We cut fresh vWAT tissues into 0.25-0.75 cm² sized pieces and incubated them with fixing buffer for 30 minutes at RT with gentle rocking.
- B.** We washed the pieces in PBST (0.1% Tween 20 in 1XPBS, Himedia, India) thrice for 5 minutes each time.
- C.** Then we incubated the tissues in permeabilization buffer (0.5% TritonX-100 in 1XPBS, Himedia, India) for 5 minutes at RT.
- D.** We repeated step 'B'.
- E.** Performed non-specific protein blocking of tissue pieces using blocking buffer (5% BSA in 1XPBS, Himedia, India) for 30 minutes at RT with gentle rocking.
- F.** We incubated the tissues in phycoerythrin (PE) conjugated antibody (rat anti-mouse, 1:100 fold diluted in blocking buffer, Invitrogen, USA) overnight at 4°C.
- G.** We repeated step 'B' with 10 minutes of washing each time.
- H.** Incubated in 4',6-Diamidino-2-Phenylindole, Dihydrochloride (DAPI) working solution (0.1 µg/ml in 1XPBS, Thermofisher, USA) for 5 minutes at RT.
- I.** We repeated step 'B' with 15 minutes of washing each time.

- J.** Using Fluoromount-G (ThermoFisher, USA), we mounted the tissues in slides and observed and imaged the tissue using SP8 LIGHTNING confocal microscope (Leica, Germany) at 20X magnification. We calculated the numbers of F4/80 +ve regions from the images to measure macrophage infiltration rates.

2.13. Image analysis by ImageJ software.

We quantified the relevant parameters of both the bright field and fluorescence images using ImageJ software (Version 1.8.0_112, USA). Our results depicted the adipocyte sizes, lipid content, and ATM infiltration rates following the dietary interventions.

2.14. RNA isolation and cDNA preparation from vWAT.

We performed RNA isolation, cDNA preparation, and relative mRNA level quantification (qRT-PCR), using commercially available kits, following the manufacturer's protocols with slight modifications. Below, we provide the details of the processes.

2.14.1. RNA isolation from vWAT

- A.** We used RNeasy Lipid Tissue Mini Kit (142) (Qiagen, USA) for isolating total RNA from vWAT tissues, following the manufacturer's protocol with slight modifications.
- B.** We cut 200 mg of tissue into small pieces after taking them out of the Allprotect tissue reagent and washing them in 1XPBS twice.

- C.** We homogenized the tissue in liquid nitrogen, after which we added 1ml QIAzol lysis reagent (provided). We performed the homogenization in a porcelain mortar and pestle (TARSONS, India).
- D.** We incubated the homogenate at RT for 5 minutes after pipetting it in a nuclease-free 2 ml MCT (TARSONS, India).
- E.** Next, we added 200 μ l molecular biology grade chloroform (Sigma, USA) and thoroughly vortexed (Select Bioproducts, USA) for 15 seconds. Following this, we incubated the samples at RT for 3 minutes.
- F.** We then centrifuged (Eppendorf, Germany) the tubes at 12000 x g for 15 minutes at 4°C.
- G.** Following centrifugation, we could visualize the upper clear aqueous phase. We carefully isolated the aqueous phase into a new 2 ml MCT and added 1 volume of 70% molecular grade ethanol (Millipore, USA).
- H.** After briefly vortexing the mixture, we transferred 700 μ l aliquots into the RNeasy Mini spin column. The column was centrifuged at RT for 15 seconds at 8000 x g. The flow-through was discarded. We repeated this step until the entire content of step 'G' was utilized.
- I.** We now added 700 μ l buffer RW1 to the spin column and centrifuged at 8000 x g. We discarded the flow through.
- J.** We added 500 μ l buffer RPE to the column and centrifuged at 8000 x g for 15 seconds. We repeated the same step but centrifuged for 2 minutes.
- K.** We performed centrifugation at full speed for 2 minutes to dry the membrane.

- L. We removed the column and placed it in a new 1.5 ml MCT. We added 30 μ l of nuclease-free water (NFW, Himedia, India) and, after incubating at RT for 1 minute, centrifuged the tube for 1 minute at 8000 x g. The tube elute was used for further quality control of RNA, which we will discuss in subsequent section.

2.14.2. *Determination of concentration and integrity of RNA by spectrophotometry and agarose gel electrophoresis*

We used the MultiscanGO plate reader for evaluating the concentration of nucleic acids in the isolated RNA samples. We checked the absorbance from 210-340 nm wavelengths and determined an absorbance spectrum for each sample in the instruments. We used the absorbance value at 260 nm to quantify the concentration of RNA samples. Then, from the absorbance at 280, 260, and 230 nm, we determined the $A_{260/280}$ and $A_{260/230}$ ratios. The samples with a concentration \geq of 300 ng/ μ l, an $A_{260/280}$ of around 2, and $A_{260/230}$ of about 2-2.2 were used for further processing. We next performed agarose (1.2%) gel electrophoresis to check the integrity of the RNA samples. We then used the RNA samples to produce cDNA.

2.14.3. *Preparation of cDNA from total RNA*

- A. We used a commercially available Affinity Script One-Step RT-PCR Kit (Agilent, USA) (143) for converting the RNA into cDNA. We conducted the reactions to convert a total of 3 μ g mRNA into cDNA.
- B. The kit consisted of a buffer containing dNTPs, necessary metallic ions, Polymerase enzyme (Herculase II), a reverse transcriptase/

RNAse block enzyme mixture (RT/RNase block), and a random 9-mer mix.

- C. We first added the buffer into a nuclease-free MCT. The buffer volume was the sum of RNA, 9-mer, and RT/RNase block needed for the reaction.
- D. Then we added 1 μ l of 9-mer to the mix.
- E. Then we added the RNA.
- F. We next incubated the mix at 65°C for 5 minutes in a heat block (Eppendorf, Germany).
- G. Then we added 1 μ l of RT/RNase block to the mixture and incubated for 60 minutes at 45°C.
- H. We then added NFW to a final volume of 100 μ l and terminated the reaction.

2.15. Relative mRNA expression analysis of select metabolic genes from vWAT.

- A. The relative mRNA expression levels were assessed by qRT-PCR analysis using QuantStudio™ 7 Real-Time PCR System (Applied Biosystems™, USA).
- B. We used a total of 10 μ l of reaction mix for each reaction well.
- C. We added 5 μ l of master mix (Containing dNTPs, metallic ions, SYBR green, Taq-DNA polymerase, GoTaq® 1-Step RT-qPCR, Promega, USA) (144) to the wells.
- D. Next, we added 1 μ l of 10 μ M forward and reverse primers (IDT, USA) to the reaction mix.

E. We finally added 1 μ l of cDNA (previously described) and adjusted the reaction volume to 10 μ l.

F. We used the following cycle steps for amplification (denaturation at 95°C for 15 seconds, annealing at 60°C for 30 seconds, and extension at 72°C for 30 seconds, a total of 40 cycles).

G. We noted the cycle threshold (C_t) values for each gene and used them to plot the fold change in gene expression using the following formula

$$\text{Fold change} = 2^{-\Delta [(C_t \text{ of the gene of interest in the treatment group} - C_t \text{ of the house-keeping gene in the treatment group}) - (C_t \text{ of the gene of interest in the control group} - C_t \text{ of the house-keeping gene in the control group})]}$$

H. We have provided the details of the primers used for the genes of interest and house-keeping gene (*Gapdh*) in Table 3.

Table 3: List of primers used in *in vivo* experiments.

Gene name	Sense strand	Antisense strand	NCBI Accession number
<i>Acaca</i>	5'- GCTCACA CACTTCTGAACAC-3'	5'-GCCGAGTCA CCTTAAGTACA-3'	NM_ 133360.2
<i>Il6</i>	5' -TTCCATC	5' -GTTGGGAG	NM_

	CAGTTGCCTTCTT-3'	TGGTATCCTCTG-3'	001314054.1
<i>Caveolin-1</i>	5' - ATACGTAGACT CCGAGGGAC - 3'	5' - GTGAGGACA GCAACCAATTC - 3'	NM_ 007616.4
<i>Tnfa</i>	5'-CCCACGTCGTAG CAAACCACCAAG-3'	5'-TGCCCGGACT CCGCAAAGTCTAAG-3'	NM_ 013693.2
<i>Tgf-β</i>	5'-CCCAGCATC TGCAAAGCT-3'	5'-GTCAATGT ACAGCTGCCGCA-3'	NM_ 011577.2
<i>Arg-1</i>	5'-GATTGGCAAG GTGATGGAAGAGAC-3'	5'-TCTGTAA GATAGGCCTCCCAGAAC-3'	NM_ 007482.3
<i>Fabp4/</i> <i>Ap2</i>	5'-AAATCACCGCAG ACGACAGGAAGG-3'	5' -CACATTC CACCACCAGCTTGTCAC-3'	NM_ 024406.3
<i>Pparγ</i>	5' - GCCCTGGCAAAGC ATTTGTATGAC -3'	5' - TGATCT CTTGCACGGCTTCTACGG - 3'	NM_ 001127330.2
<i>Gapdh</i>	5' -TTCCAGG AGCGAGACCCCACT-3'	5'-CGGCA GAAGGGGCGGAGATG-3'	NM_ 008084.3

2.16. Isolation of genomic DNA (gDNA) from cecal content of mice.

Cecal content of mice was used to study the gut microbiota profile. Cecum is the major SCFA production site for mice (145). Cecal SCFA uptake fluxes by the host directly correlate with metabolic markers (146). Also in humans, cecum produces a huge amount of SCFA accounting to 10% of their energy requirements. The cecal SCFA levels depends largely on the consumed diets (147). As we intended to understand the roles of SCFA and their producers in regulation of host metabolic parameters, we studied the cecal microbiota composition for better understanding the link between microbiome, meta-metabolome and host physiology. Genomic DNA from cecal content was isolated as follows.

- A.** We isolated gDNA from mouse cecal samples using the QIAamp Fast DNA Stool Mini kit (148).
- B.** We weighed approximately 180-220 mg cecal content in a nuclease-free 2 ml MCT and placed it on ice.
- C.** Next, we added 1 ml InhibitEX buffer to each stool sample and vortexed them continuously for 1 minute until the samples were thoroughly mixed.
- D.** We heated the suspension for 10 minutes at 95°C. Then it was vortexed for 15 seconds.
- E.** We then centrifuged the MCT at full speed for 1 minute to pellet the stool particles.
- F.** Then we added 15 µl of Proteinase K (QIAGEN, USA) into a 1.5 ml MCT and added 200 µl of supernatant from step 'E' into the tube.
- G.** Then, we added 200 µl buffer AL to the mix and vortexed for 15 seconds.

- H.** We heated this mixture for 10 minutes at 70°C.
- I.** We added 200 µl of molecular grade ethanol to the lysate and mixed it by vortexing.
- J.** We took 600 µl of this lysate into a QIAamp spin column and centrifuged it at full speed for 1 minute.
- K.** We discarded the flow-through, added 500 µl Buffer AW1 to the column, centrifuged at full speed for 1 minute, and discarded the flow through.
- L.** Next, we added 500 µl Buffer AW2 to the column and centrifuged at full speed for 3 minutes. The flow-through was discarded.
- M.** We placed the column in a new collection tube and centrifuged it at full speed for 3 minutes.
- N.** We then placed the column in a new 1.5 ml MCT, and 50 µl of NFW was added before centrifuging at full speed for 1 minute to elute the DNA.
- O.** We performed quality control of the DNA by spectrophotometry and agarose gel electrophoresis (0.8%) as described previously.

2.17. Assessment of cecal microbial diversity by 16S rRNA-based next-generation sequencing of cecal content gDNA.

From the gDNA extracted in the previous section, we performed 16S rRNA-based next-generation sequencing (NGS). We outsourced the samples to AgriGenome Labs Pvt Ltd (Kerala, India) for NGS, since we do not have the facility at NISER. Quality control (QC) of the library and amplification of NGS samples were done using Qubit Fluorimeter (V.3.0, ThermoScientific, USA). We performed amplification for V3-V4

region of 16S rRNA using universal primers (specific for V3-V4 region) V3 Forward primer 5'-CCTACGGGNBGCASCAG-3' and V4 Reverse primer 5'-GACTACNVGGGTATCTAATCC-3'. The amplified product integrity and purity was checked on 2% agarose gel, following gel purification to remove non-specific amplifications. We used 5 ng of amplified product for library preparation using the "Next Ultra DNA library preparation" kit (NEB, USA). The quantification and quality estimation of the library was done on Agilent 2200 TapeStation (Agilent, USA) before it was sequenced on Illumina HiSeq 2500 platform (Illumina, USA) (paired-end sequencing 250bpX2).

Following sequencing, we performed bioinformatics analysis of the sequencing data using the following pipeline.

- A.** The Fastq base quality (Phred score quality > 30 was considered), base composition, and GC content was checked for the samples.
- B.** From the paired-end data, read trimming was done using the PERL script. We considered the properly paired-end reads with Phred score >20 (149) for V3-V4 generation. We merged the resultant reads using the FLASH program (Version 1.2.11 and trimmed the chimeras present in the reads using the de-novo chimera removal method UCHIME (150) (version 11) implemented in the tool VSEARCH.
- C.** We performed OUT picking from the reads using the Uclust program, available with QIIME-I software (151).
- D.** OTUs were assigned to different taxonomic hierarchies from which we performed the diversity analysis.

- E. We have uploaded the raw sequences to NCBI, sequence read archive (sra) database. The BioProject ID is “PRJNA733025”.
- F. We represented the microbial data in terms of percent abundance of major microbial phyla and genera with respect to total microbial taxa at respective taxonomic stages.

2.18. Assessment of cecal microbial diversity by Shannon diversity index

We assessed the overall diversity of the cecal microbiota using the Shannon diversity index (152). Calculations were done using the following formula.

$$\text{Shannon diversity index} = -\sum p_i \log p_i$$

Where p_i is the ratio of percent abundance of respective microbial phyla divided by the total abundance of all the microbial phyla in that group. $\ln p_i$ is the natural logarithm of p_i with a base of natural exponent (e) and $-\sum$ stands for the negative of the sum of $p_i \ln p_i$ for a mouse in a particular treatment condition.

2.19. Clustering of different diet treated mice based on cecal microbial diversity, using LDA

We clustered the mice from different diet-treated groups based on the relative abundances of respective microbial phyla using the LDA as described in section 2.9.

2.20. Assessment of serum SCFA levels from serum metabolomic data

We determined the major serum SCFA (serum acetate, propionate, and butyrate) (153) levels from the metabolomic profiling (through ^1H NMR) of serum from respective diet-treated mice.

2.21. Mammalian cell lines and cell culture conditions.

We used two cell lines for our *in vitro* experiments. The murine pre-adipocyte and macrophage cell lines 3T3-L1 and RAW264.7, respectively were used for the studies. We procured both the cell lines from the National Center for Cell Science (NCCS), Pune, India. We used DMEM (Himedia, India) for culturing the 3T3-L1 cells while RPMI (Himedia, India) for the RAW264.7 cells. For both the media, was supplemented with 10% fetal bovine serum (FBS, Himedia, India) and 1% antibiotic-antimycotic solution (Himedia, India). We used a humidified incubator (Eppendorf, Germany), maintained at 5% CO_2 and 37°C for culturing the cells. We changed the media of both cell types in every 2-3 days. We harvested the cells for sub-culturing by treatment with 0.25% trypsin and 1 mM EDTA, 1X solution (HiMedia) for 3 min at 37°C.

2.22. Probiotic bacteria culture and growth conditions.

We procured both the probiotic bacteria *Lactobacillus acidophilus* MTCC10307 (LA) and the pathogenic bacteria *Salmonella typhimurium* MTCC3232 (ST') from MTCC, India, while we received the probiotic cocktail *Lactobacillus delbrueckii* sp. *bulgaricus* strain DWT1; CCM 7992 (LDB) and *Streptococcus thermophilus* strain DWT4; CCM 7992 (ST) as a direct gift from Daflorn Ltd. (Sofia, Bulgaria). LA and

LDB-ST were cultured in MRS media (Himedia, India), while ST' was cultured in nutrient broth (Himedia, India). We grew the bacteria aerobically in an incubator kept at 37°C and shaking (200 RPM). We measured absorbance at 600 nm to determine the bacterial number, calibrated to the data of the bacterial colony-forming unit (CFU), defined previously (90, 154).

2.23. Differentiation of pre-adipocyte cell line into terminally differentiated adipocytes.

We treated the pre-adipocyte cell line 3T3-L1, being cultured with DMEM with 1 mg/ml insulin (Sigma, St. Louis, MO, USA), 0.25 mM dexamethasone (MP Biomedicals, France), 2 mM rosiglitazone (Sigma, USA), and 0.5 mM 3-Isobutyl-1-methylxanthine (MP Biomedicals, France) in the differentiation medium. The differentiation process took 7 days to acquire maximum intracellular lipid accumulation, and we considered the resulting cells to be terminally differentiated adipocytes.

2.24. Co-culturing of adipocyte and macrophage cell lines.

We used trans-well co-culture inserts (0.4 µm, Himedia, India), placing them in 6-well plates (Himedia, India). In the co-culture system, we used two experimental setups to understand the mutual impact of differentiated 3T3-L1 cells and RAW264.7 cells, under simulated chronic physiological stress conditions. We used 0.5×10^6 cells of both types for the experiment. To evaluate the effects of differentiated adipocytes on the immunological polarization potential of macrophages, we seeded the differentiated 3T3-L1 cells on the inserts. In contrast, the RAW264.7 cells were

seeded on the bottom of the wells of the 6-well plates. We reversed the cell's location in a different experimental setup to understand the effects of immune cell proximity on the adipogenic potential of differentiated adipocytes.

2.25. Stress hormone treatment of co-cultured adipocyte and macrophage cells.

To simulate a chronic psychological stress condition *in vitro*, we treated the differentiated adipocytes with cortisol (Sigma, USA) and serotonin (MP biomedical, USA) alone or together for 12 h and then co-cultured them with macrophages. Initially, we titrated the optimal dose of both hormones, to effectively induce stress conditions for the cells. We selected the dose and time points for treating the hormones by analyzing the expression of serotonin receptor and transporter genes in differentiated 3T3-L1 cells (1×10^6 cells), pre-treated with the hormones alone or together. We evaluated the expression of serotonin receptor genes *Htr5a*, *Htr2a*, and transporter gene *Sert* after pre-treating differentiated 3T3-L1 cells with cortisol or serotonin at doses of 0.001-100 μ M for 12 h and then incubating the cells with cortisol and serotonin free media from 0-72 h. We chose the receptor genes as previous research from our lab had shown they were involved in inducing cortisol and serotonin-induced adipogenesis in pre-adipocytes (78, 155). We selected the optimum effective doses and time points for both the hormones from the expression patterns of *Htr5a*, *Htr2a*, and *Sert* (dose and time duration, inducing highest expression of all three genes) used for subsequent experimentation.

2.26. Treatment of differentiated adipocyte cell line with select strains of lactic acid bacteria.

We treated differentiated 3T3-L1 cells with the probiotic bacteria, LA and LDB-ST separately at MOIs 0.1-1000. We also treated ST' (challenge) at MOI 10 as a negative control for a period of 8 h. We followed kinetics of percent survival of all treatment and challenges compared to untreated 3T3-L1 cells. We did not observe any death of untreated cells during 8 h of observation. We determined the optimum MOI and duration of probiotic treatment by evaluating the survival of the 3T3-L1 cells at 0, 2, 4, 6, and 8 h post-treatment by trypan blue dye exclusion method (156). We chose the MOI and treatment duration, based on survival of 3T3-L1 that was compromised minimally, for further experiments using both probiotic bacteria.

2.27. Oil Red O (ORO) staining of adipocytes.

- A.** We used the following protocol for staining differentiated 3T3-L1 cells' (0.5×10^6) intra-cellular lipid droplets with the lipid staining dye ORO (Himedia, India). Cells were grown on sterile coverslips (FisherScientific, USA) placed in wells of 6-well plates.
- B.** We removed the cell media and washed it thrice with 1XPBS.
- C.** We then fixed the cells with 4% PFA (Himedia, India) for 1h at 4°C.
- D.** We treated the cells with 60% isopropanol (FisherScientific, USA) for 5 minutes after washing thrice with 1XPBS.
- E.** We treated the cells with an ORO working solution (3:2 diluted 0.5% ORO stock solution, made in 100% isopropanol) for 1 h at RT.
- F.** Removed the excess stain by washing thrice in 1XPBS.

- G. Mounted the coverslips on slides in 1XPBS and observed under a brightfield microscope.
- H. We took pictures and analyzed the images.

2.28. Quantification of cellular lipid content by extraction of intracellular ORO and measurement of its absorbance.

For quantifying the intracellular lipid content of differentiated 3T3-L1 cells at different treatment conditions, we performed spectrophotometric quantification of cellular lipid extracts. Briefly, we stained 0.5×10^6 differentiated 3T3-L1 cells with ORO as described previously. For extracting the intra-cellular ORO, we added 500 μ l of 100% isopropanol for 1 h at RT. We took the supernatant from the wells, measured their absorbance at 510 nm, and considered it a relative measure of cellular lipid content.

2.29. RNA isolation, cDNA preparation, and qRT-PCR analysis of select genes from differentiated adipocyte and macrophage cell lines.

We performed the RNA isolation, cDNA preparation, and qRT-PCR analysis as described in section 2.14. We used 1×10^6 cells for RNA isolation from each condition. We are describing the primers used to assess gene expression from differentiated 3T3-L1 and RAW264.7 cells in table 4. We used *β -Actin* as the housekeeping gene for these experiments.

Table 4: List of primers used in *in vitro* experiments.

Gene name	Sense strand	Antisense strand	NCBI Accession number
<i>Htr2a</i>	5'-TGCTGCTGGGTTT CCTTGTCATGC-3'	5'-TCTGGAGTTG AAGCGGCTATGGT-3'	NM_ 172812.3
<i>Htr5a</i>	5'-GGCTAACA GCAGCCATGAGCTATC-3'	5'-CTGTGGCCG TATAAACACTGTGTC-3'	NM_ 008314.2
<i>Sert</i>	5'-GACCAGT GTGGTGAAGTGCATGAC-3'	5'-GGCCTGCG AACGTACTATCCAAAC-3'	NM_ 010484.2
<i>Il1b</i>	5'-TTGAAGA AGAGCCCATCCTCTGTG-3'	5'-TGTGAGG TGCTGATGTACCAGTTG-3'	NM_ 008361.3
<i>Il12</i>	5'-CGCCCAA GAACTTGCAGATGAAGC-3'	5'-CGCCTTT GCATTGGACTTCGGTAG-3'	NM_ 001303244.1
<i>Nos2</i>	5'-GCAACT ACTGCTGGTGGTGACAAG-3'	5'-GGAAGTGAA GCGTTTCGGGATCTG-3'	NM_ 001313922.1
<i>Tgfbr1</i>	5'-TGGCA GTGGAAGTTGGCCTCAG-3'	5'-GGGCCTC AAGGCACTTCTGGAG-3'	NM_ 009370.3
<i>Arg1</i>	5'-GATTGG CAAGGTGATGGAAGAGAC-3'	5'-TCTGTAA GATAGGCCTCCCAGAAC-3'	NM_ 007482.3
<i>Ap2</i>	5'-AAATCA CCGCAGACGACAGGAAGG-3'	5' -CACATTC CACCACCAGCTTGTCAC-3'	NM_ 024406.3
<i>Cd36</i>	5'-GGCTAA ATGAGACTGGGACCATTG-3'	5' -CAAGTAA GGCCATCTCTACCATGC-3'	NM_ 001159558.1
<i>Ppary</i>	5' - GCCCTG GCAAAGCATTGTATGAC -3'	5' - TGATCT CTTGCACGGCTTCTACGG - 3'	NM_ 001127330.2

β -Actin	5'-CTGACG GCCAGGTCATCACTATTG-3'	5'-GACAGC ACTGTGTTGGCATAGAGG-3'	NM_ 007393.3
----------------	------------------------------------	------------------------------------	-----------------

2.30. Assessment of probiotic bacteria association/uptake inside differentiated 3T3-L1 cells.

We followed three separate methods for assessing the capacity of the probiotic bacteria to be associated or up taken by the differentiated 3T3-L1 cells. Following staining the probiotics with CFDA/SE dye, we incubated them with the differentiated 3T3-L1 cells and assessed the fluorescence of later via flow cytometry and fluorescent imaging. Then, to evaluate the exact number of associated/up taken bacteria, we plated the probiotics, following lysis of the treated differentiated 3T3-L1 cells. We have provided the details of the methods in the following sub sections. Also, we have described the method for flow cytometric staining of RAW264.7 cell surface markers, co-cultured with stress hormone treated differentiated 3T3-L1 cells, simultaneously.

2.30.1. Labeling of probiotic bacteria with CFDA/SE stain.

We labeled the probiotic bacteria with 5-(and-6)-carboxyfluorescein diacetate, succinimidyl ester (CFDA/SE) (Invitrogen, CA, USA). Briefly, we suspended 10^8 viable probiotic bacteria (LA and LDB-ST) in a 1 ml MRS medium. We took 1 μ l (from 25 mg/ml stock solution) CFDA/SE for bacterial staining and added the stain to the bacterial suspension. We incubated the bacterial suspension inside a shaker incubator programmed at 37°C for 2 h to achieve the desired labeling. Following incubation, we centrifuged the suspension at 4000 rpm for 12 min at 4°C, and

discarded the supernatant. To remove the excess stain, we washed the cells thrice with 1XPBS. We incubated the stained bacteria with 10^6 differentiated 3T3-L1 cells for 1 h at desired MOIs. After bacterial treatment, we washed the mammalian cells with 1XPBS to remove unbound bacteria.

2.30.2. *Flow cytometry analysis of select surface markers on macrophage cell line and probiotic association/uptake on differentiated 3T3-L1 cells.*

We performed flow cytometric analyses to identify the immunological polarization status of RAW264.7 cells, co-cultured with differentiated 3T3-L1 cells under the influence of cortisol and serotonin. Also, we evaluated the probiotic association/uptake efficiency of LA or LDB-ST treated differentiated 3T3-L1 cells by flow cytometry. We carried out both processes following the protocol described below.

- A.** Following the desired pre-treatment with stress hormones or probiotic bacteria, we analyzed 0.5×10^6 RAW264.7 cells or 1×10^6 differentiated 3T3-L1 cells respectively with flow cytometry analysis.
- B.** The cells were detached from the wells with ice-cold 1XPBS after fixing in 4% PFA.
- C.** We resuspended the cells in ice-cold FACS buffer (1XPBS, 1% BSA, 0.1% sodium azide).
- D.** We applied CD11c (Abcam, UK), CD206(Abcam), CD80 (Abcam), CD163 (Abcam), and also NOS (Abcam) and ARG (Abcam) antibodies at appropriate dilutions and for indicated intervals to the

resuspended RAW264.7 cells following manufacturer's instructions.

In contrast, we used the CFDA/SE stained probiotic treated differentiated 3T3-L1 cells for further analysis.

- E. We evaluated cell fluorescence using BD FACS Calibur (BD, San Jose, CA).

2.30.3. *Fluorescent imaging of differentiated adipocytes, pre-treated with probiotic bacteria for measuring bacterial association/uptake.*

We seeded differentiated 3T3-L1 cells (5×10^4 per well) on a glass coverslip placed in each well of a six-well plate for adherence. We incubated the stained bacteria (as described in the preceding section) with differentiated 3T3-L1 cells for 1 h at select MOIs. We removed the unbound bacteria by washing with 1XPBS following 1 h of incubation. We then fixed the cells with 4% PFA for 30 min. We stained the cytoplasm of cells with Cell Mask Red (Invitrogen, USA) at pH 7.2 for 15 min. We washed each coverslip with 1XPBS twice to remove the excess staining agent. We then mounted the coverslips on a glass slide with Fluormount G (Thermo Fisher Scientific, USA). We kept the glass slides at room temperature for 12 h in the dark, then imaging on a fluorescence microscope (Olympus, Japan).

2.30.4. *Bacterial association/uptake assay for measuring attached or internalized probiotic bacteria inside differentiated adipocytes.*

We treated differentiated, 1×10^6 3T3-L1 cells with probiotics at different MOIs for 1 h. After media aspiration, we washed the mammalian cells thrice with 1XPBS to remove unbound bacteria. We lysed the cells using 350 μ l of lysis buffer containing

0.025% sodium dodecyl sulfate (SDS, Himedia, India) in 1XPBS. We adjusted the lysate volume before plating on MRS agar and then incubated overnight at 37°C. We counted cell numbers (in CFU) and plotted them against respective MOIs to quantify internalized/ attached bacteria.

2.31. Graphs and statistical analysis.

We generated all the graphs and performed the statistical analysis in GraphPad Prism (Version 5.00 and 7.00, USA). Statistical significance has been derived based on the indicated sample sizes for each experiment.

Chapter 2

**Evaluating the effects of starch or fat-rich diets
on visceral adiposity, lipidemia, glycemia, and
serum lipid profile of immune biased mice**

3.1. Introduction

The objective behind the experiments described in this chapter was to evaluate the adipogenic and glycaemic effects of starch- or fat-rich diets on immune biased mice. Diet being the primary energy source, dictates several aspects of mammalian nutrition. The absorption, metabolism, utilization, and storage of each type of nutrient defines whether a particular dietary practice would lead to beneficial or pathophysiological outcomes (157). The comparative ratio of carbohydrates to fats in the diet is an important parameter to consider when assessing the nutritional value (158). The digestibility and assimilative properties of carbohydrates and fats can be different because of the constituent molecules' varied origin and chemical structures (159). We have discussed in chapter 1 how some nutrients can lead to pathogenic health outcomes. We will try to understand further the primary reason for such health outcomes of the nutrients.

We have reported in this section the temporal changes that take place following consumption of a) non-resistant starch-rich diet (SRD), b) unsaturated fat rich-diet (USFD), and c) saturated fat rich-diet (SFD), in comparison to the control diet. We used six-week-old male C57BL/6 and BALB/c mice for all the studies and subjected them to either control or treatment diets (SRD, USFD, SFD) for a period of four and eight weeks, as discussed previously in the methods section. We assessed various cellular, molecular and functional parameters of the mice following the dietary intervention. After considering calorie intake and body compositions, we generated basic understandings of the assimilation efficiency of the treatment diets compared to the control groups. Then we evaluated the metabolic hormone and serum lipid profile levels along with visceral adipose tissue (vWAT) morphology, adiposity, and metabolic gene expression patterns. The serum and vWAT adiposity levels helped to

evaluate the adipogenic potential of the diets. Assessment of glycemic indices from the control and treatment diet treated mice showed us how the diets imposed glycemic changes and how the adiposity levels were associated with glycemia. Further, we performed serum metabolomic analysis to understand the fundamental molecular processes controlling the adiposity and glycemia of the mice. We identified critical metabolites related to various pathways of physiological importance. We finally linked the pathways with the observed adipogenic and glycemic changes and determined which pathways most prominently affected the physiology of the mice. The results of all the univariate and multi-variate assays are described below in detail, in the following sections.

3.2. Effects of starch and fat-rich diets on calorie intake and body composition.

We evaluated the calorie intake and body compositions of the mice from all the groups. We normalized the calorie intake relative to mouse body weight to understand how the diets influenced the body compositional changes. Also, we wanted to know how the altered body composition affected the calorie intake of the mice (Figure 5A-5D). We observed a significantly greater calorie intake by the C57BL/6 mice compared to the corresponding BALB/c mice undergoing the same dietary regime. The differential caloric intake showed that C57BL/6 mice were more significantly affected by the diets than their BALB/c counterparts. We observed that the control diet, SRD, and USFD were consumed in greater amounts by C57BL/6 mice than BALB/c throughout the experimental period. SFD showed significant differences in consumption rates only after five weeks between the mice strains. We further investigated the physiological differences of the mice at the initial (less pronounced

difference) and later (more pronounced difference) treatment durations, seeing differences in the consumption rates of the diets in the mouse strains. The differential consumption rates guided the choice of the four- and eight-week time points for conducting detailed studies on the physiological effects of the diets. For further understanding the body composition, we evaluated the changes in body weight (Figure 5E, 5F) and visceral adipose tissue (vWAT) weight of the mice and calculated the vWAT index (Figure 5G, 5H). After eight weeks of dietary intervention, we found more noticeable changes in body weight and adipose tissue mass. Also, higher adiposity was found in C57BL/6 mice than BALB/c. After eight weeks, we found the most enhanced vWAT indices in SRD and USFD fed C57BL/6 mice. Enhanced vWAT indices corroborated with these groups' enhanced calorie intake rates. We monitored other molecular and cellular changes in the mice, discussed in the following sections.

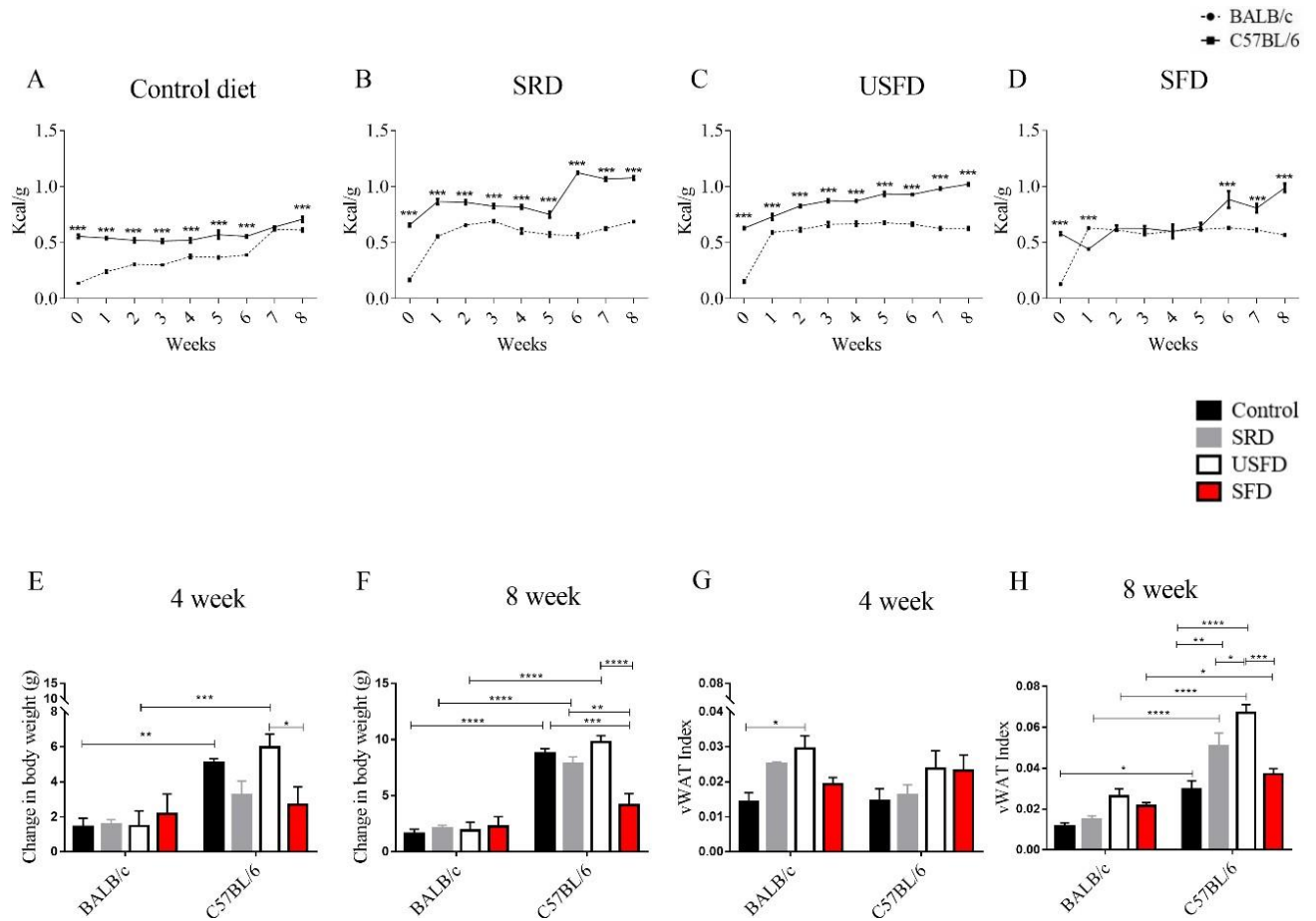


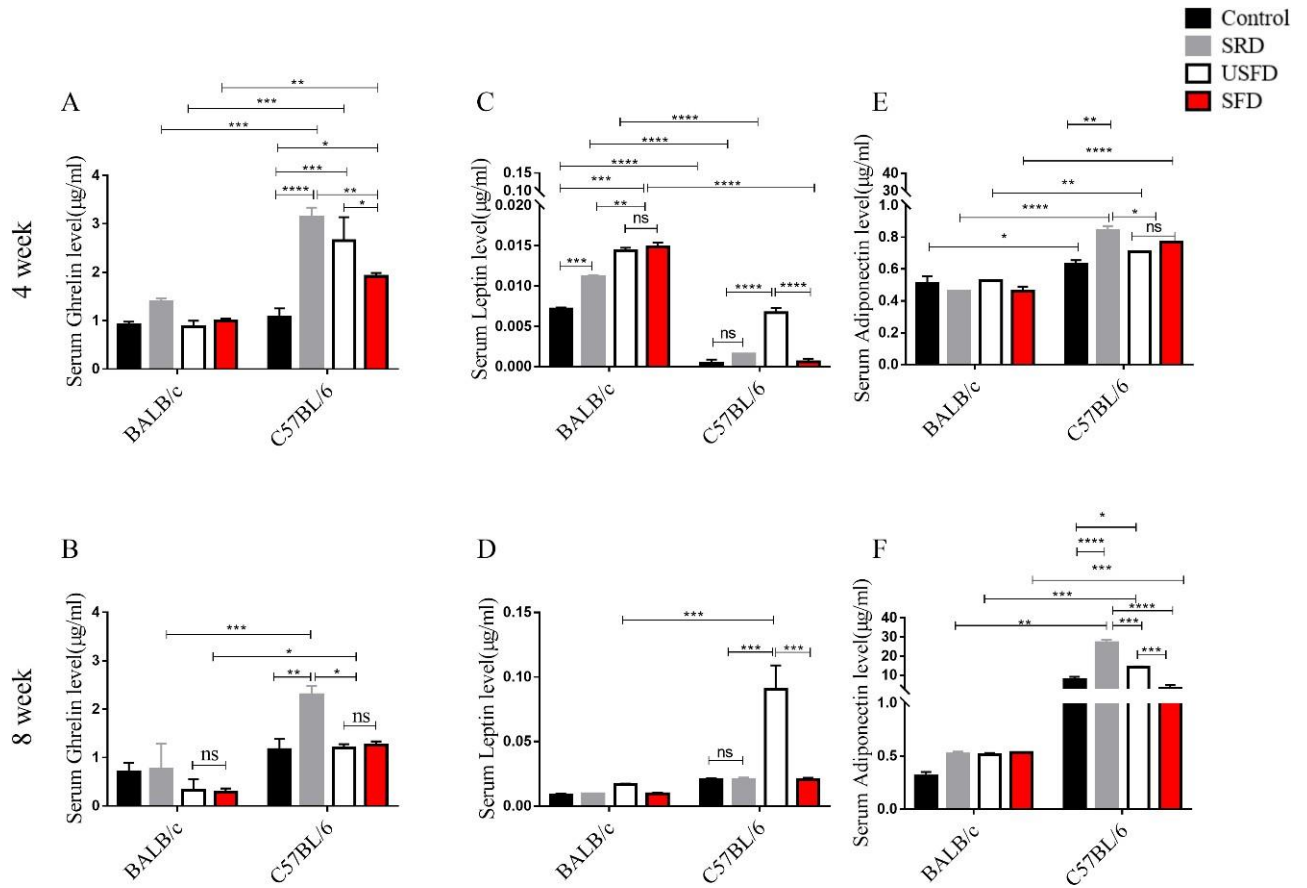
Figure 5. Comparative overview of calorie intake and resultant body composition changes in control and treatment (SRD, USFD, and SFD) diet-fed C57BL/6 and BALB/c mice.

Inter-strain comparison of the bodyweight normalized calorie intake of (A) control, (B) SRD, (C) USFD, and (D) SFD fed C57BL/6 and BALB/c mice for a period of eight weeks. A comparison of change in body weight after (E) four and (F) eight weeks and vWAT index after (G) four and (H) eight weeks of control and treatment diet consumption in C57BL/6 and BALB/c mice. We represented the data as mean ($n=6$ for A, B, C, D and $n=3$ for the rest) \pm SEM. We used 2-way ANOVA coupled with the Bonferroni post-test to determine the significance of changes in the data. We

denoted the significance by *($p \leq 0.05$), **($p \leq 0.01$), ***($p \leq 0.001$), ****($p \leq 0.0001$).

3.3. Starch and fat-rich diets differentially affect physiological energy homeostasis by regulating metabolic hormones.

We next evaluated the concentrations of metabolic hormones in the serum to determine how the hormones affect the physiology of the mice. We found the concentration of ghrelin, a primal orexigenic hormone in the serum, to be altered similarly to the calorie intake rates in the mice. We found, other than the control group, the concentrations of ghrelin were higher in C57BL/6 than corresponding BALB/c mice at both time points. The ghrelin levels of SRD fed C57BL/6 mice were highest compared to all other groups, showing that ghrelin was associated with increased consumption in the said group throughout the experimental time points (Figure 6A, 6B). Next, we found the levels of leptin and adiponectin, two predominant adipokines were influenced by the adiposity levels of the mice. The serum concentrations of both the adipokines increased over ten folds with time for certain treatment groups (Figure 6C-6F). After eight weeks of dietary intervention, we found the leptin levels in USFD fed C57BL/6 mice were significantly increased compared to all other groups. A similar scenario took place for adiponectin in SRD fed C57BL/6 mice. BALB/c mice showed less significant changes during the eight weeks period. To combat the enhanced adipose tissue mass following SRD and USFD feeding, we assume that the adipokines tried to maintain the energy homeostasis process. Both the adipokines are known for enhancing lipolysis and decreasing visceral and systemic adiposity (160). Hence, we checked the adiposity status by assessing various parameters in serum and vWAT level, following the hormonal assays.



3.4. Starch and fat-rich diets regulate visceral adiposity and lipidemia differently to maintain energy homeostasis.

We looked into the systemic adiposity levels of the diet-treated mice by checking the serum TG and FFA levels, which are important markers of serum lipid profile (161). The assessment showed that TG levels were always significantly higher in BALB/c mice than in the C57BL/6 (Figure 7A, 7B). The TG levels were increased greatly in USFD diet-fed mice after four weeks, while after eight weeks, TG levels spiked in SRD fed C57BL/6 mice. We found the FFA levels were significantly higher in BALB/c mice than corresponding C57BL/6 groups at four weeks. After eight weeks, the FFA levels showed an increased concentration in SRD fed C57BL/6 mice (Figure 7C, 7D). The cumulative analysis of the serum TG and FFA levels revealed that the diets stimulated systemic adiposity, i.e., the condition of lipidemia in BALB/c mice fed the USFD at four weeks but SRD at the eight weeks time point. In C57BL/6 mice, SRD enhanced the FFA levels at both time points. SRD seemed to be a potent enhancer of lipidemia levels in both mice strains, rendering it as an enhancer of systemic adiposity.

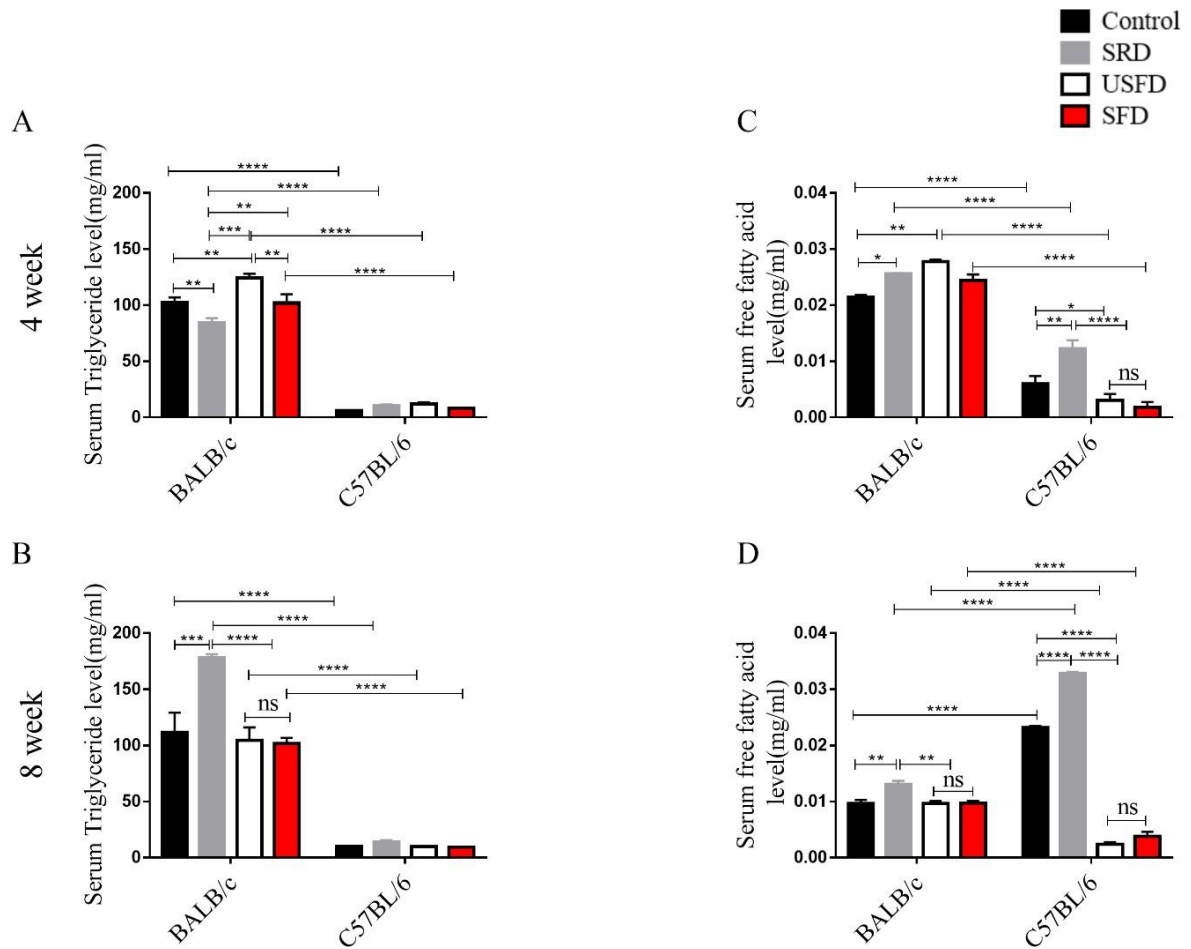


Figure 7. Comparative overview of serum lipid profile levels from control and treatment (SRD, USFD, and SFD) diet-fed C57BL/6 and BALB/c mice.

Comparative serum levels of triglyceride and free fatty acids in C57BL/6 and BALB/c mice after consumption of control and treatment (SRD, USFD, and SFD) diet for (A, C) four and (B, D) eight weeks, respectively. We represented the data as mean (n=3 for all conditions) \pm SEM. We used 2-way ANOVA coupled with the Bonferroni post-test to determine the significance of changes in the data. We denoted the significance by *($p \leq 0.05$), **($p \leq 0.01$), ***($p \leq 0.001$), ****($p \leq 0.0001$).

We next tried to determine whether the visceral adiposity responded similarly to lipidemia, induced by the diets. We performed cellular and molecular assays of the vWAT. Histology of the vWAT revealed that the adipocytes of C57BL/6 mice were affected more severely by the diets compared to BALB/c adipocytes (Figure 8A, 8B). We found hypertrophy of adipocytes to be more significant in C57BL/6 mice fed control and fat-rich diets than BALB/c (Figure 8C-8F). For SRD, at both time points, adipocyte sizes were reduced in C57BL/6, compared to BALB/c.

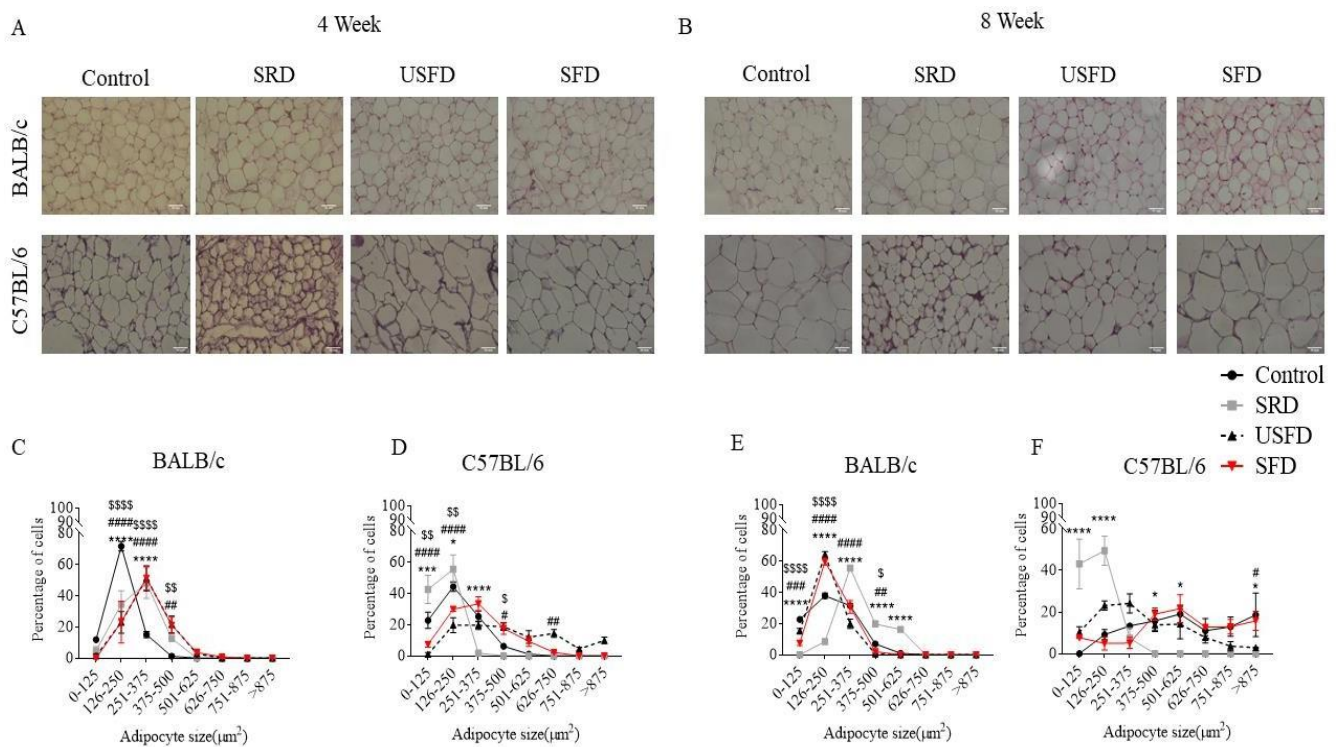


Figure 8. Micrographs representing vWAT histology from control and treatment (SRD, USFD, and SFD) diet-fed C57BL/6 and BALB/c mice.

Representative images of vWAT cellular morphology (40X magnification, H & E stained) from C57BL/6 and BALB/c mice after consumption of control and treatment (SRD, USFD and SFD) diet for (A) four and (B) eight weeks. We represent frequency distribution curves of the quantified adipocyte sizes from vWAT of BALB/c and

C57BL/6 mice after (C, D) four and (E, F) eight weeks of control and treatment diet consumption, respectively. We represented the data as mean (n=3 for all conditions) \pm SEM. We used 2-way ANOVA coupled with the Bonferroni post-test to determine the significance of changes in the data. We denoted the significance by *(p \leq 0.05), **(p \leq 0.01), ***(p \leq 0.001), ****(p \leq 0.0001) as a comparison between control and SRD. We denoted the significance by #(p \leq 0.05), ##(p \leq 0.01), ###(p \leq 0.001), ####(p \leq 0.0001) as a comparison between control and USFD. We denoted the significance by \$(p \leq 0.05), \$\$\$(p \leq 0.01), \$\$\$\$(p \leq 0.001), \$\$\$\$\$(p \leq 0.0001) as a comparison between control and SFD.

Next, we quantified the intracellular lipid contents of vWAT from all the groups to further check if the adiposity levels expressed by the lipid contents in the adipocytes were consistent with the cellular architecture. We quantified the intracellular lipid contents of vWAT from all the groups. Both the cellular lipid content and visceral adiposity levels (expressed as the compiled lipid amount of vWAT) showed us that SFD stimulated the adiposity levels most significantly in both the mouse strains after eight weeks (Figure 9A-9F). The visceral adiposity of C57BL/6 mice was further intensified than BALB/c, which ultimately gave us the idea that SFD influenced the visceral adiposity more prominently in C57BL/6 mice than in any other group. We also assessed the temporal changes in visceral adiposity, at four- and eight-week intervals (Figure 9 G and 9 H). We found that other than SFD fed group, BALB/c mice showed a gradual reduction in visceral adiposity, temporally. Interestingly, for C57BL/6 mice we did not observe any temporal adiposity changes in any group. Rather, the mice accumulated a consistent amount of adiposity, which was higher in SFD fed group, further showing the adipogenic efficiency of SFD.

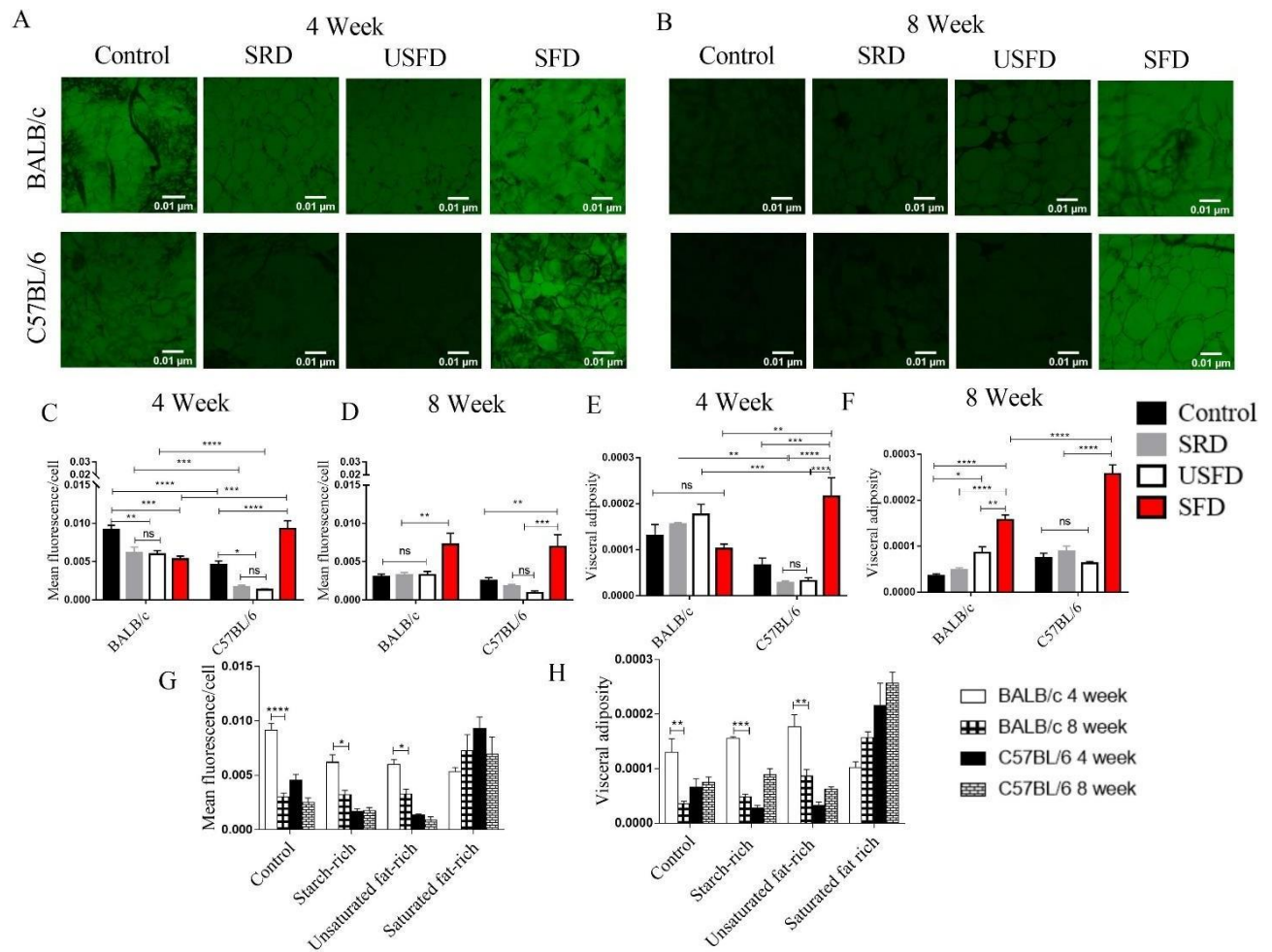


Figure 9. Comparative overview of vWAT lipid content from control and treatment (SRD, USFD, and SFD) diet-fed C57BL/6 and BALB/c mice.

Representative images of vWAT cellular lipid content (20X magnification, BODIPY stained) from C57BL/6 and BALB/c mice after consumption of control and treatment (SRD, USFD, and SFD) diet for (A) four and (B) eight weeks. Bar graphs of the quantified adipocyte lipid content and visceral adiposity (total vWAT lipid content) from vWAT of BALB/c and C57BL/6 mice after (C, E) four and (D, F) eight weeks of control and treatment diet consumption, respectively. Comparative account of the temporal changes in (G) cellular lipid content and (H) Cumulative visceral adiposity

in vWAT of control and treatment diet fed BALB/c and C57BL/6 mice. We represented the data as mean (n=3 for all conditions) \pm SEM. We used 2-way ANOVA coupled with the Bonferroni post-test to determine the significance of changes in the data. We denoted the significance by *($p \leq 0.05$), **($p \leq 0.01$), ***($p \leq 0.001$), ****($p \leq 0.0001$).

Further, we checked the expression of select adiposity-related genes to identify the probable mode of action by which diets induced the visible changes. We first studied the relative (referenced to strain and time-matched control diet-fed mice) mRNA levels of the *Fabp4* gene (Figure 10A, 10B), which is a transporter of fatty acids in adipocytes (162). At four weeks, we found the expression of *Fabp4* was not significantly higher than the controls in both strains. Still, considerably higher expression was observed at eight weeks for SRD and SFD groups of BALB/c mice. For C57BL/6, we saw increased *Fabp4* expression only for the SRD group. Next, we checked the expression of the gene *Acaca* (Figure 10C, 10D), which governs the rate-limiting step of fatty acid synthesis (163). Throughout, the expression of this gene was highest in C57BL/6 mice fed with SRD. *Acaca* might have helped to synthesize more fatty acids in the vWAT of the SRD fed mice, while for BALB/c mice, the expression of *Acaca* did not exceed the time-matched controls. The levels of the *Caveoli-1* gene, associated with lipid trafficking (164) (Figure 10E, 10F) was less in the SFD fed C57BL/6 mice at both time points. Expression of *Caveoli-1* indicated lipid transport might be less in the SFD fed C57BL/6 mice, that resulted in enhancement of the visceral adiposity levels. Finally, the expression of the adipogenesis marker gene *Ppar γ* (165) (Figure 10G, 10H) was higher in SFD fed mice, which supported enhanced adiposity following SFD consumption. We found down-regulation of

Ppar γ , *Fabp4* and *Acaca* genes in control diet fed BALB/c mice when we analyzed the relative mRNA expressions with respect to control diet fed C57BL/6 mice (Figure 10I) at both timepoints. Down regulation of the metabolic genes in BALB/c mice indicated at the probable cause of temporal reduction in visceral adiposity in the BALB/c mice while for C57BL/6 mice, we did not find similar changes. Also, for BALB/c mice the overall adiposity seemed to be reduced than C57BL/6, which might be the probable cause of the reduced adipocyte sizes in BALB/c.

Cumulatively the cellular and transcriptional data revealed that the SFD enhanced adiposity levels in both mice strains. As enhanced adiposity levels are frequently associated with altered metabolism, we tried to determine how the overall metabolism of the mice treated with the diets had changed. We started by checking the glycemic levels of mice to further our understanding of the altered systemic metabolism, described subsequently. We also compared the glycemia between all the control and treatment diet groups and measured their temporal changes to better understand how age dependent changes in glycemia could be affected by the altered diets.

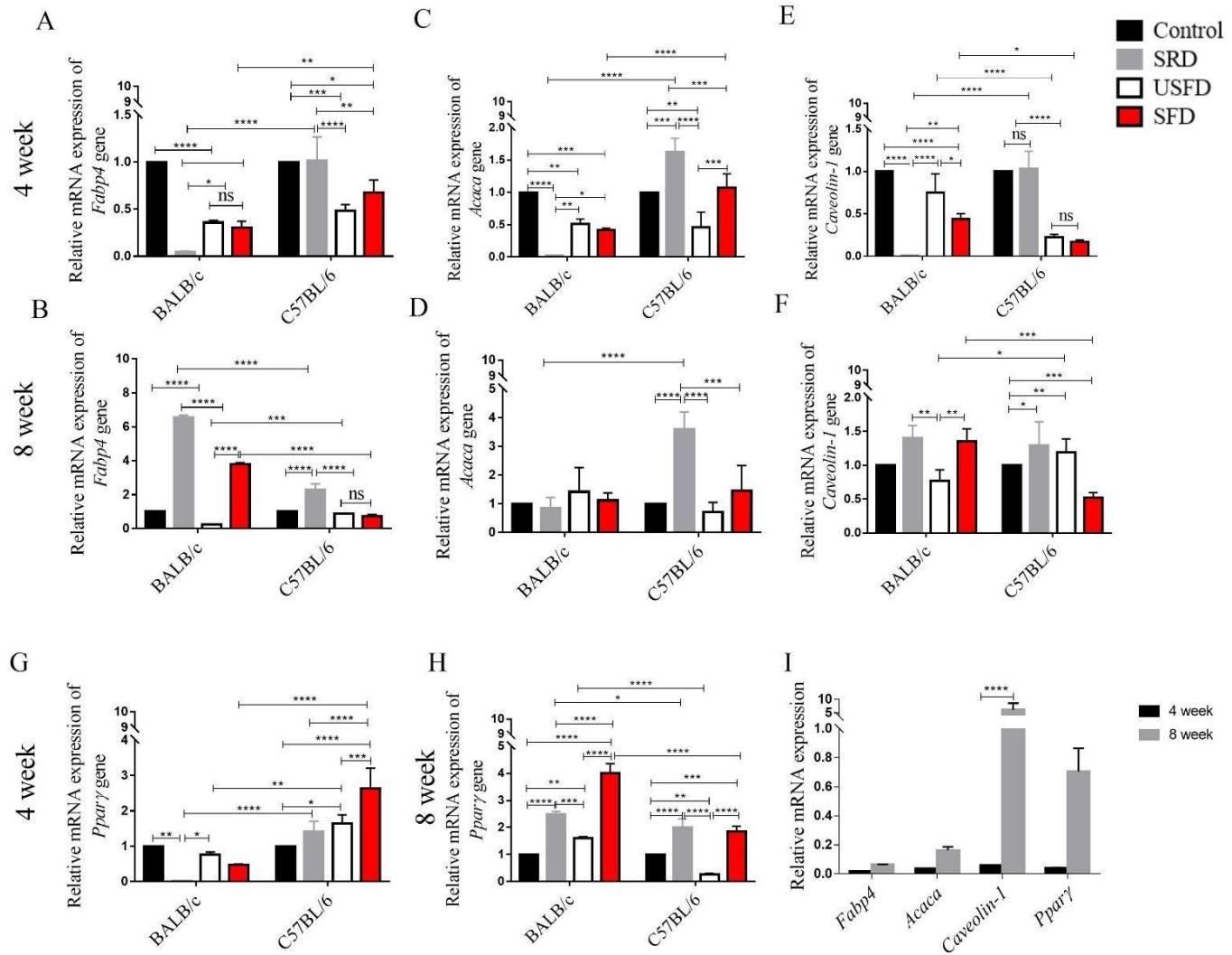


Figure 10. Comparative overview of relative mRNA expressions (fold change relative to control mice) of select metabolic genes from vWAT of control and treatment (SRD, USFD, and SFD) diet-fed C57BL/6 and BALB/c mice.

Fold change of (A, B) *Fabp4*, (C, D) *Acaca*, (E, F) *Caveolin-1* and (G, H) *Pparγ* gene expressions from the vWAT of C57BL/6 and BALB/c mice after consumption of control and treatment (SRD, USFD, and SFD) diet for four and eight weeks respectively. (I) Temporal changes in the relative mRNA expression levels of *Fabp4*, *Acaca*, *Caveolin-1* and *Pparγ* in vWAT of BALB/c mice compared to C57BL/6 mice, fed a control diet. We represented the data as mean (n=3 for all conditions) \pm SEM.

We used 2-way ANOVA coupled with the Bonferroni post-test to determine the significance of changes in the data. We denoted the significance by *($p \leq 0.05$), **($p \leq 0.01$), ***($p \leq 0.001$), ****($p \leq 0.0001$).

3.5. Glycemia is differentially affected by starch and fat-rich diets.

We checked the glycemic indices of the mice to determine dietary effects on glucose metabolism. OGTT revealed blood glucose levels were significantly higher in C57BL/6 mice following SRD consumption for four weeks, which declined at eight weeks. The blood glucose levels were consistently higher in SRD fed C57BL/6 mice, irrespective of the exogenous glucose challenge, showing the severe hyperglycemia-inducing potential of SRD after four weeks. For the fat-rich diet-fed C57BL/6 mice, we saw an increase in blood glucose level following glucose administration at eight weeks compared to the four weeks (Figure 11A, 11B). Interestingly, in most of the groups, we observed an increase in blood glucose levels 15 minutes after glucose administration which was delayed for SFD. In SFD, the spiking of blood glucose was observed after 30 minutes of glucose administration which hinted at a delayed insulin response (166, 167). In BALB/c mice, we found the entire GRC of USFD fed mice was significantly higher than the control group at four weeks. while at eight weeks, most time points of the GRC derived from the treatment diets were considerably higher than the control diet (Figure 11C, 11D). The AUC values derived from the GRC further confirmed the differential effects of the diets on the glucose response (Figure 11E, 11F). Inter-strain comparison of the control diet fed mice revealed the intrinsic glycemic differences (Figure 11G, 11H) between the strains. The inter-strain differences were less prominent at four weeks, which enhanced at eight weeks. Also, it was interesting to note that glycemia didn't change much significantly over time (4

to 8 weeks) in control, USFD and SFD fed BALB/c mice (Figure 11I-11L). In C57BL/6 mice, however glycemia gradually increased in control, USFD and SFD fed groups (Figure 11M-11P). The SRD fed mice showed an ameliorative property in terms of blood glucose levels. In BALB/c mice SRD consumption reduced the glycemia significantly (Figure 11J) over time while the effect was less prominent for C57BL/6 mice (Figure 11N). These ameliorative properties corroborated with the smaller adipocyte sizes observed in SRD fed mice, further connecting adiposity with glycemia (168). To further our understanding about the cause of the glycemia changes, we analyzed the serum insulin levels and calculated the insulin resistance levels in all the groups.

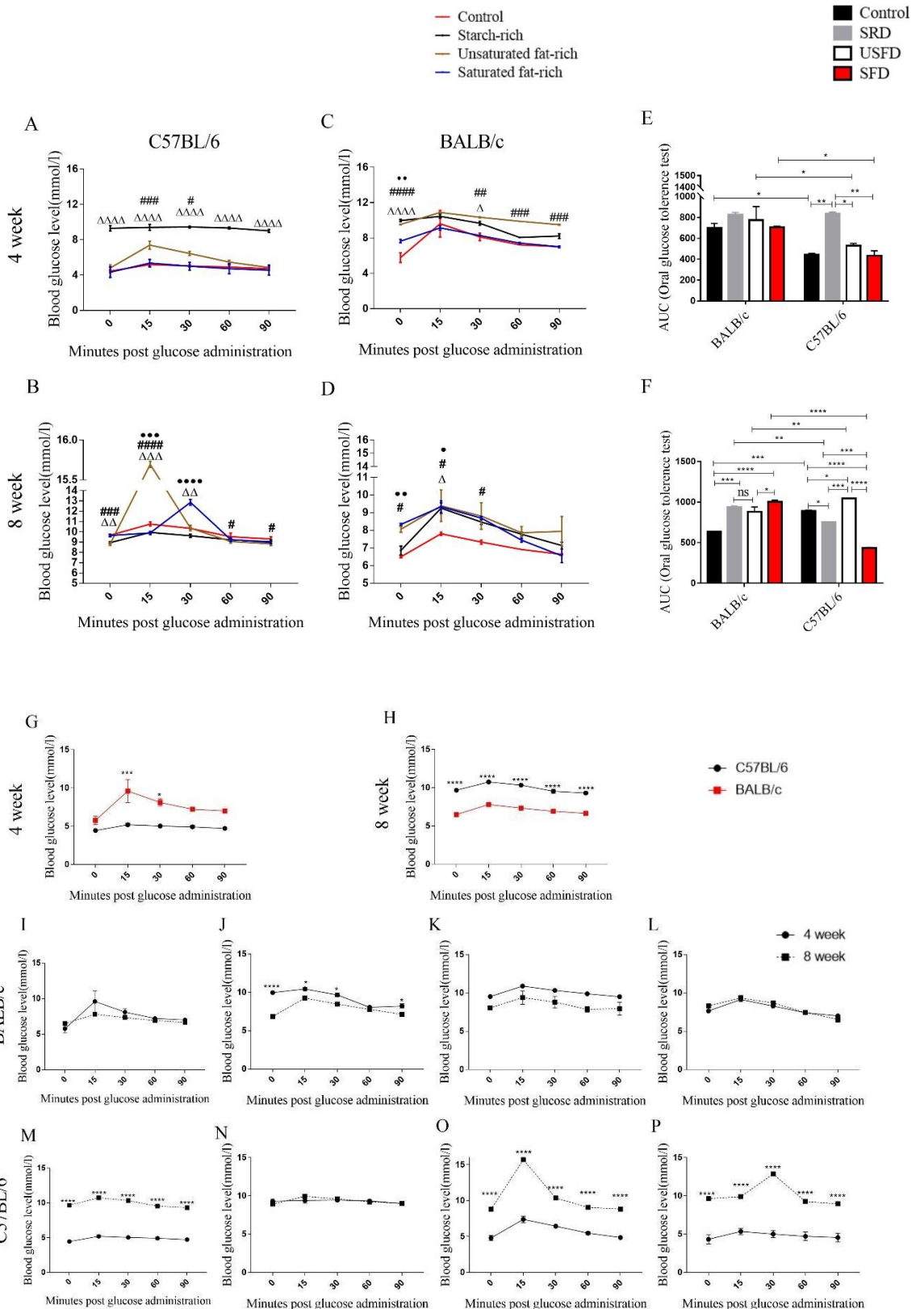


Figure 11. Comparative overview of glycemia levels from control and treatment (SRD, USFD, and SFD) diet-fed C57BL/6 and BALB/c mice.

Glucose response curves (GRCs) generated from oral glucose tolerance test (OGTT) of C57BL/6 and BALB/c mice after consumption of control and treatment (SRD, USFD and SFD) diet for (A, B) four and (C, D) eight weeks respectively. Area under the curve (AUC) of the GRCs after (E) four and (F) eight weeks, respectively. Comparison of GRCs between control C57BL/6 and BALB/c mice at (G) four and (H) eight weeks. Temporal changes in GRCs of (I, J, K and L) BALB/c and (M, N, O, P) C57BL/6 mice fed control, SRD, USFD and SFD. We represented the data as mean (n=3 for all conditions) \pm SEM. We used 2-way ANOVA coupled with the Bonferroni post-test to determine the significance of changes in the data. We denoted the significance by Δ ($p \leq 0.05$), $\Delta\Delta$ ($p \leq 0.01$), $\Delta\Delta\Delta$ ($p \leq 0.001$), $\Delta\Delta\Delta\Delta$ ($p \leq 0.0001$) between control and SRD group; # ($p \leq 0.05$), ## ($p \leq 0.01$), ### ($p \leq 0.001$), #### ($p \leq 0.0001$) between control and USFD group and by • ($p \leq 0.05$), •• ($p \leq 0.01$), ••• ($p \leq 0.001$), •••• ($p \leq 0.0001$) between control and SFD group for data in A-D. We denoted the significance by * ($p \leq 0.05$), ** ($p \leq 0.01$), *** ($p \leq 0.001$), **** ($p \leq 0.0001$) for data in E-P.

Fasting insulin levels showed us that SRD enhanced serum insulin levels similar to the blood glucose at four weeks in C57BL/6 mice, while in BALB/c, similar effects were seen in USFD fed mice (Figure 12C, 12D). At eight weeks' time point, we found the fasting insulin levels to rise severely in SFD fed BALB/c mice compared to other groups. Finally, we evaluated the IR levels in the mice by the HOMA-IR model (Figure 12E, 12F), taking into account both fasting blood glucose (Figure 12A, 12B) and serum insulin levels. The IR assessment further corroborated with the blood glucose and insulin levels, showing higher IR levels in SRD fed C57BL/6 mice at four weeks, later reduced. In BALB/c mice, we found the SFD to enhance the IR after eight

weeks. Collectively the analysis of the glycemc indices indicated SRD improved glycemia with time. The SFD enhanced glycemia and IR gradually, and the effect was more pronounced in BALB/c mice. Moreover, we found SRD to significantly ameliorate the IR in both BALB/c and C57BL/6 mice over time while SFD augmented IR in both strains (Figure 12I).

We finally performed metabolomic profiling of serum from the diet-treated mice to understand how the systemic metabolome changed following dietary interventions.



Figure 12. Comparative overview of blood and serum glycemc indices from control and treatment (SRD, USFD, and SFD) diet-fed C57BL/6 and BALB/c mice.

Fasting blood glucose, serum insulin, and HOMA-IR levels of C57BL/6 and BALB/c mice after consumption of control and treatment (SRD, USFD, and SFD) diet for (A, C, E) four and (B, D, F) eight weeks, respectively. Temporal changes in (G) fasting blood glucose, (H) fasting insulin and (I) HOMA-IR levels following control and treatment diet consumption. We represented the data as mean (n=3 for all conditions) \pm SEM. We used 2-way ANOVA coupled with the Bonferroni post-test to determine the significance of changes in the data. We denoted the significance by *(p \leq 0.05), ***(p \leq 0.001), *****(p \leq 0.0001).

3.6. Immune-biased mice are differentially impacted by the starch and fat-rich diets, leading to changes in their systemic metabolic profile.

To understand the dramatic changes occurring as a result of dietary alterations, we performed untargeted serum metabolomics. From the concentrations of the metabolites, we generated the LDA plot, which differentially clustered the mice from different diet-treated groups (Figure 13A). We quantified the extent of changes in each treatment group (including the untreated control group) by calculating the distance of individual points in each cluster from the origin of the two-dimensional cartesian axis of the LDA vector space. Further to quantify how the immune background of the mice impacted the metabolism of the diets, we calculated the vector displacement occurring between C57BL/6 and BALB/c clusters treated with the identical diets for the same duration (Figure 13B). Inter-strain vector distances for a particular type of diet gave us an idea of the differential effects of the diets on immune-biased mice. To know whether the metabolomic changes, estimated by the vector displacement, were induced by changes in expression of all the metabolites, we calculated the metabolomic index from the control and treatment diet-fed mice groups

(Figure 13C, 13D). We observed significant differences in the metabolomic index intra-strain besides inter-strain after four and eight weeks, for certain groups but not all. Such metabolomic changes suggested that, specific important metabolites could be governing the physiology besides the overall metabolite diversity. We next hypothesized that the metabolites, whose concentrations were significantly different between C57BL/6 and BALB/c mice treated with identical diets, should contribute to the observed changes in metabolism and result in alterations in visceral adiposity and IR. We identified pathways from the list of significantly altered metabolites between mouse strains subjected to dietary modifications to address this hypothesis. Next, we analyzed the potential of involvement of these pathways and their constituent metabolites in the changes in adiposity and IR observed for respective groups.

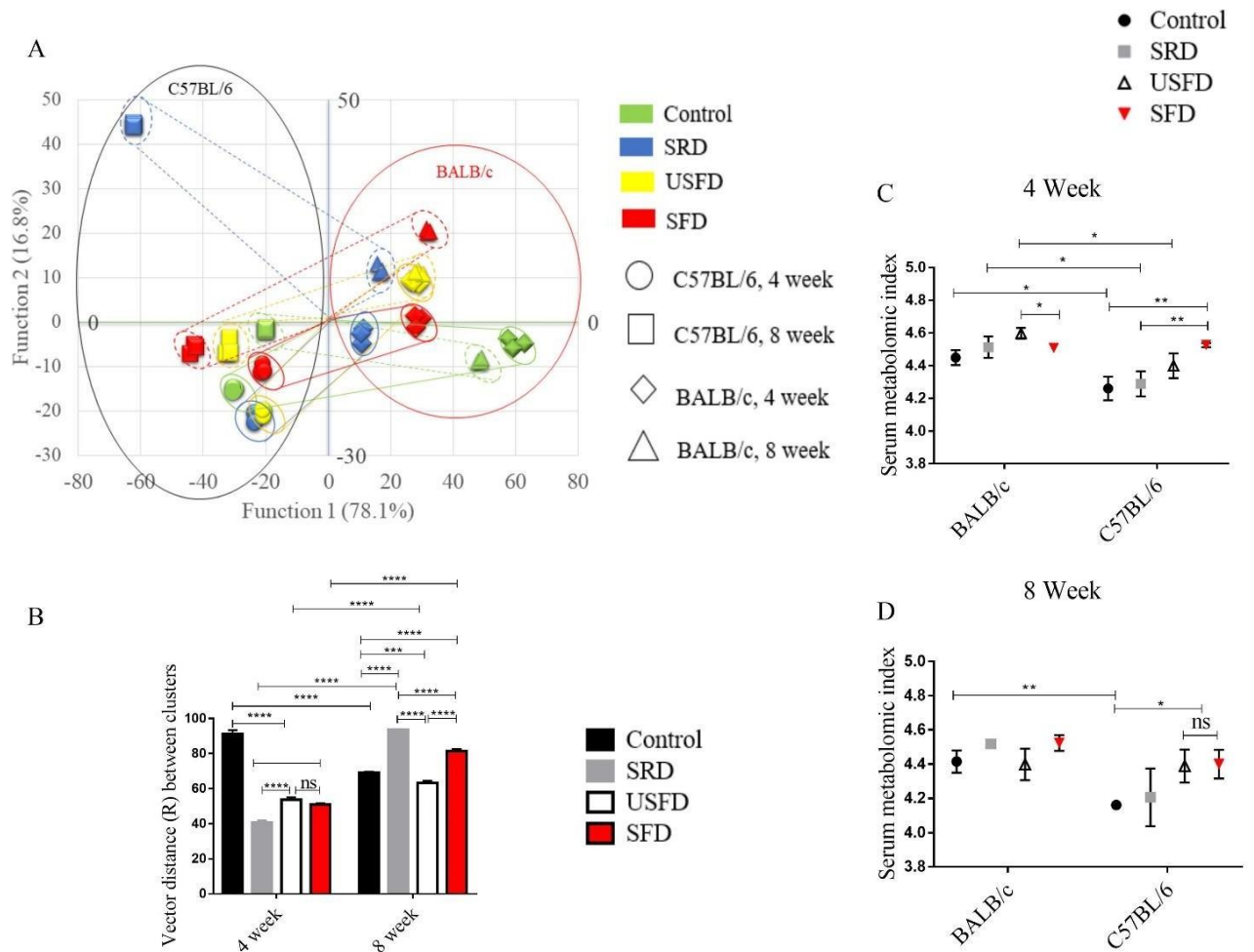


Figure 13. Effect of diets on serum metabolomic changes of C57BL/6 and BALB/c mice, subjected to dietary alteration for a period of four and eight weeks.

Clustering control, SRD, USFD, and SFD fed C57BL/6 and BALB/c mice using Linear discriminant analysis (LDA). Individual points in LDA clusters represent individual mice from respective groups. We used solid lines to show the connection between the center and the points of C57BL/6 and BALB/c mouse clusters treated with either of the four diets for four weeks, while dotted lines represent parallel connections between the center and points of the mouse clusters treated for eight weeks. The magnitude of the connectivity represented by solid or dotted lines drawn between C57BL/6 and BALB/c mouse clusters have been estimated by vector

analysis, considering the LDA plot as a 2D vector space. (B) Graphical representation of the vector distances between individual diet treated C57BL/6 and BALB/c mouse clusters, depicting the extent of differences at metabolomic level following diet consumption. Metabolomic index, representing the metabolomic diversity of C57BL/6 and BALB/c mice treated with different diets after (C) four and (D) eight weeks. Error bars in B, C, and D, represent (mean \pm SEM of data, $n = 3$). We used 2-way ANOVA coupled with the Bonferroni post-test to determine the significance of changes in the data shown for figure B, and one-tailed t -test for the value shown in figure C and D. We denoted the significance by *($P \leq 0.05$), **($P \leq 0.01$), ***($P \leq 0.001$), ****($P \leq 0.0001$).

3.7. Altered metabolites reveal several pathways leading to the observed physiological changes.

We predicted several critical pathways from the array of significantly altered metabolites, identified by inter-strain comparison of serum metabolite concentrations following dietary interventions. We found differential enrichment of specific pathways in different diet-treated groups after four and eight weeks of consumption (Figure 14A-14H).

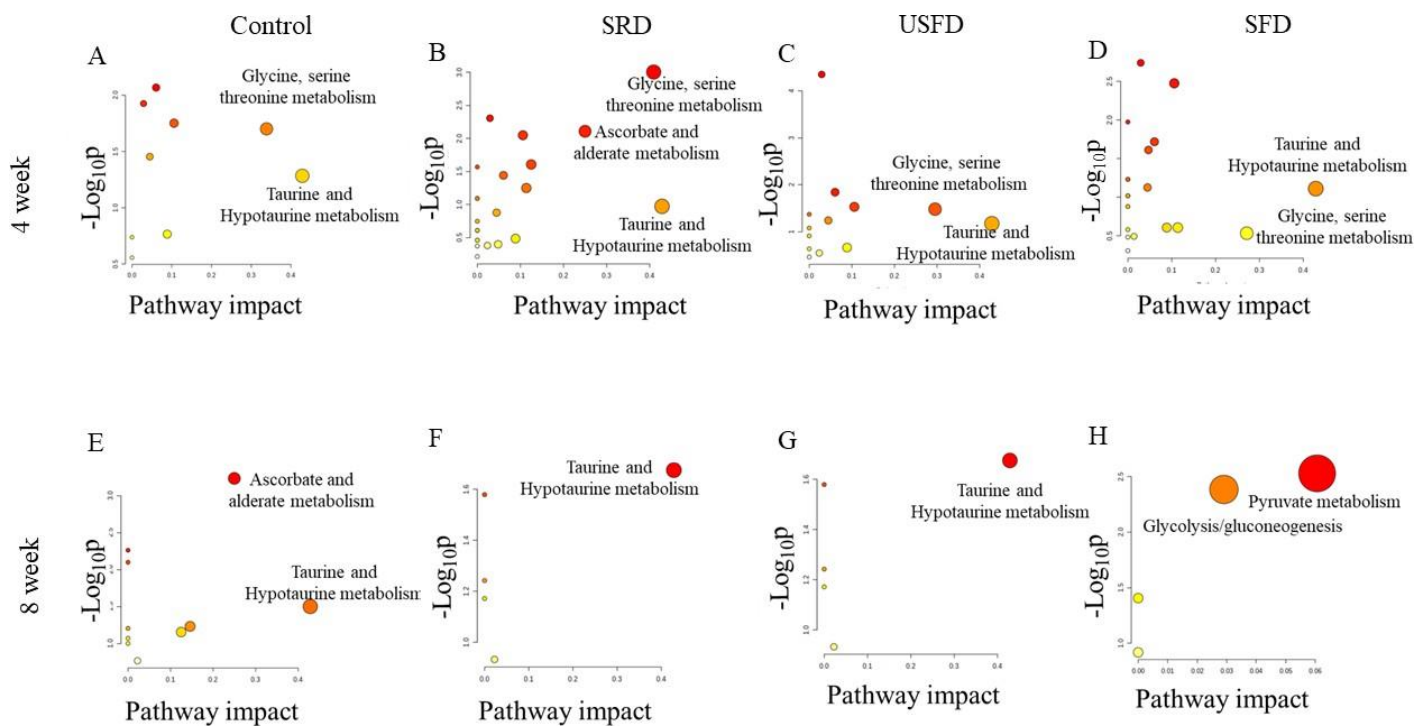


Figure 14. Pathways predicted to affect primary metabolic functions following dietary alterations in C57BL/6 and BALB/c mice, subjected to dietary alteration for four and eight weeks.

(A-H) Figure panels represent the results of metabolomic pathway analysis (MetPA), using MetaboAnalyst 5.0. We predicted the pathways using the significantly altered metabolites between C57BL/6 and BALB/c mice, fed with either control, SRD, USFD, and SFD for four and eight weeks. We used 2-way ANOVA following Bonferroni post-test to identify the altered metabolites.

We found the four-week dietary alteration mainly impacted the glycine, serine, threonine metabolism pathway, and taurine and hypotaurine metabolism pathway.

Though the pathways were identical, the degree of enrichment of the pathways differed between different groups. We found the glycine, serine, threonine metabolism pathway to be highly enriched following SRD consumption, while enrichment was less after USFD and SFD consumption. Also, we found the ascorbate and alderate metabolism pathway to be highly enriched in SRD fed mice. At four-week, we also found the diets to impact the taurine and hypotaurine metabolism pathway, with their highest enrichment in the SFD-fed group. Again, at the eight-week-time point, we found the taurine and hypotaurine metabolism to be highly affected in all the groups except for SFD-fed mice, where pyruvate metabolism and glycolysis were enriched. We could trace the changes in the pathways with the significant physiological alterations in adiposity and IR, which have been discussed in table 5A-5D.

Table 5: Major metabolites and pathways impacting the physiology of control and treatment (SRD, USFD, SFD) diet treated C57BL/6 and BALB/c mice.

A. Major pathways impacted following control diet consumption for four and eight weeks in C57BL/6 v/s BALB/c mice

Treatment duration	Major pathway/s	Important metabolite/s	Fold change (Mean \pm SEM)	Major biological function/s	Observed physiological change (Mean \pm SEM)
four weeks	Glycine, serine,	Glycine	1.51 \pm 0.222	Decreases adiposity and insulin	Reduced visceral adiposity (-

	threonine metabolism			resistance (IR) (169, 170)(169).	2±0.09) and IR (-4.54±0.005)
		Creatine	1.15±0.112	Decreases adiposity (171).	
	Taurine and hypotaurine metabolism	Taurine	1.82±0.161	Decreases adiposity and IR (170, 172).	
eight weeks	Ascorbate and alderate metabolism	Glucuronate	4.37±1.449	Associated with enhanced glycemia (173).	Enhanced fasting blood glucose level (1.55±0.044).

B. Major pathways impacted following SRD consumption for four and eight weeks in C57BL/6 v/s BALB/c mice

Treatment duration	Major pathway/s	Important metabolite/s	Fold change (Mean ± SEM)	Major biological function/s	Observed physiological change (Mean ± SEM)
--------------------	-----------------	------------------------	--------------------------	-----------------------------	--

four weeks	Glycine, serine, threonine metabolism	Glycine	6.12±0.71	Decreases adiposity (169, 170).	Reduced visceral adiposity (-5.88±0.02) and enhanced IR (1.55±0.044)
		Creatine	1.75±0.192	Decreases adiposity (171).	
	Taurine and hypotaurine metabolism	Taurine	12.19±1.485	Decreases adiposity (170, 172).	
	Ascorbate and alderate metabolism	Glucuronate	3.72±0.192	Associated with enhanced glycemia (173).	
eight weeks	Taurine and hypotaurine metabolism	Taurine	2.95±0.619	Reduces IR (174).	Reduced IR (-2.63±0.019).

C. Major pathways impacted following USFD consumption for four and eight weeks in C57BL/6 v/s BALB/c mice

Treatment duration	Major pathway/s	Important metabolite/s	Fold change (Mean ± SEM)	Major biological function/s	Observed physiological change

					(Mean \pm SEM)
four weeks	Glycine, serine, threonine metabolism	Glycine	2.78 \pm 0.119	Decreases adiposity and IR (169, 170).	Reduced visceral adiposity (-5.55 \pm 0.03) and IR (-20 \pm 0.0003)
		Creatine	-1.51 \pm 0.071	Decreases adiposity (171).	
	Taurine and hypotaurine metabolism	Taurine	1.97 \pm 0.16	Decreases adiposity and IR (170, 172).	
eight weeks	Taurine and hypotaurine metabolism	Taurine	3.44 \pm 0.107	Reduces adiposity and IR (172, 174).	Reduced visceral adiposity (-1.38 \pm 0.03) and IR (-1.61 \pm 0.032)

D. Major pathways impacted following SFD consumption for four and eight weeks in C57BL/6 v/s BALB/c mice

Treatment duration	Major pathway/s	Important metabolite/s	Fold change (Mean \pm SEM)	Major biological function/s	Observed physiological change (Mean \pm SEM)
four weeks	Glycine, serine, threonine metabolism	Glycine	2.21 \pm 0.051	Decreases IR (169, 170).	Enhanced visceral adiposity (2.1 \pm 0.32) and reduced IR (-9.09 \pm 0.009)
		Creatine	-1.04 \pm 0.089	Decreases adiposity (171).	
	Taurine and hypotaurine metabolism	Taurine	2.25 \pm 0.098	Decreases IR (174).	
eight weeks	Pyruvate metabolism	Lactate	1.33 \pm 0.292	Enhances adipose tissue lipid content (175).	Enhanced adiposity (1.64 \pm 0.1).
	Glycolysis	Glucose	1.44 \pm 0.053	Enhances glucose utilization, decreased IR (176).	Reduced IR (-5.88 \pm 0.004).
		Glucose-6-phosphate	1.84 \pm 0.446		

3.8. Discussion and conclusion

The experiments described in this chapter revealed significant differential effects of SRD, USFD, and SFD in immune-biased mice strains. The pathways predicted from metabolomic studies helped identify probable molecular mechanisms regulating diet-induced physiological changes. We found that body weight and visceral adiposity indices were higher in C57BL/6 than BALB/c mice. Our results further revealed that feeding with the SRD and USFD for eight weeks led to significant a) body weight increase, b) enhanced adipose tissue volume. It was reported earlier that increased adiposity might trigger leptin (177) and adiponectin (178) to regulate energy homeostasis. We observed an increase in adipose tissue mass in C57BL/6 mice by feeding USFD. Eight-week of USFD feeding increased serum leptin levels while SRD enhanced adiponectin secretion. These changes were less prominent in BALB/c mice, irrespective of treatment duration or type of diets consumed. Following the observations related to body composition and metabolic hormones, we tried to determine the effects of the diets on systemic and visceral adiposity. The serum triglyceride levels were higher in BALB/c mice compared to C57BL/6 at both time points, which suggested the diets affected lipidemia (179) in BALB/c mice more than C57BL/6 mice. Also, we found that the SRD diets led to a significant increase in serum TG levels in BALB/c at eight weeks post-treatment, highlighting the considerable impact of SRD on lipidemia. While the serum FFA levels showed similar trends as the TG levels at four weeks, FFA levels significantly increased in SRD fed C57BL/6 mice at eight weeks compared to all other groups. Cumulatively, the serum TG and FFA levels highlighted a significant impact of the SRD on lipidemia in mice.

Evaluation of adiposity at the vWAT levels showed, control, USFD, and SFD enhanced the adipocyte size in C57BL/6 over BALB/c mice.

SRD led to a significant shrinkage of adipocyte size in both strains, which was more pronounced in C57BL/6 mice. Further evaluation of the lipid content of vWAT revealed that both the cellular and visceral adiposity levels were significantly enhanced by SFD, most prominently in C57BL/6 mice. Both mice strains showed significant visceral lipid storage following SFD feeding after eight weeks. The cumulative assessment of adiposity at serum and vWAT levels made it clear that the BALB/c mice were affected mainly by the diets at the systemic levels while C57BL/6 mice were affected primarily at the adipose tissue level by the fat-rich diets. While the above mentioned pattern of systemic and visceral adiposity was valid for fat-rich diets, for SRD, the effects were different. SRD enhanced the FFA levels in C57BL/6 while their adiposity levels were compromised at vWAT levels compared to BALB/c mice after eight weeks of treatment. Some of the observed serum and adipose tissue level changes were consistent with select metabolic gene expression patterns in vWAT.

Interestingly, we looked into the expressions of the fatty acid synthesis and transporter genes *Acaca* and *Fabp4* (162, 163). We found that the fatty acid synthesis was consistently high for SRD fed C57BL/6 mice (at both time points), which may be the reason for the significantly elevated levels of FFA of these mice. Again, the fatty acid transport gene expression was higher in BALB/c mice following SRD consumption for eight weeks, which may be a reason for higher levels of serum TG. The expression of the adipogenesis marker gene *Ppar γ* (165) was also higher following SFD consumption in both mice strains which may be one reason for observing higher visceral adiposity.

The systemic glycemia levels indicated additional features related to the effects of the diets. The temporal increase in blood glucose levels following fat-rich diet consumptions, coupled with amelioration of the parameter following SRD consumption in C57BL/6 mice, revealed the adverse effects of the fat-rich diets on glycemia in these mice. Similarly, in BALB/c, the fat-rich diets had enhanced the glycemic levels, which further reveals a potential adverse effect. The severe spiking of the blood glucose levels following glucose consumption (post 15 minutes of oral glucose consumption) in the fat-rich diet group of C57BL/6 mice was much higher than their BALB/c counterparts. The difference could be due to the allelic variants of the *Nlrp1b1* gene in C57BL/6 and BALB/c mice, making the mice differentially prone to diet-induced glycemic changes (41). Finally, we found the IR levels were significantly enhanced following SFD consumption in BALB/c mice, with time, while in C57BL/6, such changes were less pronounced.

We finally tried to understand the probable mode of action of the diet-induced physiological changes. For this, we analyzed the serum metabolite profile (180) of the mice. LDA analysis effectively segregated the different diet-treated mouse groups into distinct clusters. The clustering of C57BL/6 and BALB/c mice at opposite quadrants of the functional axis 1 (Function1) indicated distinct metabolic differences. The vector distances between the same diet treated C57BL/6, and BALB/c mice clusters, further helped quantify the magnitude of inter-strain differences of the metabolic profile.

Interestingly, we found the vector distances to reveal that the inter-strain differences between the control diet treated mice reduced with time while it gradually increased significantly for the treatment diet groups. The higher temporal increase in the vector distances for the SRD and SFD diets revealed progressive metabolic changes occurred

over time, which could cause the observed adiposity and glycemia-related changes in SRD and SFD fed groups. Further, the differences in the metabolomic indices also revealed that changes in the concentrations of specific metabolites between mice strains might contribute to the observed physiological changes. We found the nature of the metabolomic changes marked by the altered metabolic pathways in respective diet-treated groups. The glycine, serine, threonine metabolism, taurine, and hypotaurine metabolism pathways were mainly affected in all the control, SRD, and USFD treated groups at different magnitudes (Table 5), which explained the probable cause of the observed changes in adiposity and glycemia related parameters. Further, we linked the pyruvate metabolism, and glycolysis pathways with the observed enhancement in adiposity and IR in the SFD fed mice after eight weeks.

In conclusion, we can state that all the diets had significant but different impacts on the physiology of the immune-biased mice, which implicated how the immune system is regulating metabolism. The parameters of visceral adiposity mainly affected the C57BL/6 mice, while the systemic adiposity and glycemia took their effects on BALB/c mice mostly. The adipogenic and glyceemic effects were moderately altered by the SRD and USFD diets, while SFD drove the most notable changes in these parameters. We have summarized the work, discussed in this chapter in figure 15. Further, effects of diets on parameters such as meta-inflammation and the overall impacts of cecal microbiota on all the physiological changes are described in the subsequent chapters.

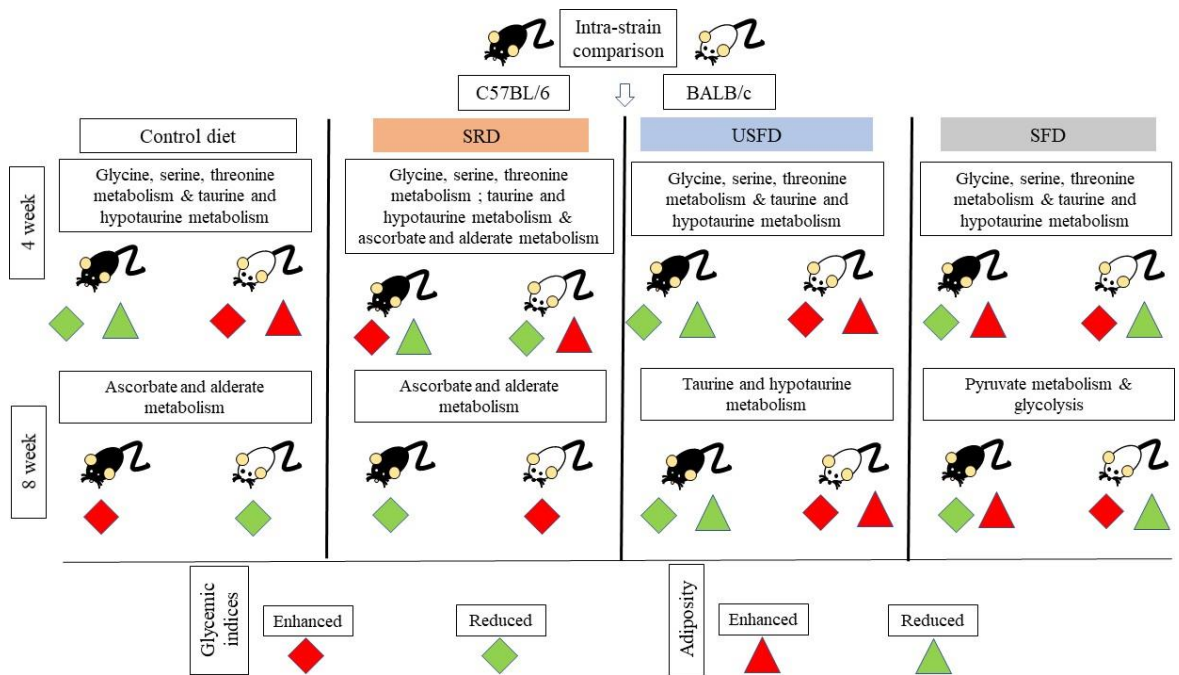


Figure 15. Schematic representation of the significant metabolic changes impacting adiposity and glycemia of immune-biased C57BL/6 and BALB/c mice following intervention with control, SRD, USFD, and SFD for four and eight weeks, respectively.

Chapter 3

Impact of diets on visceral adipose tissue meta- inflammation and elucidation of the immune- metabolic interactions occurring in the adipose tissue microenvironment

4.1. Introduction

The objective behind the experiments described in this chapter was to evaluate the meta-inflammatory effects of starch- or fat-rich diets on immune biased mice. Also, we tried to understand how the meta-inflammation and adiposity could be interlinked. Adiposity in animals is a dynamic process that can eventually lead to several metabolic disorders. During the development of severe adiposity, an interaction between the adipocytes and the immune system is indispensable (181). The enhanced adiposity often initiates a cascade of molecular interactions that leads to the secretion of various adipokines, among which various chemotactic factors are also present. These chemotactic molecules often attract several antigen-presenting cells (APCs) to the adipose tissue, among which macrophages are predominant (182–184). The infiltrated macrophages are called adipose tissue macrophages (ATMs), which often potentiate lipid-filled adipocytes' engulfment to become foam cells (185).

Along with acquiring lipids, the macrophages also become immunologically polarized into pro-inflammatory macrophages, ultimately affecting other immune and non-immune cells in the adipose tissue microenvironment (186). The adipose tissue gradually becomes a site of chronic inflammation through the effect of the immunologically active cells (187). The persistent pro-inflammatory condition, accompanied by any metabolic disorder, thus has its origin in the adipose tissue microenvironment. To develop a chronic inflammatory state, energy homeostasis plays a predominant role (188). Chronic inflammation is sustained at the cost of excessive energy expenditure, which requires energy-rich nutrients in the body (189, 190). Hence, nutrients with different energy values are required to sustain metabolic pathogenicity. To explore the diet-immune-metabolic interactions, we investigated how the metabolism associated with inflammation or meta-inflammation is affected

by dietary alteration. Other than diets, irregular lifestyle and unhealthy practices also contribute to metabolic abnormality. The deleterious lifestyle practices often join hands with psychological stress that, governed by stress hormones, may further stimulate the meta-inflammation (80). With the assumptions of finding a correlation between dietary alteration or chronic psychological stress and meta-inflammation, we performed *in vivo* and *in vitro* experiments using a murine model system.

As before, we used the control, SRD, USFD, and SFD treated C57BL/6 and BALB/c mice for our study. After four and eight weeks of dietary alterations, we analyzed macrophage infiltration of adipose tissues using direct immune fluorescence. Additionally, we analyzed the inflammatory gene expressions in the adipose tissue to evaluate the inflammatory state of the tissue. In addition to this *in vivo* work, we performed *in vitro* assays using a co-culture system of differentiated murine adipocyte and macrophage cell lines. The co-culture system simulated the adipose tissue microenvironment and facilitate a better understanding of the effects of chronic psychological stress. By applying the stress hormones cortisol and serotonin, we tried to replicate the impact of stress on adiposity and inflammation. Below, we describe the results of these studies.

4.2. Effect of starch and fat-rich diets on adipose tissue immune cell infiltration in immune-biased mice.

By labeling the protein F4/80, a specific marker for tissue macrophages (191), we quantified the macrophage infiltration rates in C57BL/6 and BALB/c adipose tissues following dietary alterations (Figure 16A, 16B). We observed that macrophage infiltration increased significantly following SRD consumption on BALB/c mice at

four weeks. Also, we found a moderate but significant increase in ATM infiltration following SFD consumption from both mouse strains (Figure 16C). At eight weeks, however, we found macrophage infiltration increased only following consumption of SFD in both mouse strains (Figure 16D). The magnitude of infiltration was higher in BALB/c compared to C57BL/6.

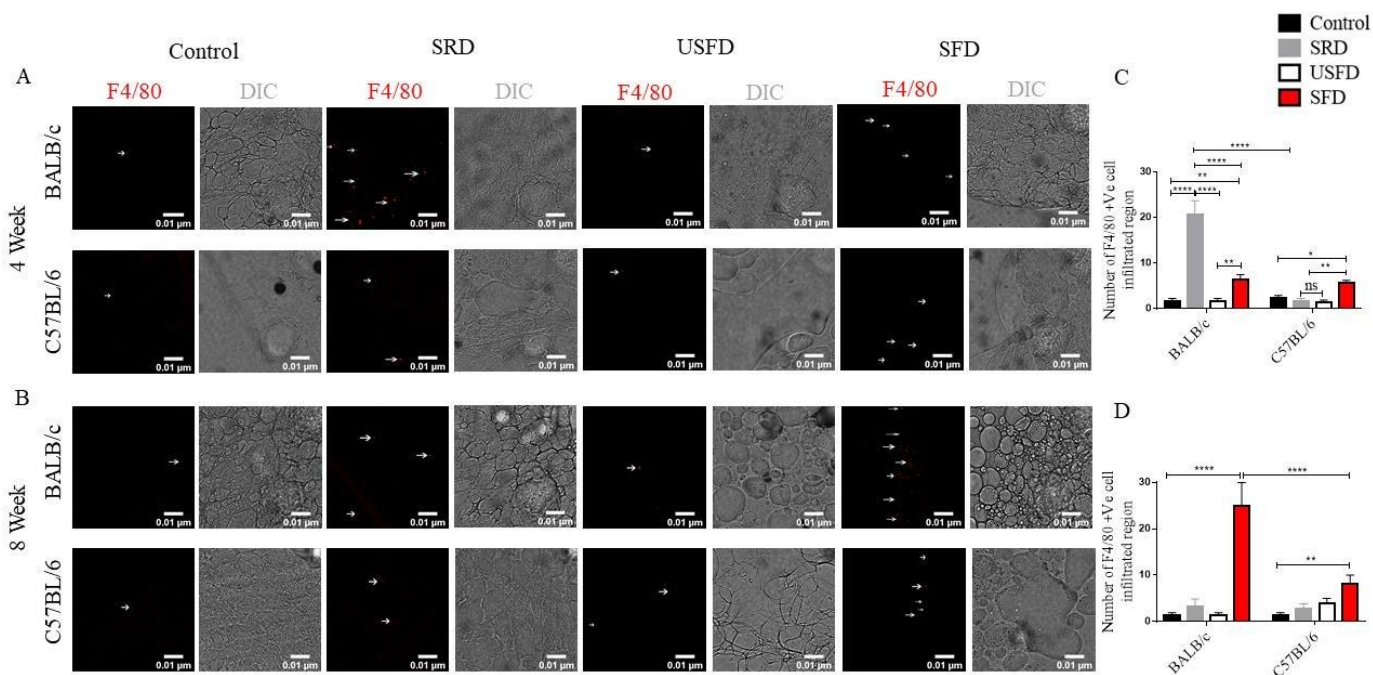


Figure 16. Comparative overview of macrophage infiltration levels from control and treatment (SRD, USFD, and SFD) diet-fed C57BL/6 and BALB/c mice.

(A, B) Fluorescent (in red, white arrow marked) and differential interference contrast (DIC, grey) images representing the macrophage (F4/80 positive cells) infiltrated inside vWAT of control and treatment diet-fed C57BL/6 and BALB/c mice after four and eight weeks of dietary alterations. The quantification of macrophage infiltrated regions, after (C) four and (D) eight weeks. We represented the data as mean (n=3 for

all conditions) \pm SEM. We used 2-way ANOVA coupled with Bonferroni post-test to determine the significance of changes in the data. We denoted the significance by *($p \leq 0.05$), **($p \leq 0.01$), ***($p \leq 0.001$), ****($p \leq 0.0001$).

Following observations related to macrophage infiltration, we checked the immune status of the tissue by analyzing inflammatory and anti-inflammatory gene expression (Figure 17A-17H). SFD consumption upregulated the pro-inflammatory genes *Il6* and *Tnfa* (192) at four weeks in C57BL/6 mice. Coincidental with this, there was increased expression of *Tgf- β* in this group. Increased *Il6* and *Tnfa* signifies a pro-inflammatory condition while *Tgf- β* stimulates angiogenesis (193, 194), needed for immune cell infiltration. We could corroborate the expression of these cytokines with the enhanced macrophage infiltration and meta-inflammatory condition in the adipose tissue (195) of C57BL/6 mice following SFD consumption. In C57BL/6 mice, fed SRD for 4 week we observed *Arg-1* and *Tgf- β* had expressed at an increased level, indicating a possible anti-inflammatory condition in these mice (196). In BALB/c mice fed SRD and SFD for four weeks, we didn't find any significant changes in the expression of either pro- or anti-inflammatory genes. The gene expression analyses suggested that macrophage infiltration and inflammatory conditions could involve mechanisms other than through the classical chemokines. At eight weeks, we found higher expression of *Il6*, *Tnfa*, and *Arg-1* in SFD fed BALB/c mice is consistent with that the severe macrophage infiltration occurring in this group. The co-occurrence of macrophage infiltration with up-regulation of *Tnfa*, and *Arg-1* suggest that both pro and anti-inflammatory macrophages may be involved. In SFD fed C57BL/6 mice, we found significantly increased expression of pro-inflammatory cytokines only. Enhanced pro-inflammatory cytokines suggest that macrophages residing in the adipose tissue of

SFD fed C57BL/6 mice may be primarily pro-inflammatory, resulting in an increased meta-inflammatory situation in the adipose tissues of SFD fed mice. When we compared the intrinsic differences between the mice strains by analyzing the differences in the gene expression of the control groups, we found *Tnfa*, *Arg-1* and *Tgf- β* expressions were down-regulated in BALB/c mice, compared to C57BL/6. The expression of *Il6* was significantly enhanced at eight weeks time point (Figure 17I). The enhanced *Il6* levels may signify higher meta-inflammation compared to C57BL/6 mice, after eight weeks.

The improved meta-inflammatory condition in the SFD fed mice further supported that enhanced adiposity was associated with increased meta-inflammation following the dietary intervention. Cumulative understanding from the macrophage infiltration and gene expression data supported the conclusion that specific diets may stimulate adiposity and meta-inflammation in murine adipose tissue. After finding the interaction between adipocytes and macrophages in the adipose tissue, under the influence of various diets, we investigated whether a similar relationship could exist under the influence of chronic psychological stress. The said relationship was evaluated subsequently.

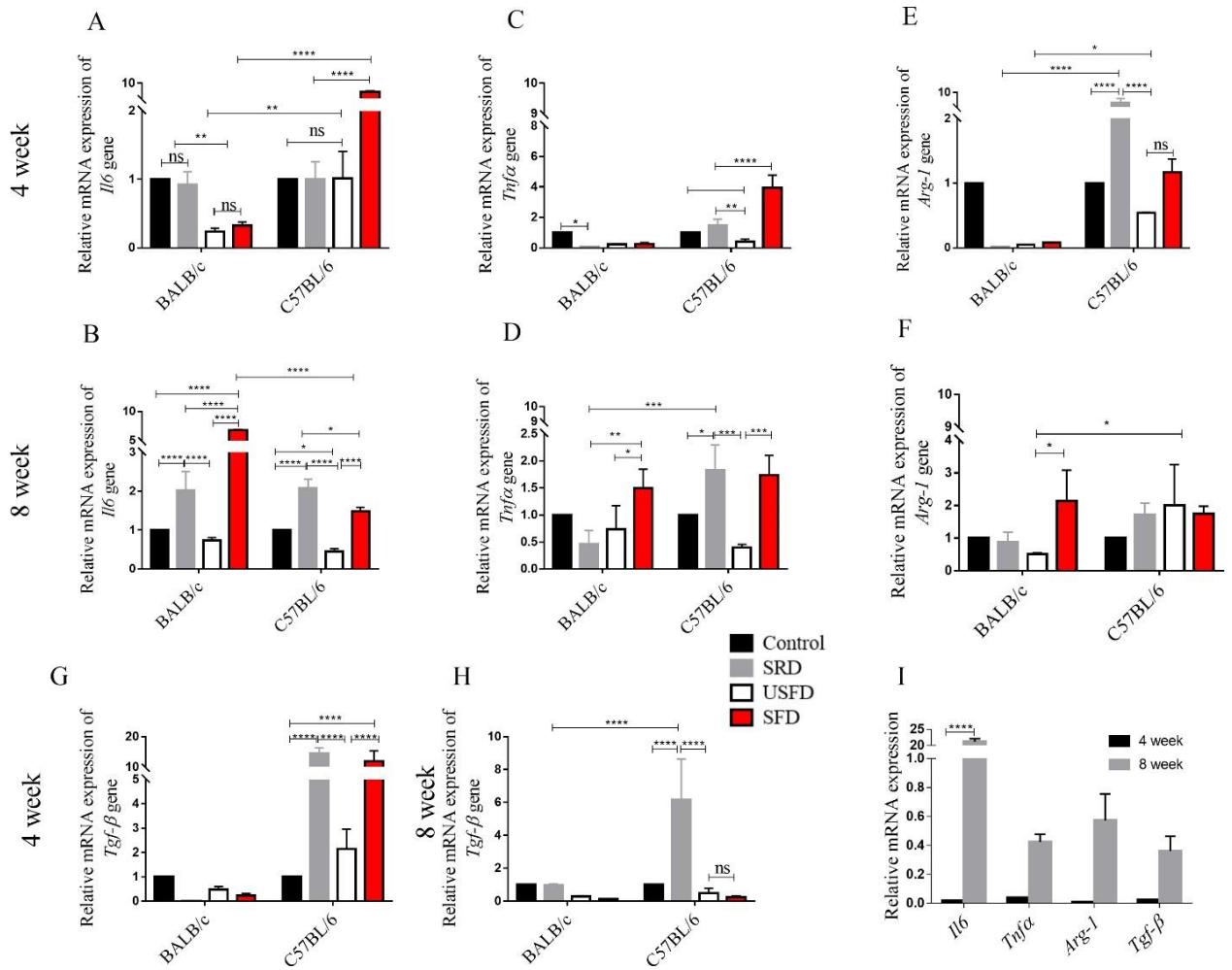


Figure 17. Comparative overview of relative mRNA expressions (fold change to control mice) of select immune genes from vWAT of control and treatment (SRD, USFD, and SFD) diet-fed C57BL/6 and BALB/c mice.

Fold change of (A, B) *Il6*, (C, D) *Tnfa*, (E, F) *Arg-1* and (G, H) *Tgf-β* gene expressions from C57BL/6 and BALB/c mice after consumption of control and treatment (SRD, USFD, and SFD) diet for four and eight weeks respectively. (I) Temporal changes in the relative mRNA expression levels of *Il6*, *Tnfa*, *Arg-1* and *Tgf-β* in vWAT of BALB/c mice compared to C57BL/6 mice, fed a control diet. We represented the data as mean (n=3 for all conditions) ± SEM. We used 2-way ANOVA coupled with the

Bonferroni post-test to determine the significance of changes in the data. We denoted the significance by *($p \leq 0.05$), **($p \leq 0.01$), ***($p \leq 0.001$), ****($p \leq 0.0001$).

4.3. Chronic psychological stress as an effector of murine metabolic processes.

We performed the following *in vitro* experiments to understand how chronic psychological stress may influence adiposity and meta-inflammation. Also, we investigated possible interactions between adipocytes and macrophages on adiposity and meta-inflammation. We first recapitulated the adipose tissue microenvironment *in vitro* by co-culturing differentiated 3T3-L1 and RAW264.7 cells for this study. In this co-culture system, we treated the cells with the stress hormones cortisol and serotonin. We first performed time and dose standardization of the stress hormones and evaluated their adipogenic and inflammatory effects.

4.3.1. Differentiation of murine pre-adipocyte cell line 3T3-L1 to terminally differentiated adipocytes

We differentiated the pre-adipocyte cell line, 3T3-L1 using differentiation media (composition given in materials and methods section) as standardized previously (156). The entire differentiation process took seven days since the lipid accumulation did not change significantly after seven days. We used these terminally differentiated cells (differentiated for seven days) for all the *in vitro* experiments. The morphology and lipid contents of the 3T3-L1 cells through the course of differentiation are described in figure 18.

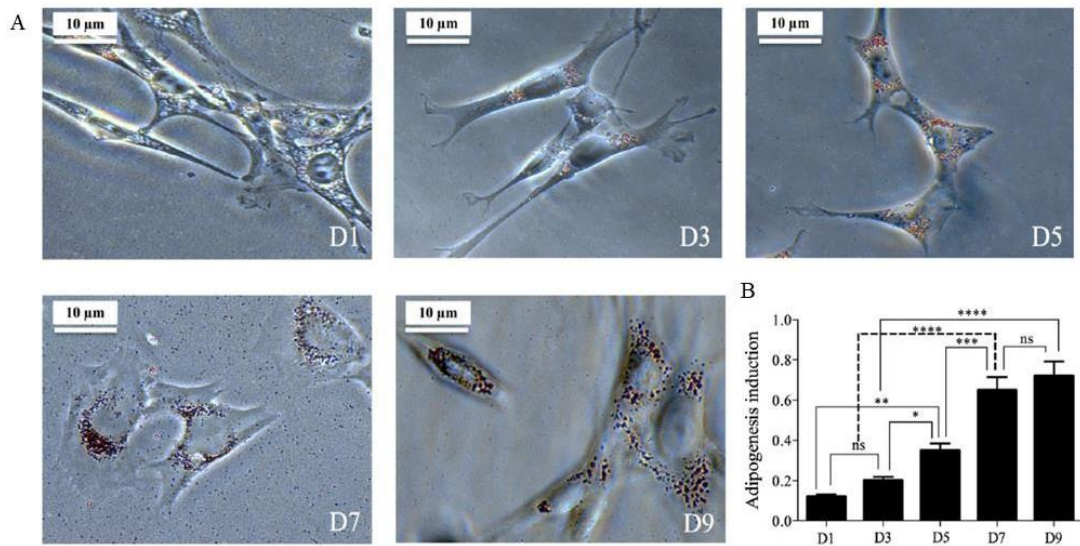


Figure 18. Time course of 3T3-L1 differentiation.

Accumulation of ORO stained lipid droplets in 3T3-L1 cells following treatment with differentiation medium for nine days (D1, D3, D5, D7, and D9). (B) Bar graph showing induction of adipogenesis (as quantitated by measuring the amount of ORO that stains lipid droplets in the 3T3-L1 cells) over time. We repeated the experiment five times. We used 1-way ANOVA followed by Bonferroni post-test to determine the significance of changes in the data. We represented the data as mean ($n = 5$) \pm SD of the data. We denoted the significance by * ($p \leq 0.05$), ** ($p \leq 0.01$), *** ($p \leq 0.001$) and **** ($p \leq 0.0001$).

4.3.2. Dose and timepoint standardization for cortisol and serotonin treatment

We checked the expression of the serotonin receptor and transporter genes *Htr5a*, *Htr2a*, and *Sert* following treatment with cortisol and serotonin alone and in combination to evaluate the effects of the stress hormones on differentiated adipocytes (47) as described in the materials and methods. Previously, we reported the roles of the receptors mentioned above and transporter genes in exerting adiposity in murine pre-adipocyte cells (78, 155). Hence, we believed *Htr5a*, *Htr2a*, and *Sert* genes might also play important roles in inducing cortisol and serotonin-mediated adiposity of differentiated 3T3-L1 cells. We found maximum expression of *Htr5a*, *Htr2a*, and *Sert* after treatment with 10 and 100 μ M cortisol or serotonin for 12 h (Figure 19A, 19B). Hence, we chose the lower 10 μ M dose for further experimentation. Next, we checked the expressions of *Htr5a*, *Htr2a*, and *Sert* after withdrawal of stress hormone treatment from differentiated 3T3-L1 cells, pre-treated with cortisol and serotonin alone and together for 12 h. Results show that expression of *Htr5a*, *Htr2a*, and *Sert* increased gradually from 0-48 h of treatment withdrawal after 12 h of pre-treatment with cortisol and serotonin alone and together (Figure 19C-19E). We chose 6, 12, 24, and 48h as optimal timepoints for evaluating adipogenic effects of the hormones.

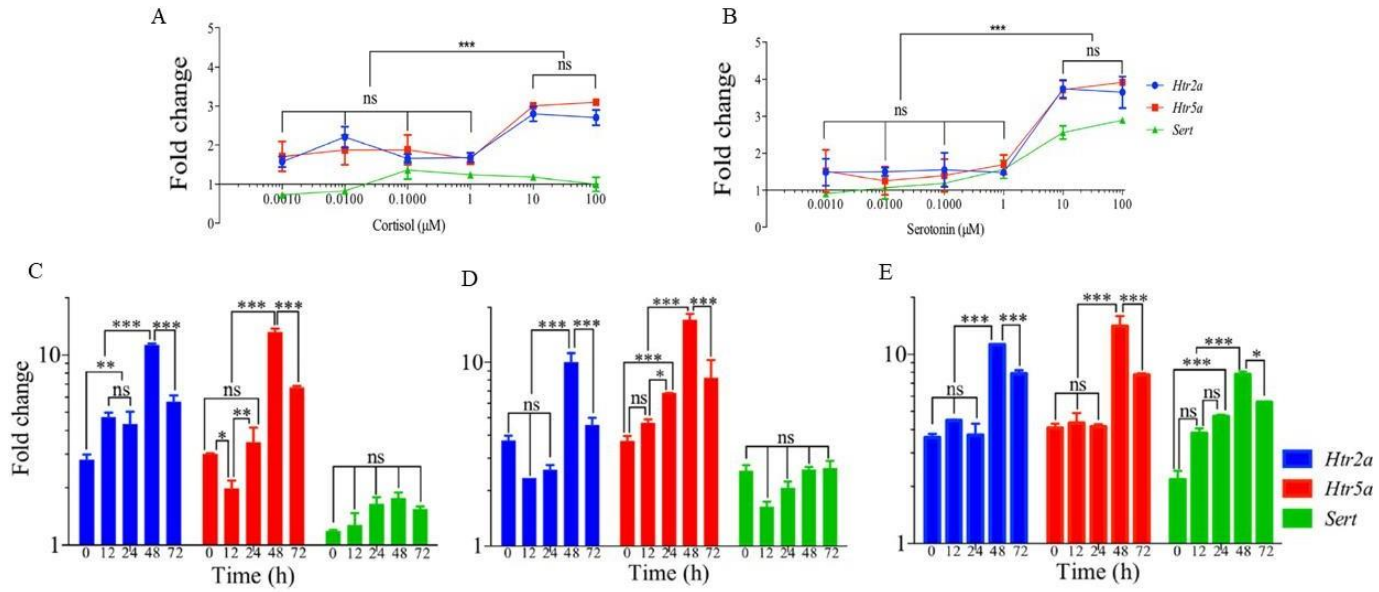


Figure 19. Dose and time titration for selecting an optimum dose for treating cortisol and serotonin on differentiated 3T3-L1 cells.

Relative mRNA expressions (fold change relative to control cells) of select serotonin receptor (*Htr2a*, *Htr5a*) and transporter (*Sert*) genes from (A) cortisol and (B) serotonin treated (12 h) differentiated 3T3-L1 cells at different doses. Fold change of these genes from (C) cortisol, (D) serotonin, and (E) cortisol and serotonin pre-treated (10 μM each) differentiated 3T3-L1 cells at different time points. We repeated the experiment three times. We represented the data as mean (n=3 for all conditions) ± SD. We used 2-way ANOVA coupled with the Bonferroni post-test to determine the significance of changes in the data. We denoted the significance by *(p ≤ 0.05), ***(p ≤ 0.01), ****(p ≤ 0.001).

4.3.3. Induction of lipid buildup in differentiated 3T3-L1 cells following cortisol and serotonin treatment

We treated differentiated 3T3-L1 cells with 10 μ M cortisol and serotonin, alone and together for 12 h, then withdrew the treatment. After 6, 12, 24, and 48 h we measured lipid accumulation in the adipocytes by staining them with ORO dye (Figure 20A). We found that intracellular lipid droplet sizes increased temporally. The lipogenic effects were even more pronounced in the cells treated with both hormones. When we extracted the intracellular ORO, we found similar results (Figure 20B). We now wanted to know whether co-culturing differentiated 3T3-L1 cells with RAW264.7 cells would further enhance lipid accumulation.

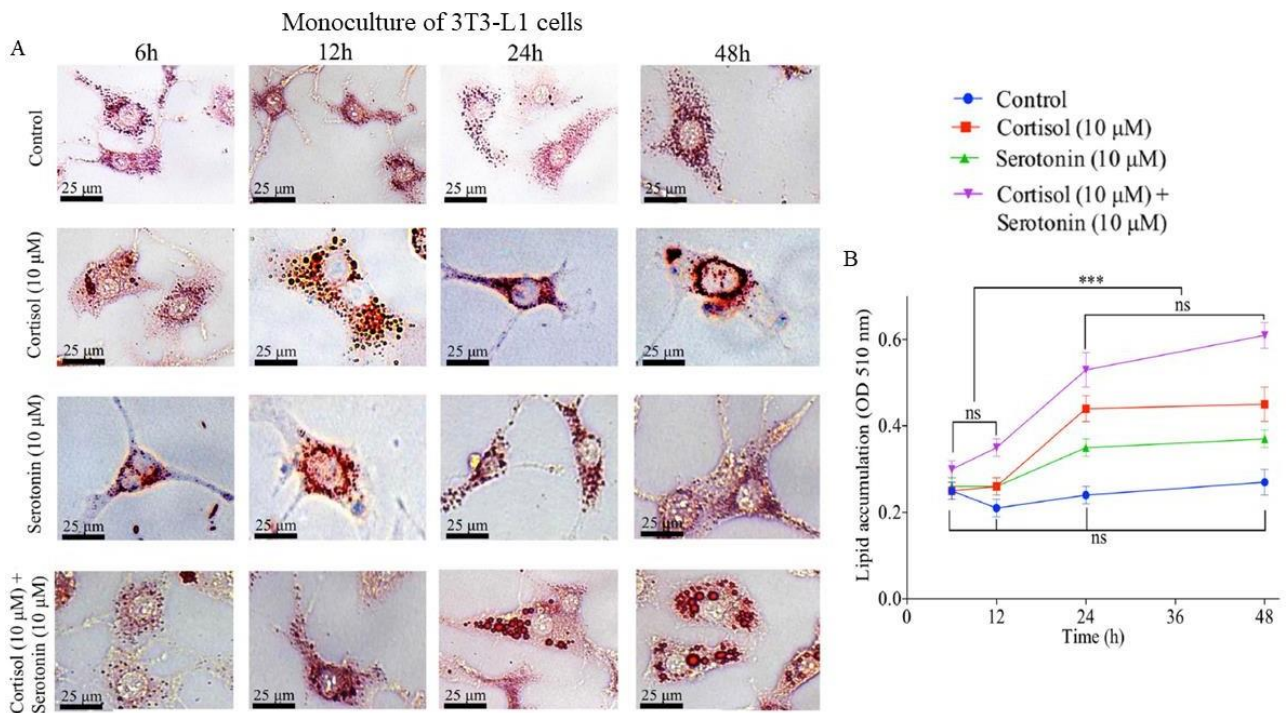


Figure 20. Effects of cortisol and serotonin treatment, alone and in combination on differentiated 3T3-L1 cells.

Representative images of ORO-stained differentiated 3T3-L1 cells pre-treated with cortisol and serotonin treatment, alone and in combination. ORO staining and imaging after 6, 12, 24, and 48 h of treatment withdrawal. (B) Spectrophotometric determination of extracted cellular ORO from the differentiated 3T3-L1 cells undergoing the same treatment. We repeated the experiment three times. We represented the data as mean (n=3 for all conditions) \pm SD. We used 2-way ANOVA coupled with the Bonferroni post-test to determine the significance of changes in the data. We denoted the significance by *(p \leq 0.05), **(p \leq 0.01), ***(p \leq 0.001).

4.3.4. Co-culturing differentiated 3T3-L1 cells with RAW264.7 cells further enhanced lipid accumulation under the influence of cortisol and serotonin

We co-cultured differentiated 3T3-L1 cells, pre-treated with cortisol and serotonin with RAW264.7 cells for 6, 12, 24, and 48 h, and evaluated the intracellular lipid contents of differentiated 3T3-L1 cells. Similar to the observations with 3T3-L1 monocultures, we observed that co-culturing with macrophages further enhanced lipid buildup in adipocytes over time (Figure 21A). ORO stained brightfield images and extracted ORO from co-cultured differentiated 3T3-L1 cells pre-treated with cortisol and serotonin alone and together revealed that the proximity of RAW264.7 further increased lipid accumulation in adipocytes (Figure 21B). We were interested in determining whether the co-culturing could influence the RAW264.7 cells and polarize them immunologically. Hence, we evaluated the immunological status of the co-cultured RAW264.7 cells.

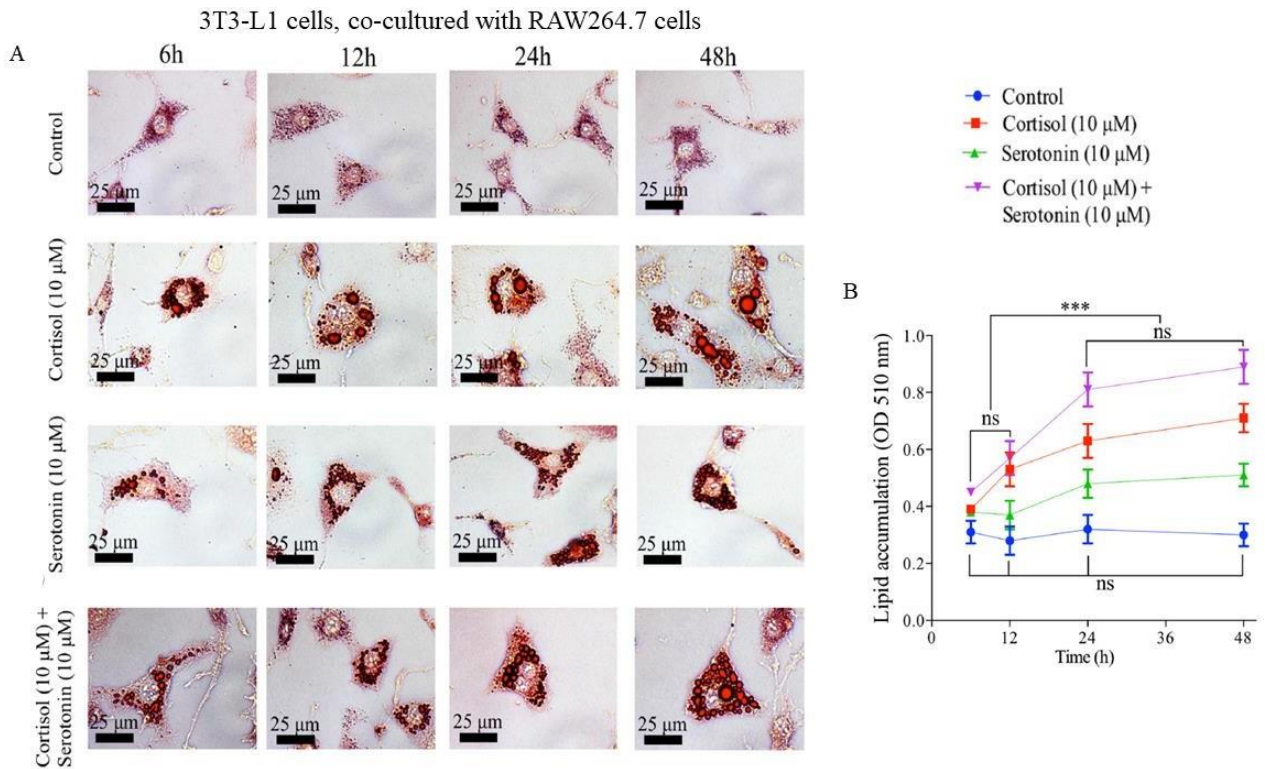


Figure 21. The effects of cortisol and serotonin treatment, combined with differentiated 3T3-L1 cells, co-cultured with RAW264.7 cells.

Representative images of ORO-stained differentiated 3T3-L1 cells pre-treated with cortisol and serotonin treatment, alone or in combination and co-cultured with RAW264.7 cells. ORO staining and imaging after 6, 12, 24, and 48 h of co-culturing.

(B) Spectrophotometric determination of extracted cellular ORO from the differentiated 3T3-L1 cells undergoing the same treatment. We repeated the experiment three times. We represented the data as mean ($n=3$ for all conditions) \pm SD. We used 2-way ANOVA coupled with the Bonferroni post-test to determine the significance of changes in the data. We denoted the significance by $^*(p \leq 0.05)$, $^{**}(p \leq 0.01)$, $^{***}(p \leq 0.001)$.

4.3.5. Immune metabolic interaction in simulated adipose tissue microenvironment in vitro.

We now tried to determine the response of the RAW264.7 cells co-cultured with differentiated 3T3-L1 cells, pre-treated with cortisol and serotonin alone and together. We assessed the immunological status of the RAW264.7 cells by evaluating the expression of select immune genes and proteins. We observed a gradual increase in expression of pro-inflammatory genes (*Il1 β* , *Il12*, and *Nos2*) and proteins (CD11C, CD80, and NOS) over time while the expression of anti-inflammatory genes (*Tgfbr1*, *Arg1*) and proteins (CD206, CD163, and ARG) were reduced (Figure 22-25). The gene and protein expression supported the conclusion that RAW264.7 cells, other than inducing additional adiposity to the cortisol and serotonin treated adipocytes, become increasingly pro-inflammatory following co-culturing with adipocytes.

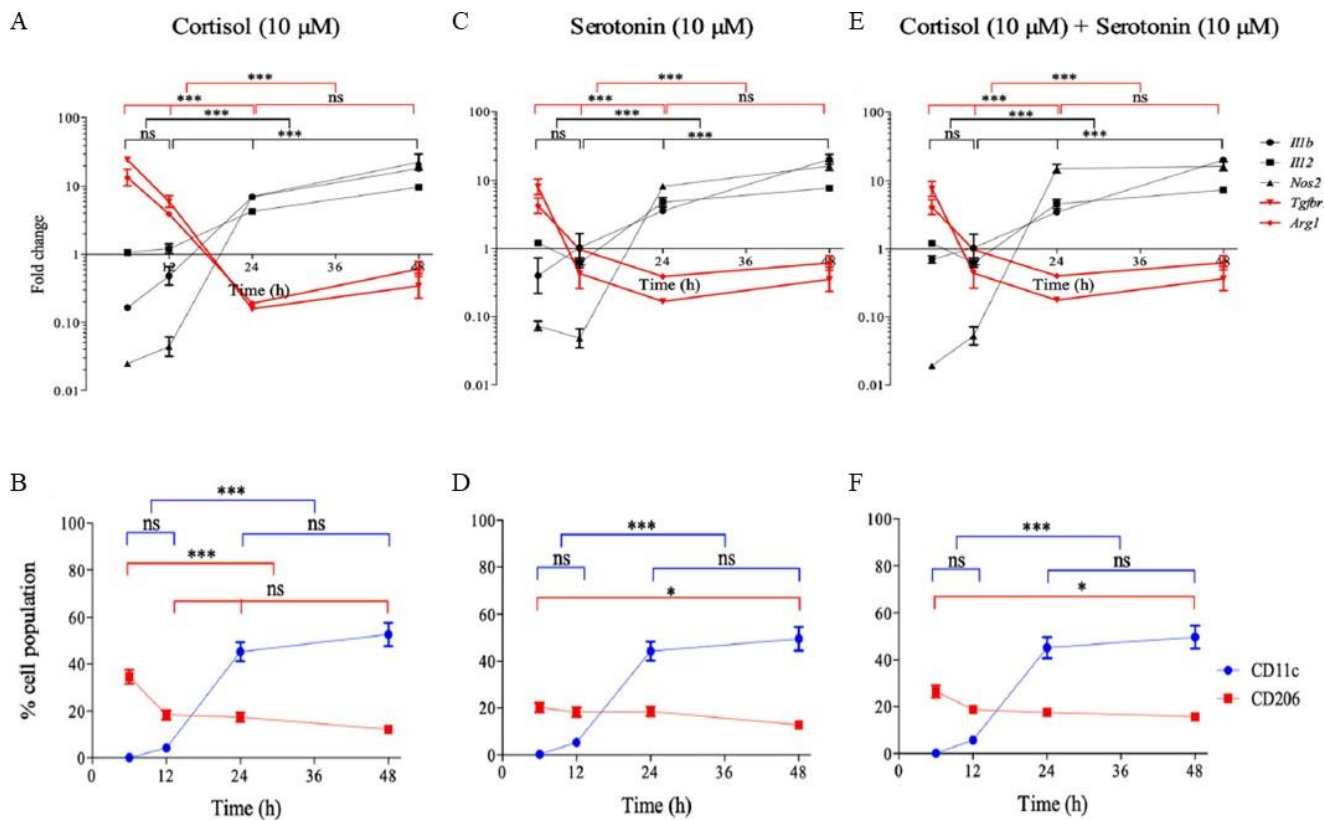


Figure 22. Effects of co-culturing RAW264.7 cells, with differentiated 3T3-L1 cells, pre-treated with cortisol and serotonin, alone and in combination.

Relative mRNA expressions (fold change to control mice) of select pro (*Il1 β* , *Il12*, *Nos2*) and anti (*Tgfb1*, *Arg1*) inflammatory marker genes from RAW264.7 cells, co-cultured with differentiated 3T3-L1 cells, pre-treated with (A) cortisol, (C) serotonin alone and (E) in combination. (B, D, F) Flow cytometric evaluation of select pro (CD11c) and anti (CD206) inflammatory marker genes from RAW264.7 cells undergoing above mentioned treatment, respectively. We repeated the experiment three times. We represented the data as mean (n=3 for all conditions) \pm SD. We used 2-way ANOVA coupled with the Bonferroni post-test to determine the significance of changes in the data. We denoted the significance by *(p \leq 0.05), **(p \leq 0.01), ***(p \leq 0.001).

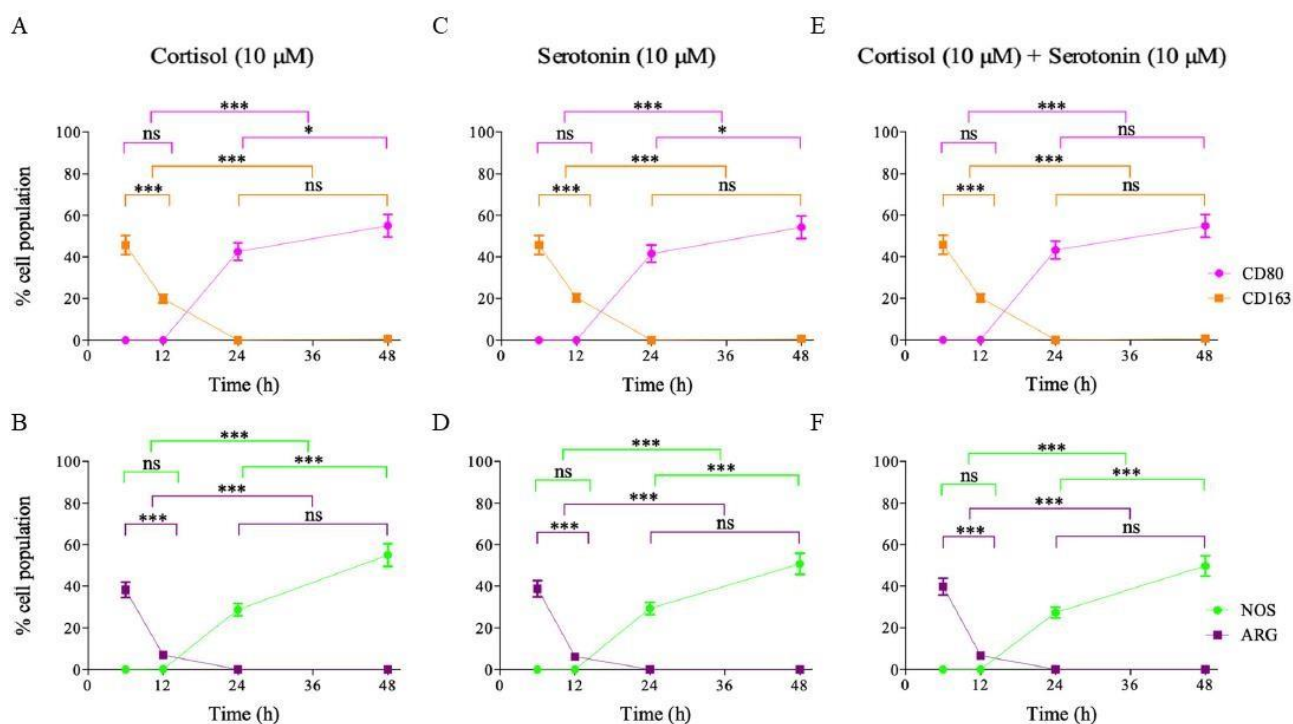


Figure 23. Flow cytometric evaluation of pro and anti-inflammatory properties of RAW264.7 cells, co-cultured with cortisol and serotonin treated, differentiated 3T3-L1 cells.

Flow cytometric evaluation of select pro (CD80, NOS) and anti (CD163, ARG) inflammatory marker genes from RAW264.7 cells, co-cultured with differentiated 3T3-L1 cells, pre-treated with (A, B) cortisol, (C, D) serotonin alone, and (E, F) in combination. We repeated the experiment three times. We represented the data as mean (n=3 for all conditions) \pm SD. We used 2-way ANOVA coupled with the Bonferroni post-test to determine the significance of changes in the data. We denoted the significance by *(p \leq 0.05), **(p \leq 0.01), ***(p \leq 0.001).

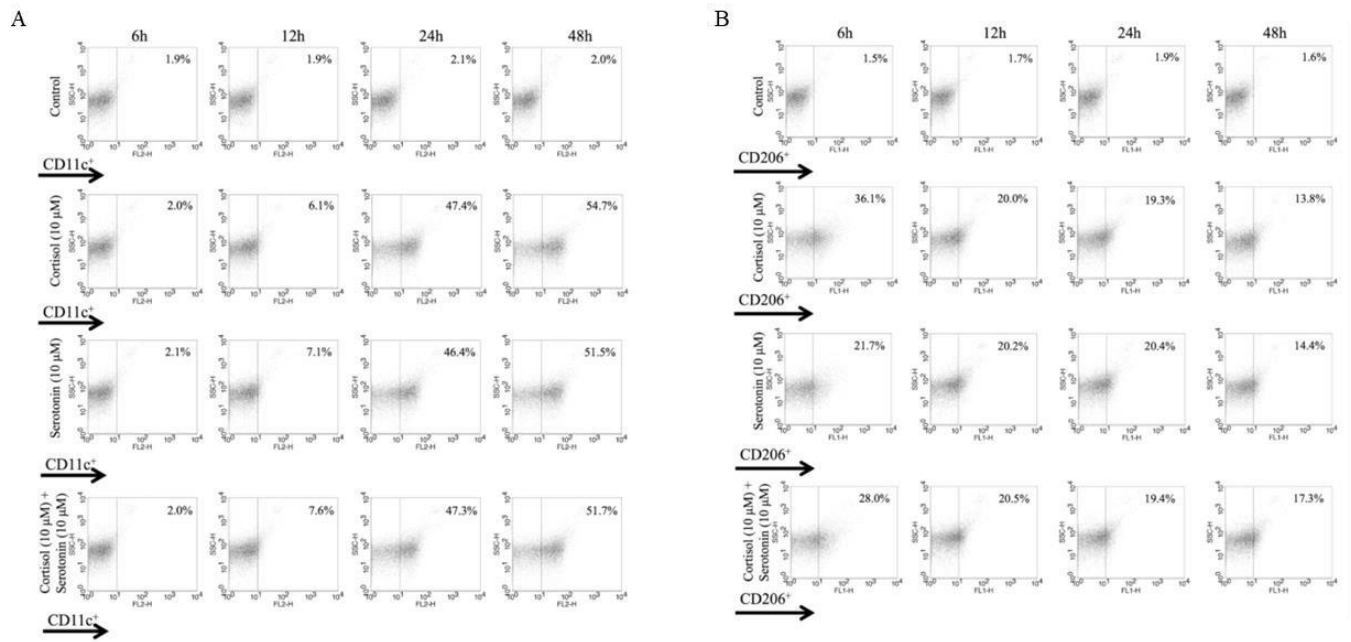


Figure 24. Scatter plots showing the population of RAW264.7 cells expressing select cell surface marker.

Scatter plots showing the population of RAW264.7 cells expressing the cell surface marker (A) CD11c and (B) CD206 following co-culturing with differentiated 3T3-L1 cells pre-treated with either cortisol and serotonin alone or together, along with time-matched controls. We repeated the experiment three times. We are showing representative scatter plots of the experiments.

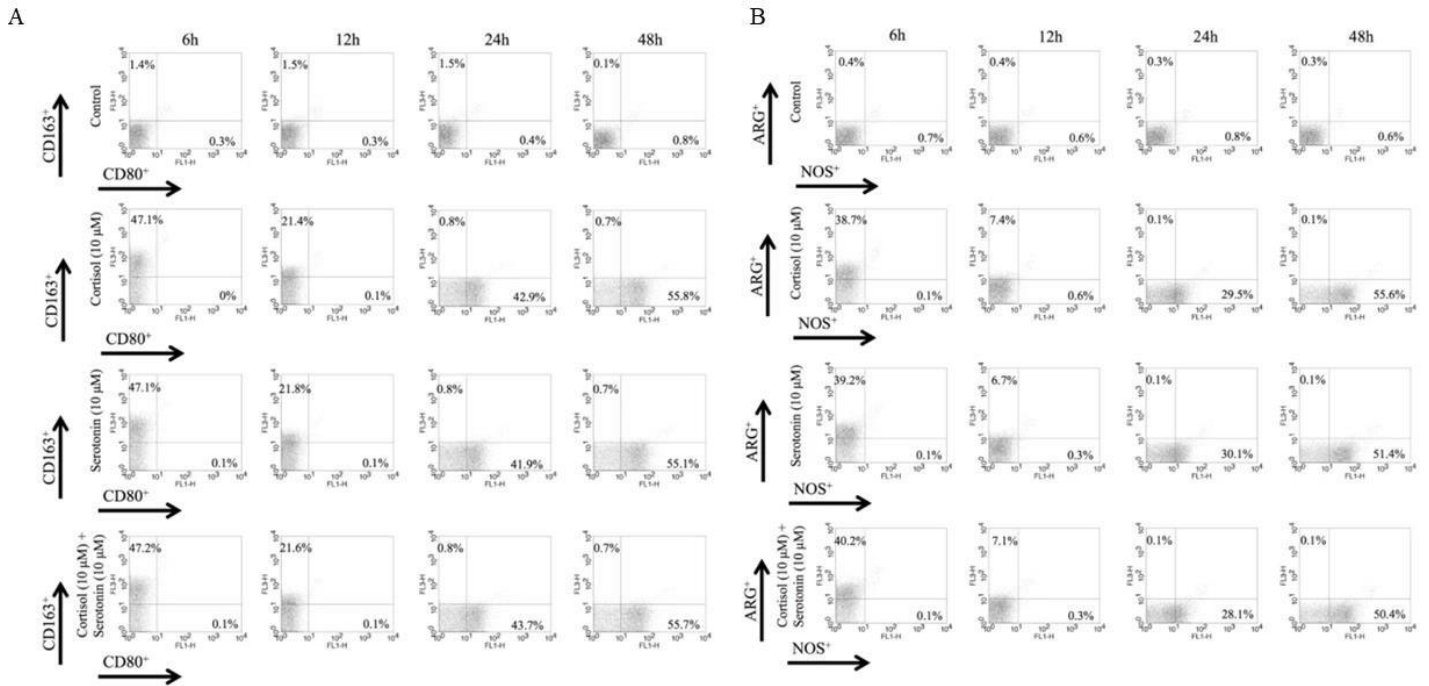


Figure 25. Scatter plots showing the population of RAW264.7 cells expressing select cell surface marker.

Scatter plots showing the population of RAW264.7 cells expressing the cell surface marker (A) CD163, CD80 and (B) ARG, NOS, following co-culturing with differentiated 3T3-L1 cells pre-treated with either cortisol and serotonin alone or together, along with time-matched controls. We repeated the experiment three times.

We are showing representative scatter plots of the experiments.

4.4. Discussion and conclusion

Results described in this chapter provided insight into how different nutrient-rich diets and chronic psychological stress condition may induce meta-inflammation in a murine model system. BALB/c mice fed SRD, showed a temporal amelioration in vWAT

macrophage infiltration rates, similar to their visceral adiposity levels. The USFD fed BALB/c mice didn't show significant changes in macrophage infiltration rates over time, while SFD enhanced infiltration. The temporal enhancement in macrophage infiltration rates corroborated the visceral adiposity and IR levels in SFD fed BALB/c. Simultaneous enhancement in adiposity, IR, and meta-inflammation following feeding a SFD prove that saturated fat consumption can most effectively induce metabolic pathogenicity over time, consistent with previous findings (197, 198). Possibly, the chemical nature of the constituent fatty acids in SFD led to the observed meta-inflammatory changes, as saturated fatty acids are known to cause enhanced adiposity and meta-inflammation (199). We concluded that SFD had initiated the process of chronic inflammation in BALB/c mice from the temporal enhancement in pro-inflammatory cytokines (*Il6* and *Tnfa*) coupled with a reduction in anti-inflammatory cytokines (*Tgf-β*) (200). We could consider the enhanced chronic inflammation as a hallmark of profound metabolic abnormality in this group (201). In C57BL/6 mice, we observed the most pronounced changes in macrophage infiltration rates in SFD fed mice, though the effects were less evident than in BALB/c mice.

Interestingly, in C57BL/6 mice, enhanced macrophage infiltration following SFD consumption was accompanied by a similar enhancement in visceral adiposity and IR levels. Hence, we can conclude that SFD diets can most effectively enhance the hallmarks of metabolic disorders in immune-biased mice. Following these findings *in vivo*, we tried to understand the immune-metabolic interactions occurring under the influence of chronic psychological stress *in vitro*. The cortisol and serotonin-induced chronic stress model helped us understand the mode of stress hormone-induced adiposity and meta-inflammation occurring in the mouse model. We found that the stress hormones can induce adiposity in differentiated 3T3-L1 cells, which is

augmented by co-culture with RAW264.7 cells. The RAW264.7 cells, on the other hand, themselves become immunologically polarized towards predominantly pro-inflammatory macrophages during co-culture. The RAW264.7 cells gradually expressed higher levels of *Il1 β* , *Il12*, *Nos2*, while *Tgfbr1* and *Arg1* expression steadily declined.

Along with these observations, we found the RAW264.7 cells expressed increased levels of CD11C, CD80, and iNOS proteins, while the levels of CD206, CD163, and ARG proteins were reduced on the cell surface over time. The expression pattern of the cytokines *Il1 β* , *Il12*, the enzymes *Nos2*, *Arg1*, and other genes and proteins, suggested that cortisol and serotonin induce RAW264.7 cells to convert from M2 to M1 state (202). The serotonin receptors play essential roles in lipogenesis-induced immune polarization, as revealed from our study. The possible mode of interaction between differentiated 3T3-L1 and RAW264.7 cells may be through glycolysis and pyruvate metabolism, as revealed from serum metabolomics study. The pyruvate metabolism was significantly enriched in SFD fed immune-biased mice, where we have found higher levels of adiposity and meta-inflammation following eight weeks of intake. Through glycolysis, cells produce pyruvate, which acts as a substrate for pyruvate metabolism (203). The pyruvate can stimulate TG synthesis in adipocytes (204). The enhanced lipid stored in adipocytes can stimulate chemokine secretion, which mediates the immune polarization of the macrophages, creating the state of meta-inflammation in adipose tissue (195). The overall molecular process of immune-metabolic interactions between adipocytes and macrophages presented schematically in Figure 26.

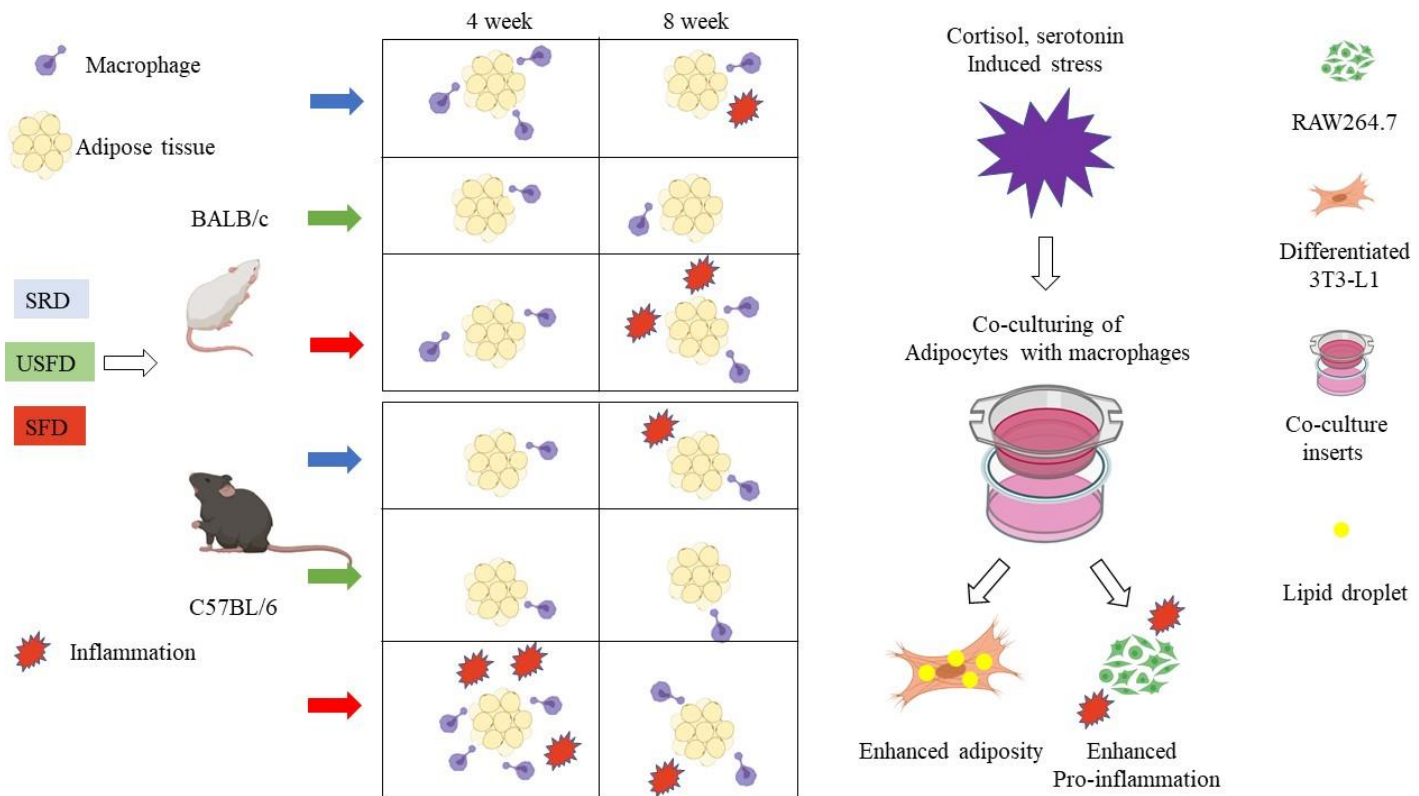


Figure 26. Schematic representation of diet and chronic psychological stress-induced meta-inflammation, in vivo and in vitro.

We evaluated the overall changes in macrophage infiltration rates in adipocytes. Also, we checked the inflammatory status of the tissue from the expression of pro-inflammatory cytokines. Cumulatively, we considered the event of macrophage infiltration and tissue inflammation had given rise to meta-inflammation in certain groups. (Icon courtesy <https://biorender.com/>). SFD consumption made the effects more pronounced. We found the adiposity to augment meta-inflammation, revealed from the *in vitro* experiments.

Chapter 4

Effects of diets on cecal microbial composition and understanding the impact of select microbes on regulating host metabolism

5.1. Introduction

The objective behind the experiments described in this chapter was to evaluate the effects of starch- or fat-rich diets on the intestinal microbial composition of the immune biased mice. Also, we evaluated how some specific microbes can influence the murine adiposity, to find out the role of microbes in regulating host metabolism. The intestinal microbes are an essential regulator of host energy homeostasis. Host nutrition, on the other hand, dictates microbial diversity. Particular types of diets augment various microbial phyla while others are hindered (205). As an intricate relationship between metabolism and the immune system exists, we assumed that the intestinal microbes might be differentially regulated by C57BL/6 and BALB/c mice, following dietary changes. The work described in this chapter concerns how the intestinal microbes are differentially affected by the control, SRD, USFD, and SFD diets in C57BL/6 and BALB/c mice after four and eight weeks of dietary alterations. The different treatment groups were further classified based on the microbial phyla diversity using LDA. The LDA effectively clustered the diet-treated groups, showing that altered diversity occurred after dietary alterations. The diversity of microbes at the genus level revealed the predominant microbial genera present in the cecum of the diet-treated immune-biased mice. As many intestinal microbes can produce meta-metabolites that affect the physiology of their hosts (206), we next assessed the levels of SCFAs from the serum of the mice by metabolomics. We observed a trend between the major SCFA producing microbial genera and SCFA abundance. We linked the microbial abundance and SCFA levels with the altered physiological conditions of the mice such as adiposity, glycemia and meta-inflammation, where we found distinct

inter-strain differences. The linking helped explain the effects of the altered microbial diversity on the physiological changes associated with different diets.

We further tried to understand the direct influence of select microbes on mammalian lipid metabolism, using murine differentiated adipocyte cell line 3T3-L1. The microbes used were established probiotic bacteria strains from the genus *Lactobacillus*, well known for their health benefits (90, 154, 156). The major aim of studying the direct anti-adipogenic effects of the probiotics was to evaluate whether bacterial metabolites or some cellular components or both had any lipid lowering capacity. We observed the probiotics *Lactobacillus acidophilus* MTCC10307 (LA) and a cocktail of *Lactobacillus delbrueckii* sp. *bulgaricus* strain DWT1, CCM 7992, and *Streptococcus thermophilus* strain DWT4; CCM 7992 (LDB-ST) were catalytic in reducing adipogenesis and intracellular lipids *in vitro*. To use LA and LDB-ST as intervention agents against lipid storage diseases, further pre-clinical and clinical studies must be done. The studies may include feeding the probiotics directly to the obese individual or model organism. Alternatively, select microbial metabolites or cellular components may be identified and used either orally or via some other route, to be circulated to the adipose tissue depot throughout the body. We describe the details of the work below.

5.2. Characterization of cecal microbial diversity following starch and fat-rich diet consumption.

We first evaluated the diversity of the intestinal microbes from different diet-treated mice at the phylum level and investigated possible associations with host physiological changes. We clustered the diet-treated groups based on the relative

abundance of the phyla to evaluate whether significant changes occurred following the dietary alterations. Then, we checked how the nutritional alterations influenced the cecal microbial genera. We identified the SCFA producing genera and linked the serum SCFA profile and physiological changes with the gut microbial genera to identify possible microbial influence on host physiology. Below, are the details of the analyses.

5.2.1. Diversity of major microbial phylum following dietary alterations for four and eight weeks

We found the diversity of major microbial phyla to change differentially, following dietary changes in C57BL/6 and BALB/c mice (Figure 27A, 27B). Significant differences existed in the gut microbial diversity between the mice strains. Also, the microbial diversity altered temporally in the mice strains. In BALB/c mice fed with control diets, we found an increase in Epsilonbacteraeota level with time. In C57BL/6 however, the percentage of Epsilonbacteraeota and Proteobacteria had reduced with time while Firmicutes level had increased. In C57BL/6 mice, after four weeks of dietary alteration, the SRD consumption increased Firmicutes and Proteobacteria levels compared to other time-matched groups. Compared to the control mice, the Firmicutes levels remained almost identical or changed little while the Epsilonbacteraeota level nearly doubled in the fat-rich diet fed mice. At eight weeks, we found SRD and USFD fed mice had an increased number of Verrucomicrobia in the cecum. The Proteobacteria levels increased markedly in all the treatment diet groups, with the greatest increase in the SFD fed mice. In contrast, we observed the Bacteroidetes level decreased almost to half of that found in the time-matched control, keeping the Firmicutes at a nearly constant level in all the treatment diet-fed mice.

For BALB/c mice, evaluation of the cecal microbial contents revealed that at four weeks, the SRD and SFD fed mice had an increased abundance of Epsilonbacteraeota in the cecum. However, in the USFD and time-matched control mice, we observed an almost identical microbial profile. We found an increase in Verrucomicrobia and Proteobacteria levels in SRD fed mice while the Bacteroidetes and Firmicutes levels decreased after eight weeks. In USFD fed mice, the microbial profile didn't change significantly other than a slight reduction in Firmicutes level. However, the SFD fed mice had almost doubled the Epsilonbacteraeota level, coupled with a slight decrease in Bacteroidetes level. We could say from the microbial profile that SRD and USFD fed mice from both strains gradually reduced their cecal bacterial phyla Proteobacteria or Epsilonbacteraeota. The phylum Verrucomicrobia level was simultaneously increased with time. SFD fed mice from both strains did not show this observed change, visualized in SRD and USFD mice. In SFD fed mice, the Proteobacteria and Epsilonbacteraeota levels remained high in the cecum throughout time, irrespective of the mouse strain. We also tried to link the microbial alterations with the host physiological changes which have been described in table 6A-6D.

We then investigated how the overall microbial diversity changed in the diet-treated mice using the Shannon diversity indices. The diversity indices suggested that the broad phyla diversity had more significant intra and inter-strain changes at four weeks than eight weeks (Figure 27C, 27D). Following dysbiosis of microbiota, the diversity of microbes is reduced and is dominated by few microbial taxa (207). Our study found that the altered diets almost uniformly enhanced microbial diversity, suggesting remodeling of the gut ecosystem rather than dysbiosis. We analyzed the spatial distribution of the different diet-treated groups to visualize the intra-strain differences among the diet-treated mice.

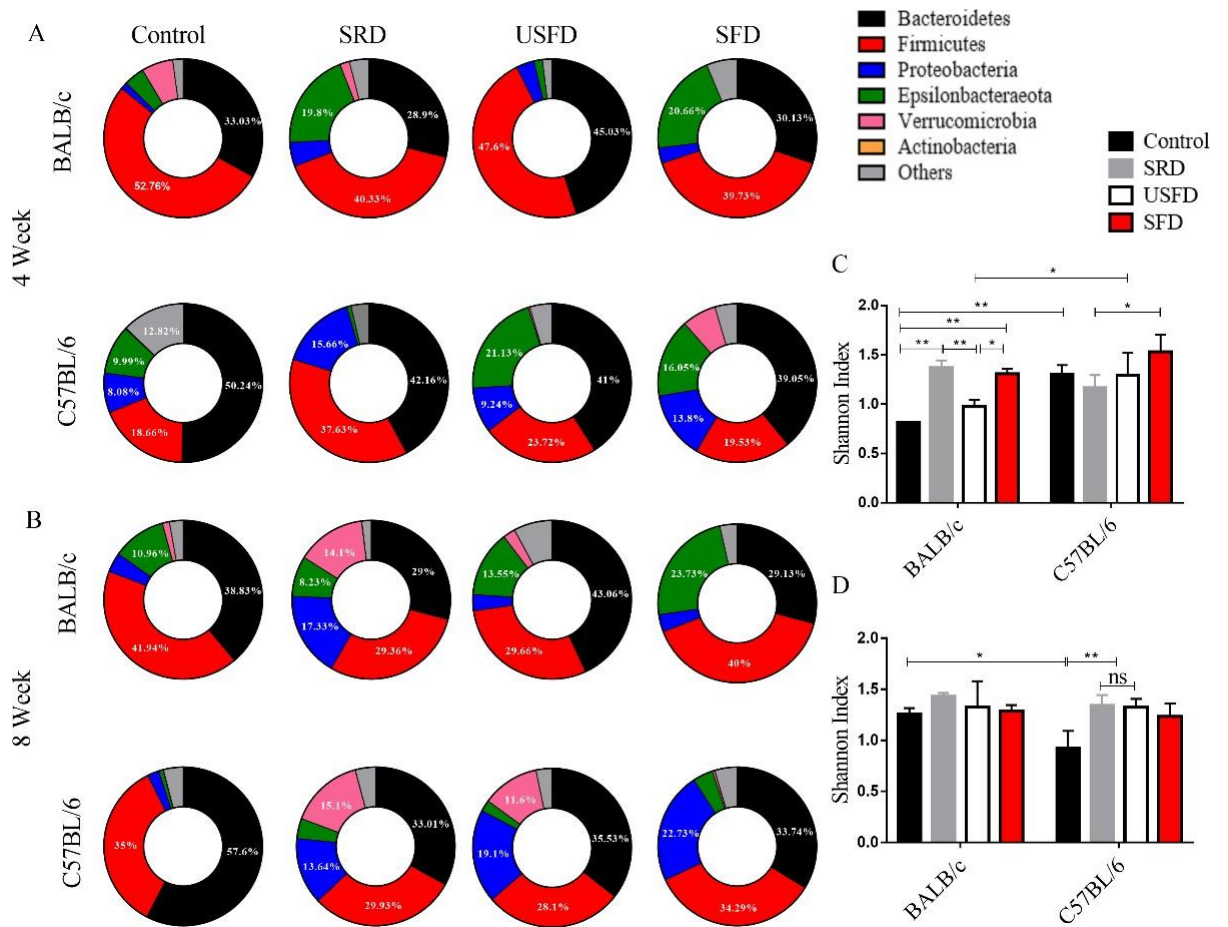


Figure 27. Comparative overview of the significant intestinal microbial phyla and their diversity in control and treatment (SRD, USFD, and SFD) diet-fed C57BL/6 and BALB/c mice.

Donut charts representing the major cecal microbial phyla of C57BL/6 and BALB/c mice after (A) four and (B) eight weeks of control and treatment diet consumption. The Shannon diversity indices of C57BL/6 and BALB/c mice after (C) four and (D) eight weeks of the aforementioned interventions. Data represented are mean (n=3) percent abundance of respective microbial phylum (A, B). We represented the data as mean (n=3 for all conditions) \pm SEM for figure C and D. We used one-tailed *t*-test to

determine the significance of changes in the data for figures C and D. We denoted the significance by *($p \leq 0.05$), **($p \leq 0.01$), ***($p \leq 0.001$), ****($p \leq 0.0001$).

Table 6: Possible associations between the major microbial phylum and the induced physiological changes following dietary alterations.

A: The abundance of major cecal microbial phyla and possible associations with host physiology of C57BL/6 mice after four weeks of dietary intervention.

Group	Changes in relative abundance	Significant physiological changes	Role of microbial phylum
SRD	Enhanced Proteobacteria (15.6%) and Firmicutes (37.6%).	Enhanced IR	Associated with enhanced IR (208, 209).
USFD	Enhanced Epsilonbacteraeota (21.1%)	Enhanced blood glucose and leptin level	Associated with enhanced metabolic abnormalities (210).

SFD	Enhanced Epsilonbacteraeota (16%)	Enhanced adiposity and meta- inflammation	Associated with enhanced metabolic abnormalities (210).
-----	---	--	---

B: The abundance of major cecal microbial phyla and possible associations with host physiology of C57BL/6 mice after eight weeks of dietary intervention.

Group	Changes in relative abundance	Significant physiological changes	Role of microbial phylum
SRD	Enhanced Verrucomicrobia (15.1%).	Reduced FBS.	Reduces IR (211).
USFD	Enhanced Verrucomicrobia (15.1%).	Reduced FBS.	Reduces IR (211).
SFD	Enhanced Proteobacteria (22.7%)	Enhanced adiposity and meta- inflammation.	Associated with enhanced metabolic abnormalities (212).

C: The abundance of major cecal microbial phyla and possible associations with host physiology of BALB/c mice after four weeks of dietary intervention.

Group	Changes in relative abundance	Significant physiological changes	Role of microbial phylum
SRD	Enhanced Epsilonbacteraeota (19.8%).	Enhanced meta-inflammation.	Associated with enhanced inflammation (213).
USFD	Enhanced Bacteroidetes (45.03%)	Reduced cellular adiposity.	Associated with reduced metabolic abnormalities (214).
SFD	Enhanced Epsilonbacteraeota (20.6%)	Enhanced meta-inflammation.	Associated with enhanced inflammation (213).

D: The abundance of major cecal microbial phyla and possible associations with host physiology of BALB/c mice after eight weeks of dietary intervention.

Group	Changes in relative abundance	Significant physiological changes	Role of microbial phylum
--------------	--------------------------------------	--	---------------------------------

SRD	Enhanced Verrucomicrobia (14.1%).	Unaltered FBS and IR.	Reduces IR (211).
USFD	Reduced Firmicutes (29.6%).	Unaltered cellular adiposity.	Reduces adiposity (215).
SFD	Enhanced Epsilonbacteraeota (23.7%).	Enhanced adiposity and meta-inflammation.	Associated with enhanced metabolic abnormalities (210).

5.2.2. Clustering of control and treatment diet fed mice based on cecal microbiota abundance

The LDA clustering revealed the intra-strain differences as a measurement of diets' impact on microbiota remodeling. LDA of BALB/c mice at four and eight weeks (Figure 28A, 28B) revealed that SRD and SFD fed mice had more microbial phyla differences than the control and USFD mice, which clustered closely. Further, the LDA classification could only moderately segregate the C57BL/6 mice based on microbial phyla at any time point (Figure 28C, 28D). The LDA clustering point out that the diets created more drastic differences in the BALB/c mice than the C57BL/6 mice. The differential clustering could also be related to the differential magnitude of physiological changes between the mice strains observed in previous sections. Next,

we will discuss the functional aspects of the microbes by analyzing some select microbial metabolic products and relating them to the physiology of the host.

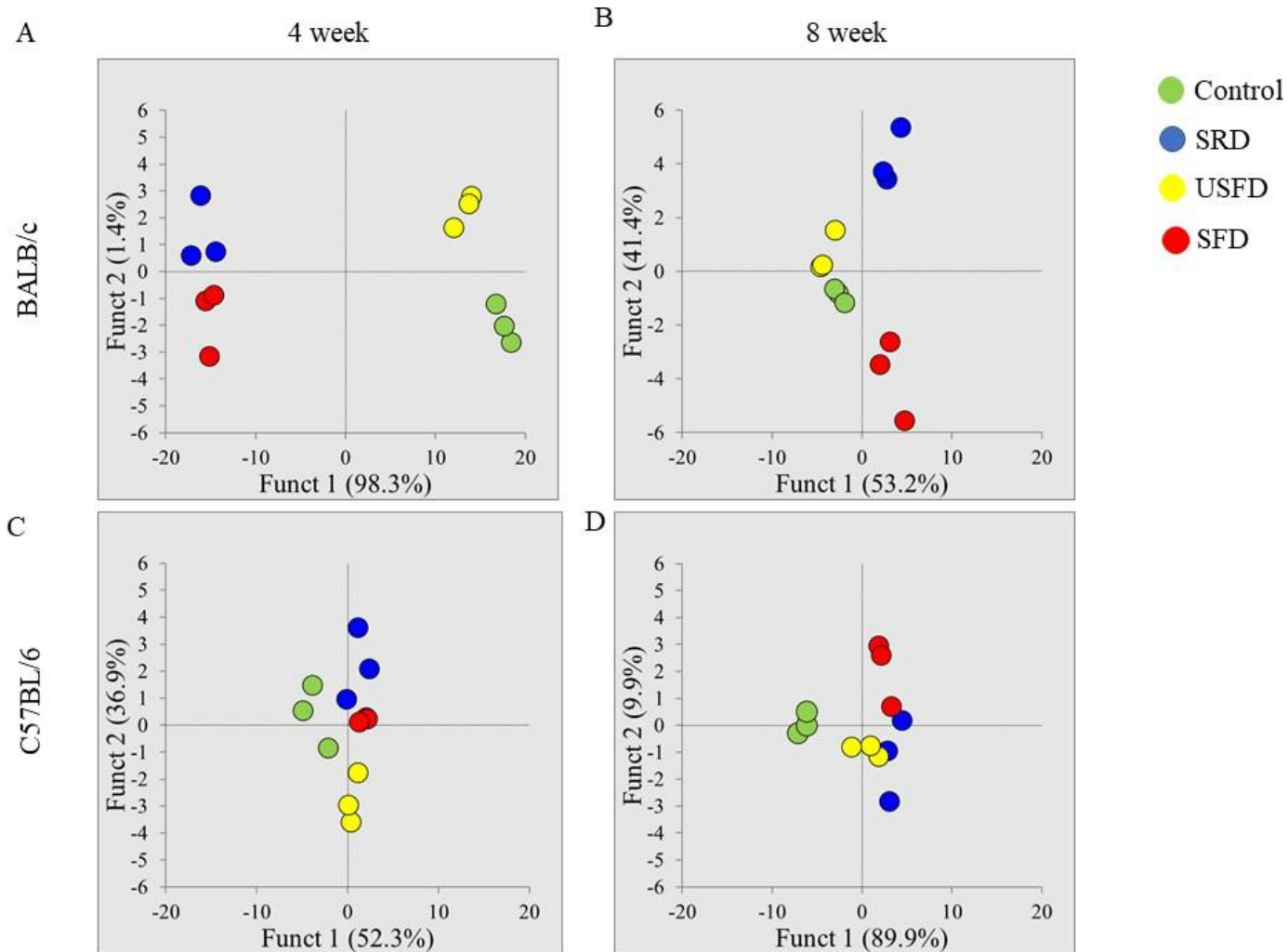


Figure 28. Clustering of different diet-fed C57BL/6 and BALB/c mice based on intestinal microbial phyla diversity using a linear discriminant analysis (LDA) plot.

LDA-based clustering of individual BALB/c mice fed control and treatment (SRD, USFD, and SFD) diet for (A) four and (B) eight weeks and C57BL/6 mice fed the

identical diets for (C) four and (D) eight weeks. We represented the data as individual mice, belonging to respective control and treatment groups.

5.2.3. Major SCFA producing microbial genera, affected by dietary alterations and their relationship with host physiology

We analyzed the serum concentrations of acetate, propionate, and butyrate as they are the major SCFAs (Figure 29A-29F), playing an essential role in host metabolism and physiology (86). We also listed the relative abundance of major SCFA producing microbial genera in table 7A-7D that had changed following dietary alterations. When we looked into the functionality of the SCFAs, we found that they can reduce adiposity and enhance insulin sensitivity (216). Our study found that four weeks of SFD consumption improves all three SCFA (acetate, propionate, and butyrate) levels in the serum of C57BL/6 mice, compared to the BALB/c. We had also found that the fasting blood glucose, serum insulin, and IR levels (Figure 12A, 12C, 12E) had reduced significantly in SFD fed C57BL/6 mice, compared to BALB/c after four weeks. We can associate the reduced glycemic levels with the relatively higher abundance of *Akkermansia* spp in SFD fed C57BL/6 mice (table 7A, 7C, 6.99 ± 2.853 and absent, in C57BL/6 and BALB/c, respectively). As *Akkermansia* spp is a well-known producer of acetate (217) and is also known for its antagonistic effects on insulin resistance (218), we propose that *Akkermansia* spp could reverse the insulin resistance in SFD-fed mice. A similar trend was found in both USFD and SFD fed C57BL/6 and BALB/c mouse after eight weeks, where the levels of *Akkermansia* spp (5.824 ± 4.755 , 0.706 ± 0.576 and 0.458 ± 0.374 , 0.006 ± 0.005 in C57BL/6 and BALB/c mice fed USFD and SFD respectively) and serum acetate varied similarly, giving rise to a reduction in IR of C57BL/6 mice compared to BALB/c. The relation between the

phenotypic changes and microbial metabolites showed that diet-induced altered microbiome could effectively impact immune-biased mice.

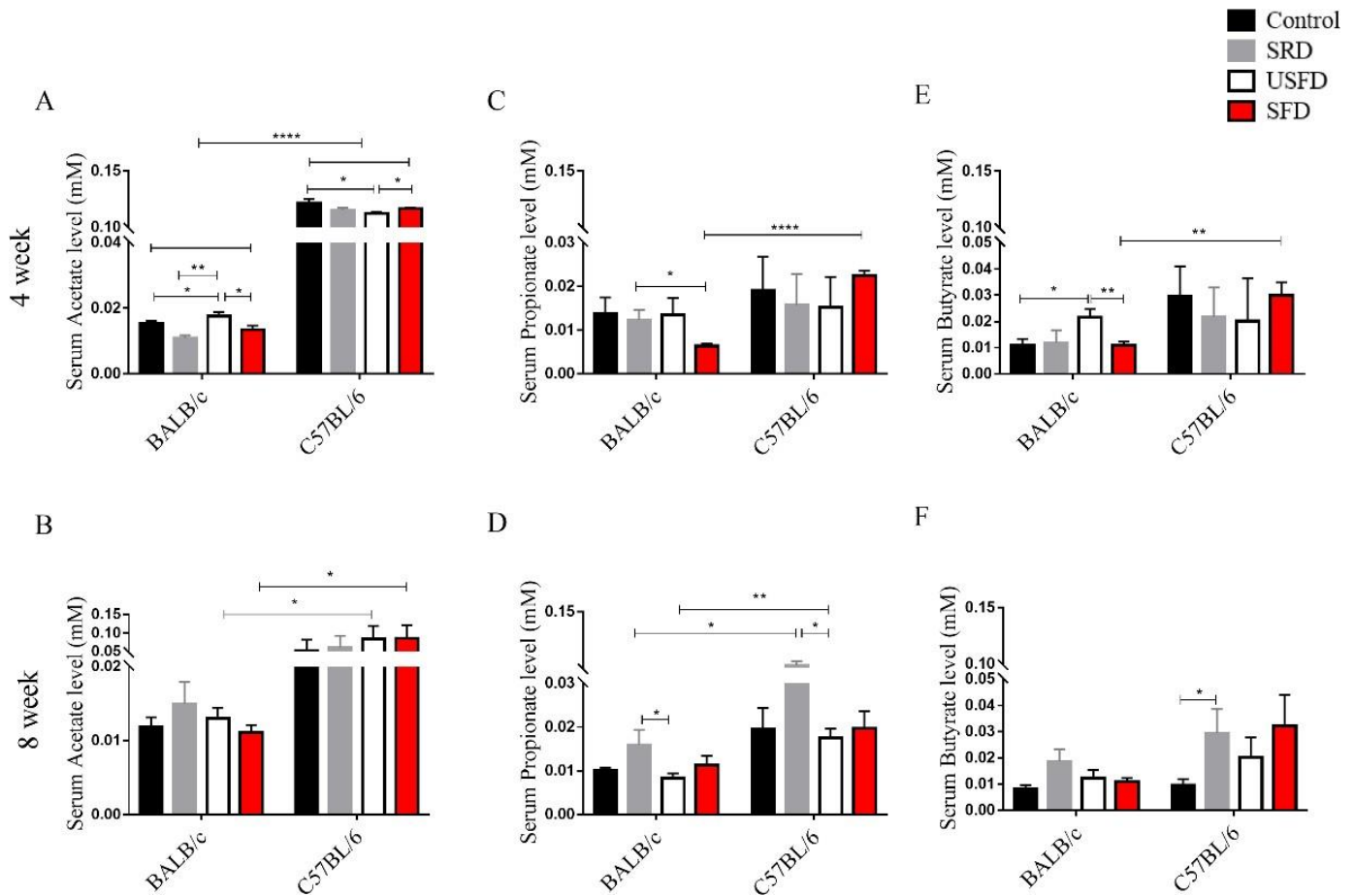


Figure 29. Comparative overview of short-chain fatty acid (SCFA) levels in serum from control and treatment (SRD, USFD, and SFD) diet-fed groups of C57BL/6 and BALB/c mice.

Comparative serum acetate, propionate, and butyrate levels of C57BL/6 and BALB/c mice following control and treatment diet consumption for (A, C, E) four and (B, D, F) eight weeks, respectively. We represented the data as mean (n=3 for all conditions)

± SEM. A one-tailed *t*-test has determined the significance of changes. We denoted the significance by *($p \leq 0.05$), **($p \leq 0.01$), ***($p \leq 0.001$), ****($p \leq 0.0001$).

Table 7. Percent abundance of Major SCFA producing microbial genera ().

A: Percent abundance in C57BL/6 mice after four weeks of dietary intervention

Major genera	Control	SRD	USFD	SFD	Major SCFA produced
<i>Bacteroides</i> spp	13.536±1.106	2.353±1.377	7.503±1.113	8.517±0.722	Acetate, propionate, butyrate (217),
<i>Lactobacillus</i> spp	0.453±0.214	0±0	0.087±0.036	0.046±0.019	Acetate (217)
<i>Akkermansia</i> spp	0.139±0.023	0±0	0.294±0.136	6.99±2.853	Acetate (217)
<i>Prevotella</i> spp	6.612±0.085	0±0	0.001±0.0004	0.001±0.0008	Acetate (217)
<i>Alistipes</i> spp	1.775±0.062	1.71±0.475	4.54±0.916	3.11±0.449	Acetate (219)
<i>Lachnospiraceae</i> spp	2.933±0.528	11.604±0.585	4.553±2.543	3.88±2.42	Butyrate (220)

B: Percent abundance in C57BL/6 mice after eight weeks of dietary intervention

Major genera	Control	SRD	USFD	SFD	Major SCFA produced
<i>Bacteroides</i> spp	6.871±2.955	10.858±3.283	9.955±3.204	8.164±2.961	Acetate, propionate, butyrate (217),
<i>Lactobacillus</i> spp	0.534±0.436	0.068±0.048	0.029±0.023	0.072±0.058	Acetate (217)
<i>Akkermansia</i> spp	0.016±0.013	8.334±6.413	5.824±4.755	0.458±0.374	Acetate (217)
<i>Prevotella</i> spp	0±0	0.001±0.001	0±0	0±0	Acetate (217)
<i>Alistipes</i> spp	3.393±1.509	2.876±1.257	2.401±1.045	2.427±1.263	Acetate (219)
<i>Lachnospiraceae</i> spp	7.073±0.561	3.955±0.865	6.166±3.918	6.486±1.617	Butyrate (220)

C: Percent abundance in BALB/c mice after four weeks of dietary intervention

Major genera	Control	SRD	USFD	SFD	Major SCFA produced
<i>Bacteroides</i> spp	10.8±1.853	8.553±0.327	15.566±6.151	9.643±1.793	Acetate, propionate, butyrate (217),
<i>Lactobacillus</i> spp	0±0	0±0	0±0	0±0	Acetate (217)
<i>Akkermansia</i> spp	6.433±5.252	0±0	0±0	0±0	Acetate (217)
<i>Prevotella</i> spp	0±0	0±0	0±0	0±0	Acetate (217)
<i>Alistipes</i> spp	6.363±0.488	5.91±2.413	0±0	3.613±1.48	Acetate (219)
<i>Lachnospiraceae</i> spp	20.99±4.975	10.176±0.715	6.596±3.961	2.37±0.599	Butyrate (220)

D: Percent abundance in BALB/c mice after eight weeks of dietary intervention

Major genera	Control	SRD	USFD	SFD	Major SCFA produced
---------------------	----------------	------------	-------------	------------	----------------------------

<i>Bacteroides</i> spp	9.706±0.274	12.4±3.225	3.406±1.573	6.923±1.341	Acetate, propionate, butyrate (217),
<i>Lactobacillus</i> spp	0.01±0.008	0.03±0.024	0.026±0.021	0.013±0.01	Acetate (217)
<i>Akkermansia</i> spp	0.9±0.734	14.161±5.794	0.706±0.576	0.006±0.005	Acetate (217)
<i>Prevotella</i> spp	0±0	0.001±0.0008	0±0	0±0	Acetate (217)
<i>Alistipes</i> spp	4.813±0.242	4.78±2.18	10.353±0.852	7.073±0.484	Acetate (219)
<i>Lachnospiraceae</i> spp	14.106±2.24	3.076±0.317	4.93±0.724	13.166±3.996	Butyrate (220)

5.3. Effect of select strains of *Lactobacillus acidophilus* and *Lactobacillus delbruckei* sp. *bulgaricus* on adiposity, when co-cultured with murine adipocytes.

We used two probiotics, LA and LDB-ST, and cultured them with the differentiated 3T3-L1 cells to check their anti-adipogenic potential. We determined the optimum doses of bacteria by performing a survival assay of the differentiated 3T3-L1 cells following treatment with the probiotics at different MOIs (Figure 30A, 30B). We then used the selected doses to evaluate the number of probiotics that are associated with or taken up by differentiated 3T3-L1 cells. We assessed the association/ uptake

efficiency of the probiotics to establish the effects they caused following treatment. At higher MOIs, the association/ uptake efficiency of probiotics might have increased. We didn't check the probiotic association/ uptake at higher doses as the higher doses had lethal effects on the mammalian cell survival and could be rendered ineffective, therapeutically. We then hypothesize that the probiotics following association/ uptake with the cells would exert their beneficial effects. Since, some bacteria has the property of replicating inside host cells following internalization (221), we assume bacterial multiplication may also be true for the studied probiotics and for that at even MOI 1 the probiotics may have shown lethal effect upon prolonged culturing. Also, at MOIs higher than 1, the probiotics may have produced toxic metabolites which may be lethal for the cells (222). Finally, we determined whether following internalization, the probiotics could reduce cellular adiposity by staining the mammalian cells with ORO and quantified the extracted intracellular lipid. We assessed the anti-adipogenesis potential of the probiotics by evaluating the expression of mammalian adipogenesis marker genes. The detailed results are discussed below.

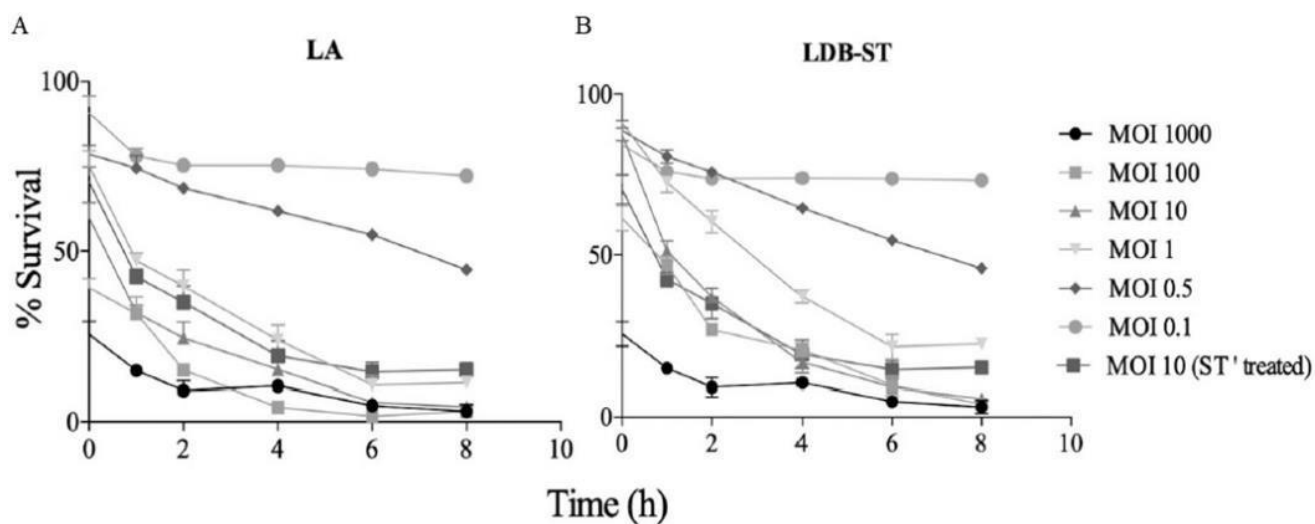


Figure 30. Survival kinetics of differentiated 3T3-L1 cells treated with either *Lactobacillus acidophilus* MTCC10307 (LA) or a cocktail *Lactobacillus delbrueckii* sp. *bulgaricus* strain DWT1; CCM 7992 (LDB) and *Streptococcus thermophilus* strain DWT4; CCM 7992 (ST). The survival of untreated 3T3-L1 cells were 100% for the entire 8 h study period.

We treated differentiated 3T3-L1 cells with (A) LA and (B) LDB-ST for 1 h, and the mammalian cell survival was estimated after 0 (post 1 h treatment), 2, 4, 6, and 8 h post-treatment withdrawal. We used *Salmonella enterica* serovar *Typhimurium* (ST') at MOI 10 as a positive control. We repeated each experiment 3 times. We represented the data as mean (n=3 for all conditions) \pm SD. We used 2-way ANOVA coupled with the Bonferroni post-test to determine the significance of changes in the data. We denoted the significance by *(p \leq 0.05), **(p \leq 0.01), ***(p \leq 0.001).

5.3.1. LA and LDB-ST were associated/up taken by differentiated 3T3-L1 cells following exposure at optimum MOIs

We treated the differentiated 3T3-L1 cells separately with different MOIs of the probiotic bacteria. Following incubation with the bacteria for 1 h, we evaluated the mammalian cells' survival until 8 h post-treatment. We found both probiotics caused significant cell death following treatment at MOI 1 or above. At MOI 0.5, LA or LDB-ST didn't cause more than 50% death to differentiated 3T3-L1 cells. At MOI 0.1, we found the extent of cell death of LA and LDB-ST treated differentiated 3T3-L1 cells was not significant even 8 h after treatment. For further studies, MOIs 0.1 and 0.5 were selected for treatment with LA or LDB-ST to understand the anti-adipogenic roles of the probiotics. Flow cytometry (Figure 31A, 31B) clearly showed that LA or LDB-ST, at MOIs 0.1 and 0.5, were associated/up taken by differentiated 3T3-L1 cells. LA treated differentiated 3T3-L1 cells were 28% and 41% positive for LA at MOIs of 0.1 and 0.5, respectively, while LDB-ST treated differentiated 3T3-L1 cells were 27% and 40% LDB-ST positive at MOIs of 0.1 and 0.5, respectively. We further validated the bacterial association/uptake by fluorescence microscopy (Figure 31C, 31D). Images depicted that at the said MOIs, probiotics effectively got associated/up taken (white arrows indicating internalized bacteria) inside differentiated 3T3-L1 cells. From the results obtained by cell lysis methodology (Figure 31E), we found the number of LA or LDB-ST associated/up taken with/by the differentiated 3T3-L1 cell membrane. We found the effective MOIs for LA treatment to be 0.1 and 0.48, compared to the experimental MOIs of 0.1 and 0.5, respectively. For LDB-ST treatment, we found the effective MOIs to be 0.17 and 0.5, when experimental MOIs were MOIs 0.1 and 0.5, respectively.

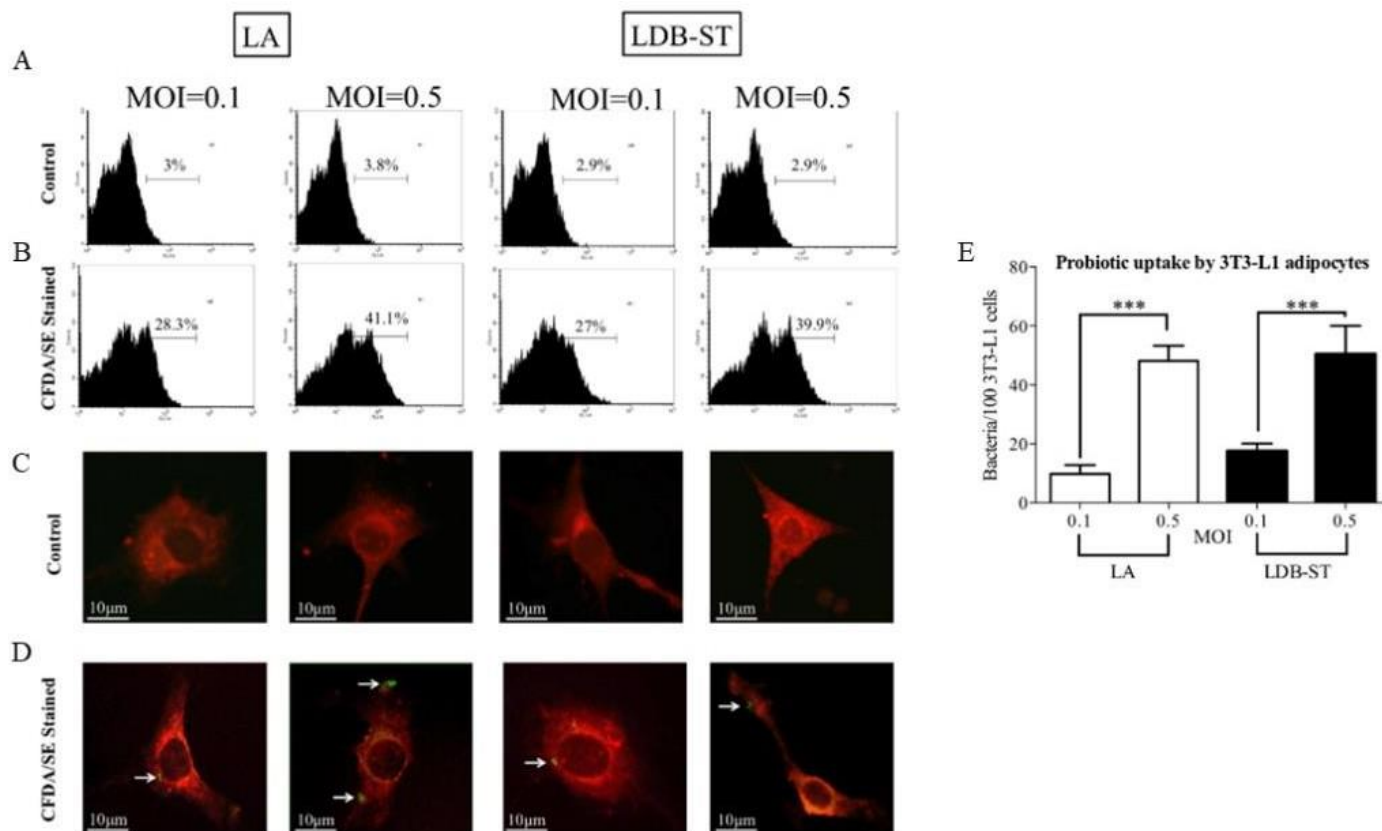


Figure 31. Association/uptake of LA or LDB-ST in differentiated 3T3-L1 cells following treatment.

Flow cytometry analysis of differentiated 3T3-L1 cells following treatment with LA or LDB-ST either (A) unstained (control) or (B) pre-stained with CFDA/SE at a multiplicity of infections (MOI) of 0.1 and 0.5 for 1 h. Fluorescence microscopic visualization of differentiated 3T3-L1 cells following treatment with LA or LDB-ST either (C) unstained and (D) pre-stained with CFDA/SE (Green dots marked by white arrow) at MOI of 0.1 or 0.5 for 1 h. (E) Amount of bacteria uptake per 100 differentiated 3T3-L1 cells done by cell lysis method. We repeated each experiment

3 times. A one-tailed t-test calculated statistical differences. We represented the data as mean ($n = 3$) \pm SD of the data. We denoted the significance by *** ($p \leq 0.001$).

5.3.2. Both LA and LDB-ST effectively reduced cellular lipid content and adipogenic gene expressions of differentiated 3T3-L1 cells.

We evaluated the lipolytic potential of the probiotics by staining the intracellular lipid droplets of the differentiated 3T3-L1 cells treated with the probiotics. We didn't find any pronounced lipolysis in the cells treated with LA and LDB-ST at MOI 0.1 for 4 h. We could only visualize a considerable amount of lipolysis in the cells after treatment with LA and LDB-ST at MOIs 0.1 for 8 h and 0.5 for 4 h (Figure 32A). Further, we confirmed our observations by spectrophotometrically estimating the ORO extracted from the control and treated cells (Figure 32B). We found that treating probiotics at MOI of 0.1 for 8 h or at MOI of 0.5 for 4 h could significantly reduce lipid accumulation in 3T3-L1 cells.

We then evaluated if the probiotics reduced the adipogenic potential of the differentiated 3T3-L1 cells. We hence checked the expressions of mammalian adipogenesis marker *Ppar γ* , *Cd36*, and *Ap2* genes (223) in control and probiotic-treated cells (Figure 32C). We didn't observe any significant changes in the expressions of *Ppar γ* and *Cd36* genes in differentiated 3T3-L1 cells treated with either LA or LDB-ST at MOI 0.1 for 4 h but there was a significant difference for *Ap2*, relative to the untreated differentiated 3T3-L1 cells. Differentiated 3T3-L1 cells, following treatment with either LA or LDB-ST at MOIs of 0.1 or 0.5 for 8 or 4 h, respectively, had a significant reduction in expression of *Ppar γ* , *Cd36*, and *Ap2*. The results were normalized in terms of house-keeping gene *β -actin*, which remained

almost similar between the groups. The consistency in house-keeping gene expression further show that the observed differences in gene expressions were not due to reduced cellular functioning but due to reduced adiposity. These results revealed that both probiotics are effective in causing lipolysis and reduce adipogenesis *in vitro*.

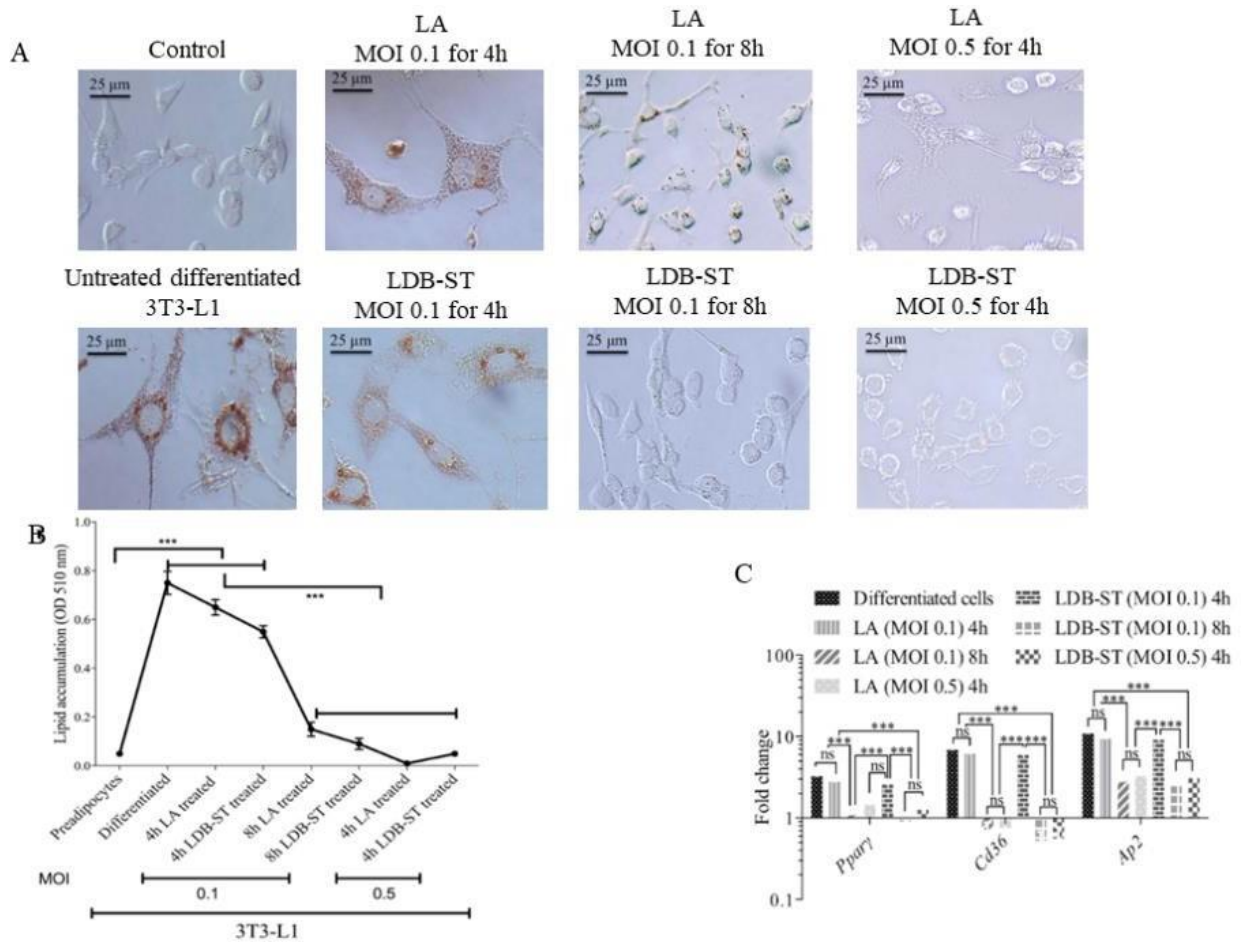


Figure 32. Effects of treatment with LA or LDB-ST on differentiated 3T3-L1 cells.

(A) Light microscopy images of ORO stained untreated undifferentiated 3T3-L1, untreated differentiated 3T3-L1 cells, and differentiated 3T3-L1 cells, following treatment with either LA at a multiplicity of infection (MOI) of 0.1 for 4 h, 0.1 for 8

h, and 0.5 for 4 h or LDB-ST at MOI of 0.1 for 4 h, 0.1 for 8 h and 0.5 for 4 h. (B) Spectrophotometric quantitation of ORO extracted from stained 3T3-L1 cells in various treatment conditions. (C) Fold change values for the expression (determined by qRT-PCR) of *Ppar γ* , *Cd36*, and *Ap2* genes in differentiated 3T3-L1 cells treated with either LA or LDB-ST at MOI of 0.1 for 4 h and 8 h and MOI of 0.5 for 4 h. We repeated each experiment 3 times. We calculated the statistical differences by 1-way ANOVA (data in B), and 2-way ANOVA (data in C) followed by Bonferroni post-test. We represented the data as mean ($n = 3$) \pm SD of the data. We denoted the significance by *($p \leq 0.05$), ** ($p \leq 0.01$), *** ($p \leq 0.001$) and **** ($p \leq 0.0001$).

5.4. Discussion and conclusion

The experiments described in this chapter found that changes in intestinal microbes are corroborated with diet-induced physiological changes. The augmentation or reduction of various microbial phyla in the immune-biased mice could be associated with observed physiological changes. Limitation of the *in vivo* study conducted in this section is that our results are mostly associative in nature and no causal conclusion can be firmly made with-out further experimentation. We need to conduct further causal studies, using germ free animal models (224) for understanding the direct influence of individual microbes. In C57BL/6, we observed that IR was significantly enhanced in SRD fed mice at four weeks which then decreased at eight weeks to almost half of its previous magnitude. At eight weeks, we correlated the changes in IR with the enhancement of the phylum Verrucomicrobia in SRD fed mice, as the microbes belonging to this phylum were previously associated with enhancing insulin sensitivity (225). In USFD fed mice, no change in IR was observed, possibly due to a higher abundance of Proteobacteria along with Verrucomicrobia. Bacteria from the

phylum Proteobacteria are known indicators of metabolic disorders. Hence we speculate the association of these microbes with the IR levels in USFD fed mice (226). In SFD fed mice, there was an association between an increased abundance of Proteobacteria, Epsilonbacteraeota, and Firmicutes with enhanced IR and adiposity (226–228). In BALB/c mice, SRD feeding resulted in the augmentation of Verrucomicrobia. We could associate the augmented Verrucomicrobia level with a milder (compared to C57BL/6) reduction in IR. At the same time, the fasting blood glucose (FBS) levels were more reduced. We could also associate the reduced visceral adiposity in USFD fed mice with a decreased relative abundance of Firmicutes. Finally, in SFD fed mice, we found the relative abundance of Firmicutes and Epsilonbacteraeota remained almost unchanged. The consistent levels of Firmicutes and Epsilonbacteraeota resulted in a gradual increase in adiposity, IR, and meta-inflammation (referred to as adipose tissue macrophage infiltration). The LDA plots, derived from the microbial abundance profile, also showed a greater alteration in the relative abundance of respective microbial phyla over time in BALB/c mice than C57BL/6. We could associate the enhanced microbial changes in BALB/c mice with the more prominent intra-strain changes in meta-inflammation and IR than observed with C57BL/6 mice. We used the serum abundance of the SCFA to identify possible associations between microbial diversity and both IR and adiposity, where we could mostly find the beneficial effects of *Akkermansia* spp.

To further support our hypothesis on the influence of microbes, specifically probiotic microorganisms, on host physiology, we evaluated the anti-adipogenic effects of LA and LDB-*Sin vitro*. We found both probiotics were associated/up taken by differentiated 3T3-L1 cells, following incubation for 1 h. The probiotics, post-treatment, were able to reduce cellular lipid storage and expression of crucial

adipogenesis marker genes, significantly after 8 h at a lower dose (0.1 MOI) and after 4 h at a higher dose (0.5 MOI). The marker gene *Ppar γ* codes for a transcription factor that is upregulated and essential for the differentiation of mammalian adipocytes (229). *Ap2* or *Fabp4* genes encode the fatty acid transporter FABP4, necessary for transporting fatty acids in adipocytes (162). *Cd36* encodes for CD36 protein, a fatty acid translocase, expressed widely during abundant fatty acid influx inside adipocytes (230). The probable cause for the probiotic mediated reduced adiposity could mostly be via certain bacterial metabolites (231) and to a lesser extent, via bacterial structural components, as previous reports from our lab using both LA and LDB-ST has proven that heat-killing of these probiotics exert negligible beneficial effects (154). Limitation of the *in vitro* study also exists as we have not identified specific metabolites responsible for the anti-adipogenic effects of the probiotics. Also, as we do not know whether the associated/up taken probiotics replicates on/inside the mammalian cells like some other bacteria (221), we cannot surely say whether the observed effects were entirely due to the associated/up taken probiotics or their enhanced number after association/incorporation on/inside the adipocytes.

Because at the lower doses, the survival of the adipocytes was not compromised, we could say that the probiotics used in our study can be an effective intervention strategy for individuals suffering from lipid metabolism-associated disorders. We have schematically deduced the relationship between diet-induced altered gut microbes with murine physiological alterations and the *in vitro* anti-adipogenic effects of LA and LDB-ST in figure 33. We have considered the adipogenic, insulin resistance, and meta-inflammation promoting properties of Firmicutes (227), Proteobacteria (232) and Epsilonbacteraeota (228). Alternatively, we considered the insulin sensitivity

enabling and anti-adipogenic properties of verrucobionia (225) and Bacteroidetes (227). *In vitro*, we have represented the anti-adipogenic effects of lactic acid bacteria.

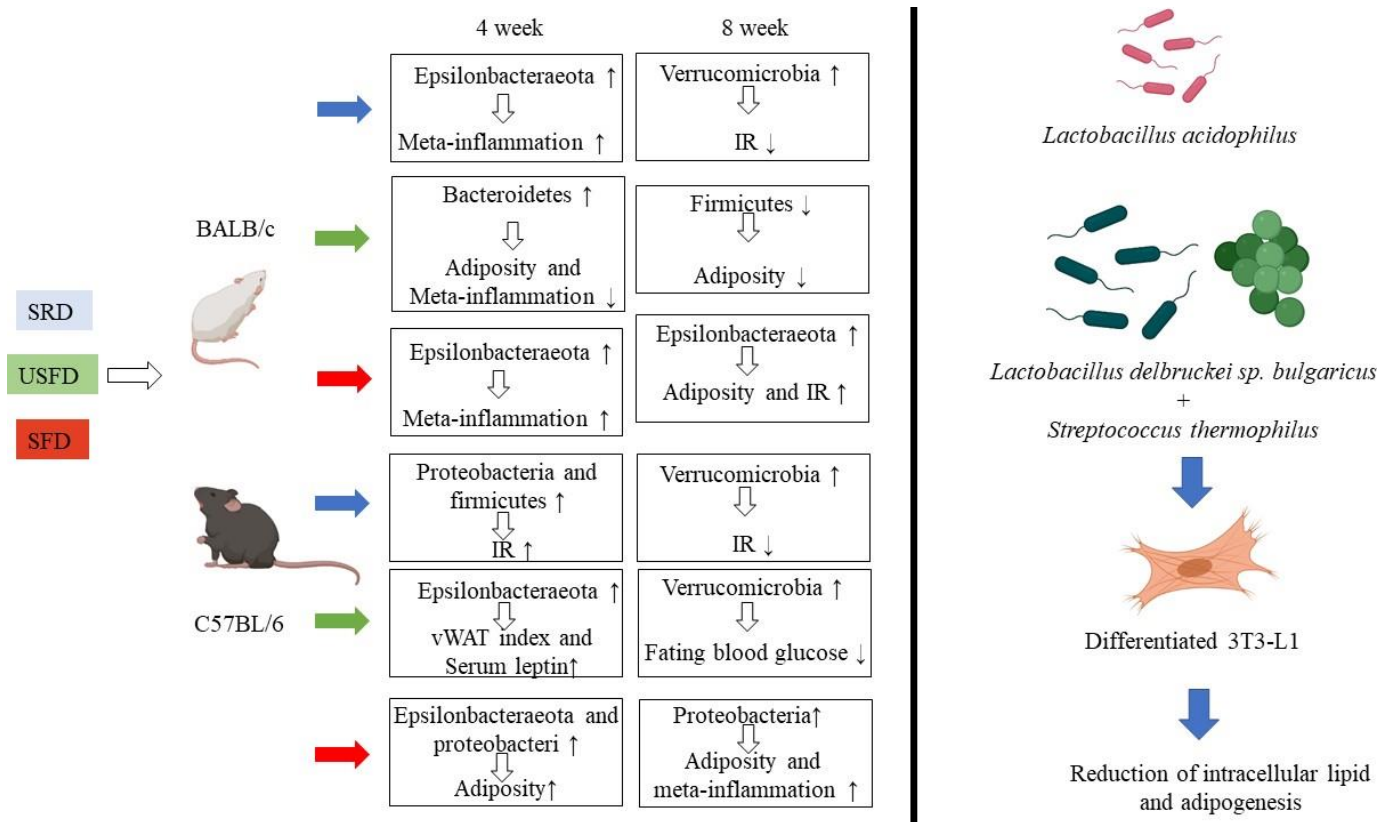


Figure 33. Schematical representation of the diet-induced changes in intestinal microbes and their relation with host physiology. (Icon courtesy <https://biorender.com/>).

References

1. D. Chapelot, K. Charlot, Physiology of energy homeostasis: Models, actors, challenges and the glucoadipostatic loop. *Metabolism* **92**, 11–25 (2019).
2. J. Korner, S. C. Woods, K. A. Woodworth, Regulation of Energy Homeostasis and Health Consequences in Obesity. *Am. J. Med.* **122**, I-CO4 (2009).
3. A. Vidal-Puig, “The Metabolic Syndrome and its Complex Pathophysiology” in *A Systems Biology Approach to Study Metabolic Syndrome*, M. Orešič, A. Vidal-Puig, Eds. (Springer International Publishing, 2014), pp. 3–16.
4. M. CLAUSS, J. HUMMEL, The digestive performance of mammalian herbivores: why big may not be that much better. *Mamm. Rev.* **35**, 174–187 (2005).
5. R. E. Ley, *et al.*, Evolution of Mammals and Their Gut Microbes. *Science* (80-.). **320**, 1647–1651 (2008).
6. D. W. Cockburn, N. M. Koropatkin, Polysaccharide Degradation by the Intestinal Microbiota and Its Influence on Human Health and Disease. *J. Mol. Biol.* **428**, 3230–3252 (2016).
7. D. J. Chivers, C. M. Hladik, Morphology of the gastrointestinal tract in primates: Comparisons with other mammals in relation to diet. *J. Morphol.* **166**, 337–386 (1980).
8. S. A. Price, S. S. B. Hopkins, The macroevolutionary relationship between diet and body mass across mammals. *Biol. J. Linn. Soc.* **115**, 173–184 (2015).
9. K. V. Kardong, *Vertebrate Comparative Anatomy Function, Evolution* (2012).
10. D. MILLER, R. K. CRANE, The Digestion of Carbohydrates in the Small

- Intestine. *Am. J. Clin. Nutr.* **12**, 220–227 (1963).
11. H. G. HERS, “Glycogen Storage Disease” in (1964), pp. 1–44.
 12. H. Liu, *et al.*, Health beneficial effects of resistant starch on diabetes and obesity via regulation of gut microbiota: a review. *Food Funct.* **11**, 5749–5767 (2020).
 13. R. A. YOUNG, Fat, Energy and Mammalian Survival. *Am. Zool.* **16**, 699–710 (1976).
 14. P. Björntorp, Body fat distribution, insulin resistance, and metabolic diseases. *Nutrition* **13**, 795–803 (1997).
 15. L. H. KULLER, Dietary Fat and Chronic Diseases. *J. Am. Diet. Assoc.* **97**, S9–S15 (1997).
 16. J. A. Alegría-Torres, A. Baccarelli, V. Bollati, Epigenetics and lifestyle. *Epigenomics* **3**, 267–277 (2011).
 17. M. Wennberg, P. E. Gustafsson, P. Wennberg, And, A. Hammarström, Irregular eating of meals in adolescence and the metabolic syndrome in adulthood: results from a 27-year prospective cohort. *Public Health Nutr.* **Volume 19**, 667–673.
 18. T. A. M. K. S. Schwartzkopf-Genswein, K. A. Beauchemin, D. J. Gibb, D. H. Crews, Jr., D. D. Hickman, M. Streeter, Effect of bunk management on feeding behavior, ruminal acidosis and performance of feedlot cattle: A review. *J. Anim. Sci.* **81**.
 19. S. Sharma, M. Kavuru, Sleep and Metabolism: An Overview. *Int. J. Endocrinol.* **2010**, 1–12 (2010).

20. O. Mesarwi, J. Polak, J. Jun, V. Y. Polotsky, Sleep Disorders and the Development of Insulin Resistance and Obesity. *Endocrinol. Metab. Clin. North Am.* **42**, 617–634 (2013).
21. R. Wolk, V. K. Somers, Sleep and the metabolic syndrome. *Exp. Physiol.* **92**, 67–78 (2007).
22. J. A. Goldstein, S. Balter, M. Cowley, J. Hodgson, L. W. Klein, Occupational hazards of interventional cardiologists: Prevalence of orthopedic health problems in contemporary practice. *Catheter. Cardiovasc. Interv.* **63**, 407–411 (2004).
23. G. Giulio Marchesini, Lifestyle modification in the management of the metabolic syndrome: achievements and challenges. *Diabetes, Metab. Syndr. Obes. Targets Ther.*, 373 (2010).
24. W. Kopp, How Western Diet And Lifestyle Drive The Pandemic Of Obesity And Civilization Diseases. *Diabetes, Metab. Syndr. Obes. Targets Ther.* **Volume 12**, 2221–2236 (2019).
25. T. Chandola, E. Brunner, M. Marmot, Chronic stress at work and the metabolic syndrome: prospective study. *BMJ* **332**, 521–525 (2006).
26. S. Garbarino, N. Magnavita, Work Stress and Metabolic Syndrome in Police Officers. A Prospective Study. *PLoS One* **10**, e0144318 (2015).
27. W. Kuo, *et al.*, The association between psychological stress and metabolic syndrome: A systematic review and meta-analysis. *Obes. Rev.* **20**, 1651–1664 (2019).
28. E. A. Lambert, G. W. Lambert, Stress and Its Role in Sympathetic Nervous

- System Activation in Hypertension and the Metabolic Syndrome. *Curr. Hypertens. Rep.* **13**, 244–248 (2011).
29. K. Widhalm, Genetic background of obesity. *Pediatr. Res.* **89**, 1584–1585 (2021).
 30. D. Z. Pan, *et al.*, Integration of human adipocyte chromosomal interactions with adipose gene expression prioritizes obesity-related genes from GWAS. *Nat. Commun.* **9**, 1512 (2018).
 31. S. Ghosh, C. Bouchard, Convergence between biological, behavioural and genetic determinants of obesity. *Nat. Rev. Genet.* **18**, 731–748 (2017).
 32. L. E. Wagar, R. M. DiFazio, M. M. Davis, Advanced model systems and tools for basic and translational human immunology. *Genome Med.* **10**, 73 (2018).
 33. N. Giridharan, Glucose & energy homeostasis: Lessons from animal studies. *Indian J. Med. Res.* **148**, 659 (2018).
 34. S. K. Wong, K.-Y. Chin, F. H. Suhaimi, A. Fairus, S. Ima-Nirwana, Animal models of metabolic syndrome: a review. *Nutr. Metab. (Lond)*. **13**, 65 (2016).
 35. T. Hattori, *et al.*, Characterization of a new animal model of metabolic syndrome: the DahlS.Z-Leprfa/Leprfa rat. *Nutr. Diabetes* **1**, e1–e1 (2011).
 36. A. Miesel, *et al.*, Overfeeding-Induced Obesity in Spontaneously Hypertensive Rats: An Animal Model of the Human Metabolic Syndrome. *Ann. Nutr. Metab.* **56**, 127–142 (2010).
 37. A. Aleixandre de Artiñano, M. Miguel Castro, Experimental rat models to study the metabolic syndrome. *Br. J. Nutr.* **102**, 1246–1253 (2009).

38. S. K. Panchal, L. Brown, Rodent Models for Metabolic Syndrome Research. *J. Biomed. Biotechnol.* **2011**, 1–14 (2011).
39. A. J. Kennedy, K. L. J. Ellacott, V. L. King, A. H. Hasty, Mouse models of the metabolic syndrome. *Dis. Model. Mech.* **3**, 156–166 (2010).
40. H. Watanabe, K. Numata, T. Ito, K. Takagi, A. Matsukawa, INNATE IMMUNE RESPONSE IN TH1- AND TH2-DOMINANT MOUSE STRAINS. *Shock* **22**, 460–466 (2004).
41. J. Salazar-León, *et al.*, Nlrp1b1 negatively modulates obesity-induced inflammation by promoting IL-18 production. *Sci. Rep.* **9**, 13815 (2019).
42. M. K. Montgomery, *et al.*, Mouse strain-dependent variation in obesity and glucose homeostasis in response to high-fat feeding. *Diabetologia* **56**, 1129–1139 (2013).
43. K. Burlikowska, *et al.*, Comparison of Metabolomic Profiles of Organs in Mice of Different Strains Based on SPME-LC-HRMS. *Metabolites* **10**, 255 (2020).
44. Y. Qian, M. Chen, H. Forsberg, R. Diaz Heijtz, Genetic variation in dopamine-related gene expression influences motor skill learning in mice. *Genes, Brain Behav.* **12**, 604–614 (2013).
45. W. Schwartz, P. Zimmerman, Circadian timekeeping in BALB/c and C57BL/6 inbred mouse strains. *J. Neurosci.* **10**, 3685–3694 (1990).
46. S. B. Park, *et al.*, Development of in vitro three-dimensional co-culture system for metabolic syndrome therapeutic agents. *Diabetes, Obes. Metab.* **21**, 1146–1157 (2019).
47. D. Guha, R. Mukherjee, P. Aich, Macrophage plays important role in cortisol

- and serotonin induced adipogenesis in vitro. *Vitr. Cell. Dev. Biol. - Anim.* **56**, 511–521 (2020).
48. R. Gebhardt, *et al.*, New Hepatocyte In Vitro Systems for Drug Metabolism: Metabolic Capacity and Recommendations for Application in Basic Research and Drug Development, Standard Operation Procedures. *Drug Metab. Rev.* **35**, 145–213 (2003).
 49. R. L. Perlman, Mouse Models of Human Disease: An Evolutionary Perspective. *Evol. Med. Public Heal.*, eow014 (2016).
 50. L. E. Pappas, T. R. Nagy, The translation of age-related body composition findings from rodents to humans. *Eur. J. Clin. Nutr.* **73**, 172–178 (2019).
 51. E. R. De Leon, *et al.*, Age-Dependent Protection of Insulin Secretion in Diet Induced Obese Mice. *Sci. Rep.* **8**, 17814 (2018).
 52. C. W. Chia, J. M. Egan, L. Ferrucci, Age-Related Changes in Glucose Metabolism, Hyperglycemia, and Cardiovascular Risk. *Circ. Res.* **123**, 886–904 (2018).
 53. A. Lomba, *et al.*, Obesity induced by a pair-fed high fat sucrose diet: methylation and expression pattern of genes related to energy homeostasis. *Lipids Health Dis.* **9**, 60 (2010).
 54. S. A. Gibson, Are High-Fat, High-Sugar Foods and Diets Conducive to Obesity? *Int. J. Food Sci. Nutr.* **47**, 405–415 (1996).
 55. C. R. Hancock, *et al.*, High-fat diets cause insulin resistance despite an increase in muscle mitochondria. *Proc. Natl. Acad. Sci.* **105**, 7815–7820 (2008).
 56. X. Xu, Y. Hua, N. Sreejayan, Y. Zhang, J. Ren, Akt2 knockout preserves

- cardiac function in high-fat diet-induced obesity by rescuing cardiac autophagosome maturation. *J. Mol. Cell Biol.* **5**, 61–63 (2013).
57. M. von Scheidt, *et al.*, Applications and Limitations of Mouse Models for Understanding Human Atherosclerosis. *Cell Metab.* **25**, 248–261 (2017).
 58. F. T. Yazdi, S. M. Clee, D. Meyre, Obesity genetics in mouse and human: back and forth, and back again. *PeerJ* **3**, e856 (2015).
 59. J. C. Russell, S. D. Proctor, Small animal models of cardiovascular disease: tools for the study of the roles of metabolic syndrome, dyslipidemia, and atherosclerosis. *Cardiovasc. Pathol.* **15**, 318–330 (2006).
 60. A. G. Dulloo, N. Mensi, J. Seydoux, L. Girardier, Differential effects of high-fat diets varying in fatty acid composition on the efficiency of lean and fat tissue deposition during weight recovery after low food intake. *Metabolism* **44**, 273–279 (1995).
 61. E. H. Ahrens, D. H. Blankenhorn, T. T. Tsaltas, Effect on Human Serum Lipids of Substituting Plant for Animal Fat in Diet. *Exp. Biol. Med.* **86**, 872–878 (1954).
 62. M. SANZ, Higher lipid accumulation in broilers fed on saturated fats than in those fed on unsaturated fats. *Br. Poult. Sci.* **40**, 95–101 (1999).
 63. C. L. Gentile, *et al.*, Resistant starch and protein intake enhances fat oxidation and feelings of fullness in lean and overweight/obese women. *Nutr. J.* **14**, 113 (2015).
 64. J. Zhang, *et al.*, Intestinal microbiota are involved in the immunomodulatory activities of longan polysaccharide. *Mol. Nutr. Food Res.* **61**, 1700466 (2017).

65. H. J. Flint, K. P. Scott, S. H. Duncan, P. Louis, E. Forano, Microbial degradation of complex carbohydrates in the gut. *Gut Microbes* **3**, 289–306 (2012).
66. Y. Zhao, *et al.*, GPR43 mediates microbiota metabolite SCFA regulation of antimicrobial peptide expression in intestinal epithelial cells via activation of mTOR and STAT3. *Mucosal Immunol.* **11**, 752–762 (2018).
67. C. Martin-Gallausiaux, L. Marinelli, H. M. Blottière, P. Larraufie, N. Lapaque, SCFA: mechanisms and functional importance in the gut. *Proc. Nutr. Soc.* **80**, 37–49 (2021).
68. M. Simonson, Y. Boirie, C. Guillet, Protein, amino acids and obesity treatment. *Rev. Endocr. Metab. Disord.* **21**, 341–353 (2020).
69. S. M. Hofmann, *et al.*, Adipocyte LDL receptor–related protein–1 expression modulates postprandial lipid transport and glucose homeostasis in mice. *J. Clin. Invest.* **117**, 3271–3282 (2007).
70. A. Rodríguez, Novel Molecular Aspects of Ghrelin and Leptin in the Control of Adipobiology and the Cardiovascular System. *Obes. Facts* **7**, 82–95 (2014).
71. S. Dey, N. Murmu, M. Bose, S. Ghosh, B. Giri, Obesity and chronic leptin resistance foster insulin resistance: An analytical overview. *BLDE Univ. J. Heal. Sci.* **6**, 7 (2021).
72. K. W. Williams, M. M. Scott, J. K. Elmquist, From observation to experimentation: leptin action in the mediobasal hypothalamus. *Am. J. Clin. Nutr.* **89**, 985S–990S (2009).
73. L. S. Morris, V. Voon, L. Leggio, Stress, Motivation, and the Gut-Brain Axis:

- A Focus on the Ghrelin System and Alcohol Use Disorder. *Alcohol. Clin. Exp. Res.* **42**, 1378–1389 (2018).
74. O. Al Massadi, M. López, M. Tschöp, C. Diéguez, R. Nogueiras, Current Understanding of the Hypothalamic Ghrelin Pathways Inducing Appetite and Adiposity. *Trends Neurosci.* **40**, 167–180 (2017).
75. T. W. K. Ng, G. F. Watts, M. S. Farvid, D. C. Chan, P. H. R. Barrett, Adipocytokines and VLDL Metabolism: Independent Regulatory Effects of Adiponectin, Insulin Resistance, and Fat Compartments on VLDL Apolipoprotein B-100 Kinetics? *Diabetes* **54**, 795–802 (2005).
76. M. Bulló, J. Salas-Salvadó, P. García-Lorda, Adiponectin Expression and Adipose Tissue Lipolytic Activity in Lean and Obese Women. *Obes. Surg.* **15**, 382–386 (2005).
77. A. R. Anderson, B. J. Fowers, Lifestyle behaviors, psychological distress, and well-being: A daily diary study. *Soc. Sci. Med.* **263**, 113263 (2020).
78. S. Priyadarshini, B. Pradhan, P. Griebel, P. Aich, Cortisol regulates immune and metabolic processes in murine adipocytes and macrophages through HTR2c and HTR5a serotonin receptors. *Eur. J. Cell Biol.* **97**, 483–492 (2018).
79. T. FIELD, M. HERNANDEZ-REIF, M. DIEGO, S. SCHANBERG, C. KUHN, CORTISOL DECREASES AND SEROTONIN AND DOPAMINE INCREASE FOLLOWING MASSAGE THERAPY. *Int. J. Neurosci.* **115**, 1397–1413 (2005).
80. Q. Yan, “Obesity, Stress, Inflammation, and Psychoneuroimmunology” in *Psychoneuroimmunology: Systems Biology Approaches to Mind-Body*

Medicine, (Springer International Publishing, 2016), pp. 65–74.

81. H. Shapiro, A. Lutaty, A. Ariel, Macrophages, Meta-Inflammation, and Immuno-Metabolism. *Sci. World J.* **11**, 2509–2529 (2011).
82. E. Thursby, N. Juge, Introduction to the human gut microbiota. *Biochem. J.* **474**, 1823–1836 (2017).
83. P. D. Cani, Human gut microbiome: hopes, threats and promises. *Gut* **67**, 1716–1725 (2018).
84. R. Sender, S. Fuchs, R. Milo, Are We Really Vastly Outnumbered? Revisiting the Ratio of Bacterial to Host Cells in Humans. *Cell* **164**, 337–340 (2016).
85. M. Priyadarshini, K. U. Kotlo, P. K. Dudeja, B. T. Layden, “Role of Short Chain Fatty Acid Receptors in Intestinal Physiology and Pathophysiology” in *Comprehensive Physiology*, (Wiley, 2018), pp. 1091–1115.
86. D. Parada Venegas, *et al.*, Short Chain Fatty Acids (SCFAs)-Mediated Gut Epithelial and Immune Regulation and Its Relevance for Inflammatory Bowel Diseases. *Front. Immunol.* **10** (2019).
87. J. Tsiaoussis, *et al.*, Effects of single and combined toxic exposures on the gut microbiome: Current knowledge and future directions. *Toxicol. Lett.* **312**, 72–97 (2019).
88. P. Ray, U. Pandey, D. Das, P. Aich, Vancomycin-Induced Changes in Host Immunity and Behavior: Comparative Genomic and Metagenomic Analysis in C57BL/6 and BALB/c Mice. *Dig. Dis. Sci.* (2021) <https://doi.org/10.1007/s10620-020-06729-x>.
89. A. K. Naik, *et al.*, *Lactobacillus rhamnosus* GG reverses mortality of neonatal

- mice against Salmonella challenge. *Toxicol. Res. (Camb)*. **8**, 361–372 (2019).
90. B. Pradhan, *et al.*, Probiotics *L. acidophilus* and *B. clausii* Modulate Gut Microbiota in Th1- and Th2-Biased Mice to Ameliorate Salmonella Typhimurium-Induced Diarrhea. *Probiotics Antimicrob. Proteins* **11**, 887–904 (2019).
91. J. Wu, *et al.*, Dietary nutrients shape gut microbes and intestinal mucosa via epigenetic modifications. *Crit. Rev. Food Sci. Nutr.*, 1–15 (2020).
92. X. Du, *et al.*, Microbial Community and Short-Chain Fatty Acid Mapping in the Intestinal Tract of Quail. *Animals* **10**, 1006 (2020).
93. I. Rowland, *et al.*, Gut microbiota functions: metabolism of nutrients and other food components. *Eur. J. Nutr.* **57**, 1–24 (2018).
94. M. S. Riaz Rajoka, *et al.*, Interaction between diet composition and gut microbiota and its impact on gastrointestinal tract health. *Food Sci. Hum. Wellness* **6**, 121–130 (2017).
95. B. S. Ramakrishna, Role of the gut microbiota in human nutrition and metabolism. *J. Gastroenterol. Hepatol.* **28**, 9–17 (2013).
96. Hernández, Canfora, Jocken, Blaak, The Short-Chain Fatty Acid Acetate in Body Weight Control and Insulin Sensitivity. *Nutrients* **11**, 1943 (2019).
97. S. Fukuda, *et al.*, Bifidobacteria can protect from enteropathogenic infection through production of acetate. *Nature* **469**, 543–547 (2011).
98. R. B. Canani, Potential beneficial effects of butyrate in intestinal and extraintestinal diseases. *World J. Gastroenterol.* **17**, 1519 (2011).

99. E. S. Chambers, *et al.*, Effects of targeted delivery of propionate to the human colon on appetite regulation, body weight maintenance and adiposity in overweight adults. *Gut* **64**, 1744–1754 (2015).
100. E. C. Deehan, *et al.*, Precision Microbiome Modulation with Discrete Dietary Fiber Structures Directs Short-Chain Fatty Acid Production. *Cell Host Microbe* **27**, 389-404.e6 (2020).
101. S. Macfarlane, G. T. Macfarlane, Regulation of short-chain fatty acid production. *Proc. Nutr. Soc.* **62**, 67–72 (2003).
102. J. H. Cummings, E. W. Pomare, W. J. Branch, C. P. Naylor, G. T. Macfarlane, Short chain fatty acids in human large intestine, portal, hepatic and venous blood. *Gut* **28**, 1221–1227 (1987).
103. G. den Besten, *et al.*, The role of short-chain fatty acids in the interplay between diet, gut microbiota, and host energy metabolism. *J. Lipid Res.* **54**, 2325–2340 (2013).
104. S. Zhang, X. Zeng, M. Ren, X. Mao, S. Qiao, Novel metabolic and physiological functions of branched chain amino acids: a review. *J. Anim. Sci. Biotechnol.* **8**, 10 (2017).
105. A. Agus, J. Planchais, H. Sokol, Gut Microbiota Regulation of Tryptophan Metabolism in Health and Disease. *Cell Host Microbe* **23**, 716–724 (2018).
106. I. Vujkovic-Cvijin, *et al.*, Dysbiosis of the Gut Microbiota Is Associated with HIV Disease Progression and Tryptophan Catabolism. *Sci. Transl. Med.* **5**, 193ra91-193ra91 (2013).
107. P. J. Kennedy, J. F. Cryan, T. G. Dinan, G. Clarke, Kynurenine pathway

- metabolism and the microbiota-gut-brain axis. *Neuropharmacology* **112**, 399–412 (2017).
108. A. S. Devlin, *et al.*, Modulation of a Circulating Uremic Solute via Rational Genetic Manipulation of the Gut Microbiota. *Cell Host Microbe* **20**, 709–715 (2016).
109. T. Bansal, R. C. Alaniz, T. K. Wood, A. Jayaraman, The bacterial signal indole increases epithelial-cell tight-junction resistance and attenuates indicators of inflammation. *Proc. Natl. Acad. Sci.* **107**, 228–233 (2010).
110. J. M. Yano, *et al.*, Indigenous Bacteria from the Gut Microbiota Regulate Host Serotonin Biosynthesis. *Cell* **161**, 264–276 (2015).
111. T. C. Fung, *et al.*, Intestinal serotonin and fluoxetine exposure modulate bacterial colonization in the gut. *Nat. Microbiol.* **4**, 2064–2073 (2019).
112. J. Gao, *et al.*, Impact of the Gut Microbiota on Intestinal Immunity Mediated by Tryptophan Metabolism. *Front. Cell. Infect. Microbiol.* **8** (2018).
113. W. Barcik, M. Wawrzyniak, C. A. Akdis, L. O’Mahony, Immune regulation by histamine and histamine-secreting bacteria. *Curr. Opin. Immunol.* **48**, 108–113 (2017).
114. A. Deiteren, J. G. De Man, P. A. Pelckmans, B. Y. De Winter, Histamine H₄ receptors in the gastrointestinal tract. *Br. J. Pharmacol.* **172**, 1165–1178 (2015).
115. L. J. Peters, J. P. Kovacic, Histamine: metabolism, physiology, and pathophysiology with applications in veterinary medicine. *J. Vet. Emerg. Crit. Care* **19**, 311–328 (2009).

116. V. Maini Rekdal, E. N. Bess, J. E. Bisanz, P. J. Turnbaugh, E. P. Balskus, Discovery and inhibition of an interspecies gut bacterial pathway for Levodopa metabolism. *Science* (80-.). **364**, eaau6323 (2019).
117. S. P. van Kessel, *et al.*, Gut bacterial tyrosine decarboxylases restrict levels of levodopa in the treatment of Parkinson's disease. *Nat. Commun.* **10**, 310 (2019).
118. M. Olle Lindvall, PhD, MD,"? Anders Bjorklund, PhD, MD," and Gunnar Skagerberg, Dopamine-Containing Neurons in the Spinal Cord: Anatomy and Some Functional Aspects. *Neurol. Prog.* <https://doi.org/10.1111/j.1365-2044.1959.tb02431.x>.
119. J. K. Nicholson, E. Holmes, I. D. Wilson, Gut microorganisms, mammalian metabolism and personalized health care. *Nat. Rev. Microbiol.* **3**, 431–438 (2005).
120. X. Cui, L. Bao, X. Wang, C. Chen, The Nano–Intestine Interaction: Understanding the Location-Oriented Effects of Engineered Nanomaterials in the Intestine. *Small* **16**, 1907665 (2020).
121. S. Bikel, *et al.*, Combining metagenomics, metatranscriptomics and viromics to explore novel microbial interactions: towards a systems-level understanding of human microbiome. *Comput. Struct. Biotechnol. J.* **13**, 390–401 (2015).
122. Y. Yan, L. H. Nguyen, E. A. Franzosa, C. Huttenhower, Strain-level epidemiology of microbial communities and the human microbiome. *Genome Med.* **12**, 71 (2020).
123. M. X. Chen, S.-Y. Wang, C.-H. Kuo, I.-L. Tsai, Metabolome analysis for

- investigating host-gut microbiota interactions. *J. Formos. Med. Assoc.* **118**, S10–S22 (2019).
124. S. Chowdhury, S. S. Fong, Computational Modeling of the Human Microbiome. *Microorganisms* **8**, 197 (2020).
 125. J.-A. Kim, *et al.*, Investigating the probiotic characteristics of four microbial strains with potential application in feed industry. *PLoS One* **14**, e0218922 (2019).
 126. S. Fijan, Microorganisms with Claimed Probiotic Properties: An Overview of Recent Literature. *Int. J. Environ. Res. Public Health* **11**, 4745–4767 (2014).
 127. D. Davani-Davari, *et al.*, Prebiotics: Definition, Types, Sources, Mechanisms, and Clinical Applications. *Foods* **8**, 92 (2019).
 128. K. R. Pandey, S. R. Naik, B. V. Vakil, Probiotics, prebiotics and synbiotics- a review. *J. Food Sci. Technol.* **52**, 7577–7587 (2015).
 129. Wegh, Geerlings, Knol, Roeselers, Belzer, Postbiotics and Their Potential Applications in Early Life Nutrition and Beyond. *Int. J. Mol. Sci.* **20**, 4673 (2019).
 130. R. Mukherjee, P. Aich, The starch-rich diet causes lipidemia while the fat-rich diet induces visceral adiposity, meta-inflammation, and insulin resistance differentially in immune biased mouse strains. *Food Biosci.* **42**, 101136 (2021).
 131. S. C. Adams, *et al.*, Effects of Pelleting, Irradiation, and Autoclaving of Rodent Feed on MPV and MNV Infectivity. *J. Am. Assoc. Lab. Anim. Sci.* **58**, 542–550 (2019).
 132. Biorad, Bradford assay protocol.

133. Raybiotech, Mouse Leptin ELISA kit.
134. RAYbiotech, Mouse Adiponectin ELISA kit.
135. Raybiotech, Mouse serum Insulin ELISA kit.
136. Raybiotech, Mouse Ghrelin ELISA kit.
137. Sigma, Serum triglyceride and glycerol determination kit.
138. Sigma, Serum free fatty acid quantification kit.
139. H. Li, *et al.*, Long term liver specific glucokinase gene defect induced diabetic cardiomyopathy by up regulating NADPH oxidase and down regulating insulin receptor and p-AMPK. *Cardiovasc. Diabetol.* **13**, 24 (2014).
140. R. Berry, *et al.*, “Imaging of Adipose Tissue” in (2014), pp. 47–73.
141. H. Kato, *et al.*, Reversible Adipose Tissue Enlargement Induced by External Tissue Suspension: Possible Contribution of Basic Fibroblast Growth Factor in the Preservation of Enlarged Tissue. *Tissue Eng. Part A* **16**, 2029–2040 (2010).
142. QIAGEN, RNeasy Lipid Tissue Mini Kit.
143. Agilent, Agilent cDNA synthesis kit.
144. Prmega, Promega qPCR master mix.
145. T. Høverstad, T. Midtvedt, Short-Chain Fatty Acids in Germfree Mice and Rats. *J. Nutr.* **116**, 1772–1776 (1986).
146. G. den Besten, *et al.*, The Short-Chain Fatty Acid Uptake Fluxes by Mice on a Guar Gum Supplemented Diet Associate with Amelioration of Major Biomarkers of the Metabolic Syndrome. *PLoS One* **9**, e107392 (2014).

147. G. den Besten, *et al.*, The role of short-chain fatty acids in the interplay between diet, gut microbiota, and host energy metabolism. *J. Lipid Res.* **54**, 2325–2340 (2013).
148. QIAGEN, QIAamp Fast DNA Stool Mini Kit.
149. Illumina, Quality Scores for Next-Generation Sequencing.
150. R. C. Edgar, B. J. Haas, J. C. Clemente, C. Quince, R. Knight, UCHIME improves sensitivity and speed of chimera detection. *Bioinformatics* **27**, 2194–2200 (2011).
151. V. D’Argenio, G. Casaburi, V. Precone, F. Salvatore, Comparative Metagenomic Analysis of Human Gut Microbiome Composition Using Two Different Bioinformatic Pipelines. *Biomed Res. Int.* **2014**, 1–10 (2014).
152. Z. Chen, Z. Yang, X. Yuan, X. Zhang, P. Hao, scSensitiveGeneDefine: sensitive gene detection in single-cell RNA sequencing data by Shannon entropy. *BMC Bioinformatics* **22**, 211 (2021).
153. H.-H. Xiao, *et al.*, Prenylated Isoflavonoids-Rich Extract of Erythrinae Cortex Exerted Bone Protective Effects by Modulating Gut Microbial Compositions and Metabolites in Ovariectomized Rats. *Nutrients* **13**, 2943 (2021).
154. D. Guha, *et al.*, A probiotic formulation containing *Lactobacillus bulgaricus* DWT1 inhibits tumor growth by activating pro-inflammatory responses in macrophages. *J. Funct. Foods* **56**, 232–245 (2019).
155. S. Priyadarshini, B. Pradhan, P. Aich, Role of murine macrophage in temporal regulation of cortisol and serotonin induced adipogenesis in pre-adipocytes when grown together. *Biol. Open* (2018) <https://doi.org/10.1242/bio.034629>.

156. D. Guha, R. Mukherjee, P. Aich, Effects of two potential probiotic Lactobacillus bacteria on adipogenesis in vitro. *Life Sci.* **278**, 119538 (2021).
157. C. L. Bush, *et al.*, Toward the Definition of Personalized Nutrition: A Proposal by The American Nutrition Association. *J. Am. Coll. Nutr.* **39**, 5–15 (2020).
158. J. L. Sievenpiper, Low-carbohydrate diets and cardiometabolic health: the importance of carbohydrate quality over quantity. *Nutr. Rev.* **78**, 69–77 (2020).
159. H. Cena, P. C. Calder, Defining a Healthy Diet: Evidence for the Role of Contemporary Dietary Patterns in Health and Disease. *Nutrients* **12**, 334 (2020).
160. J. H. Stern, J. M. Rutkowski, P. E. Scherer, Adiponectin, Leptin, and Fatty Acids in the Maintenance of Metabolic Homeostasis through Adipose Tissue Crosstalk. *Cell Metab.* **23**, 770–784 (2016).
161. S. Q. Arain, F. N. Talpur, N. A. Channa, M. S. Ali, H. I. Afridi, Serum lipid profile as a marker of liver impairment in hepatitis B Cirrhosis patients. *Lipids Health Dis.* **16**, 51 (2017).
162. M. Furuhashi, S. Saitoh, K. Shimamoto, T. Miura, Fatty Acid-Binding Protein 4 (FABP4): Pathophysiological Insights and Potent Clinical Biomarker of Metabolic and Cardiovascular Diseases. *Clin. Med. Insights Cardiol.* **8s3**, CMC.S17067 (2014).
163. L.-Y. Wang, *et al.*, Alteration of fatty acid metabolism in the liver, adipose tissue, and testis of male mice conceived through assisted reproductive technologies: fatty acid metabolism in ART mice. *Lipids Health Dis.* **12**, 5 (2013).

164. J. M. Fernández-Real, *et al.*, Study of caveolin-1 gene expression in whole adipose tissue and its subfractions and during differentiation of human adipocytes. *Nutr. Metab. (Lond)*. **7**, 20 (2010).
165. P. Ferre, The Biology of Peroxisome Proliferator-Activated Receptors: Relationship With Lipid Metabolism and Insulin Sensitivity. *Diabetes* **53**, S43–S50 (2004).
166. C. Thauvin-Robinet, *et al.*, PIK3R1 Mutations Cause Syndromic Insulin Resistance with Lipoatrophy. *Am. J. Hum. Genet.* **93**, 141–149 (2013).
167. Y. S. Oh, *et al.*, Increase of Calcium Sensing Receptor Expression Is Related to Compensatory Insulin Secretion during Aging in Mice. *PLoS One* **11**, e0159689 (2016).
168. A. Guilherme, J. V. Virbasius, V. Puri, M. P. Czech, Adipocyte dysfunctions linking obesity to insulin resistance and type 2 diabetes. *Nat. Rev. Mol. Cell Biol.* **9**, 367–377 (2008).
169. M. El Hafidi, *et al.*, Glycine intake decreases plasma free fatty acids, adipose cell size, and blood pressure in sucrose-fed rats. *Am. J. Physiol. Integr. Comp. Physiol.* **287**, R1387–R1393 (2004).
170. N. Alvarado-Vásquez, *et al.*, Effect of glycine in streptozotocin-induced diabetic rats. *Comp. Biochem. Physiol. Part C Toxicol. Pharmacol.* **134**, 521–527 (2003).
171. L. Kazak, *et al.*, Ablation of adipocyte creatine transport impairs thermogenesis and causes diet-induced obesity. *Nat. Metab.* **1**, 360–370 (2019).
172. K. S. Kim, *et al.*, Anti-obesity effect of taurine through inhibition of

- adipogenesis in white fat tissue but not in brown fat tissue in a high-fat diet-induced obese mouse model. *Amino Acids* **51**, 245–254 (2019).
173. X. Wang, *et al.*, Glucose oxidase induces insulin resistance via influencing multiple targets in vitro and in vivo: The central role of oxidative stress. *Biochimie* **94**, 1705–1717 (2012).
174. K. S. Kim, *et al.*, Taurine ameliorates hyperglycemia and dyslipidemia by reducing insulin resistance and leptin level in Otsuka Long-Evans Tokushima fatty (OLETF) rats with long-term diabetes. *Exp. Mol. Med.* **44**, 665 (2012).
175. M. Digirolamo, F. D. Newby, J. Lovejoy, Lactate production in adipose tissue; a regulated function with extra-adipose implications. *FASEB J.* **6**, 2405–2412 (1992).
176. X. Guo, *et al.*, Glycolysis in the control of blood glucose homeostasis. *Acta Pharm. Sin. B* **2**, 358–367 (2012).
177. A. Sahu, Leptin signaling in the hypothalamus: emphasis on energy homeostasis and leptin resistance. *Front. Neuroendocrinol.* **24**, 225–253 (2003).
178. E. Nigro, *et al.*, New Insight into Adiponectin Role in Obesity and Obesity-Related Diseases. *Biomed Res. Int.* **2014**, 1–14 (2014).
179. S. Venkatesan, P. Cullen, P. Pacy, D. Halliday, J. Scott, Stable isotopes show a direct relation between VLDL apoB overproduction and serum triglyceride levels and indicate a metabolically and biochemically coherent basis for familial combined hyperlipidemia. *Arterioscler. Thromb. A J. Vasc. Biol.* **13**, 1110–1118 (1993).

180. A. Zhang, H. Sun, S. Qiu, X. Wang, NMR-based metabolomics coupled with pattern recognition methods in biomarker discovery and disease diagnosis. *Magn. Reson. Chem.* **51**, 549–556 (2013).
181. L. Capuron, J. Lasselin, N. Castanon, Role of Adiposity-Driven Inflammation in Depressive Morbidity. *Neuropsychopharmacology* **42**, 115–128 (2017).
182. B. K. Surmi, A. H. Hasty, The role of chemokines in recruitment of immune cells to the artery wall and adipose tissue. *Vascul. Pharmacol.* **52**, 27–36 (2010).
183. Z. Wu, *et al.*, Mesenteric adipose tissue B lymphocytes promote local and hepatic inflammation in non-alcoholic fatty liver disease mice. *J. Cell. Mol. Med.* **23**, 3375–3385 (2019).
184. S. Nishimura, *et al.*, CD8⁺ effector T cells contribute to macrophage recruitment and adipose tissue inflammation in obesity. *Nat. Med.* **15**, 914–920 (2009).
185. H. Shapiro, *et al.*, Adipose Tissue Foam Cells Are Present in Human Obesity. *J. Clin. Endocrinol. Metab.* **98**, 1173–1181 (2013).
186. J. M. Wentworth, *et al.*, Pro-Inflammatory CD11c⁺CD206⁺ Adipose Tissue Macrophages Are Associated With Insulin Resistance in Human Obesity. *Diabetes* **59**, 1648–1656 (2010).
187. G. Ghigliotti, *et al.*, Adipose Tissue Immune Response: Novel Triggers and Consequences for Chronic Inflammatory Conditions. *Inflammation* **37**, 1337–1353 (2014).
188. D. S. Lark, D. H. Wasserman, Meta-fibrosis links positive energy balance and

- mitochondrial metabolism to insulin resistance. *F1000Research* **6**, 1758 (2017).
189. F. Eichelmann, L. Schwingshackl, V. Fedirko, K. Aleksandrova, Effect of plant-based diets on obesity-related inflammatory profiles: a systematic review and meta-analysis of intervention trials. *Obes. Rev.* **17**, 1067–1079 (2016).
190. D. Kumar, *et al.*, Chronic hyperinsulinemia promotes meta-inflammation and extracellular matrix deposition in adipose tissue: Implications of nitric oxide. *Mol. Cell. Endocrinol.* **477**, 15–28 (2018).
191. J. M. Austyn, S. Gordon, F4/80, a monoclonal antibody directed specifically against the mouse macrophage. *Eur. J. Immunol.* **11**, 805–815 (1981).
192. R. Garcia-Macedo, *et al.*, Glycine increases mRNA adiponectin and diminishes pro-inflammatory adipokines expression in 3T3-L1 cells. *Eur. J. Pharmacol.* **587**, 317–321 (2008).
193. A. A. Hill, W. Reid Bolus, A. H. Hasty, A decade of progress in adipose tissue macrophage biology. *Immunol. Rev.* **262**, 134–152 (2014).
194. C. Pang, *et al.*, Macrophage infiltration into adipose tissue may promote angiogenesis for adipose tissue remodeling in obesity. *Am. J. Physiol. Metab.* **295**, E313–E322 (2008).
195. H. L. Kammoun, M. J. Kraakman, M. A. Febbraio, Adipose tissue inflammation in glucose metabolism. *Rev. Endocr. Metab. Disord.* **15**, 31–44 (2014).
196. K. Terada, *et al.*, Transplantation of periaortic adipose tissue inhibits atherosclerosis in apoE $-/-$ mice by evoking TGF- β 1-mediated anti-

- inflammatory response in transplanted graft. *Biochem. Biophys. Res. Commun.* **501**, 145–151 (2018).
197. N. de Wit, *et al.*, Saturated fat stimulates obesity and hepatic steatosis and affects gut microbiota composition by an enhanced overflow of dietary fat to the distal intestine. *Am. J. Physiol. Liver Physiol.* **303**, G589–G599 (2012).
198. P. K. Luukkonen, *et al.*, Saturated Fat Is More Metabolically Harmful for the Human Liver Than Unsaturated Fat or Simple Sugars. *Diabetes Care* **41**, 1732–1739 (2018).
199. H. Zhou, C. J. Urso, V. Jadeja, Saturated Fatty Acids in Obesity-Associated Inflammation. *J. Inflamm. Res.* **Volume 13**, 1–14 (2020).
200. D. Liddle, *et al.*, Integrated Immunomodulatory Mechanisms through which Long-Chain n-3 Polyunsaturated Fatty Acids Attenuate Obese Adipose Tissue Dysfunction. *Nutrients* **9**, 1289 (2017).
201. W. van den Brink, *et al.*, Current and Future Nutritional Strategies to Modulate Inflammatory Dynamics in Metabolic Disorders. *Front. Nutr.* **6** (2019).
202. K. Zhou, *et al.*, Targeting tumor-associated macrophages in the tumor microenvironment (Review). *Oncol. Lett.* **20**, 1–1 (2020).
203. L. R. Gray, S. C. Tompkins, E. B. Taylor, Regulation of pyruvate metabolism and human disease. *Cell. Mol. Life Sci.* **71**, 2577–2604 (2014).
204. Y. Si, H. Shi, K. Lee, Impact of perturbed pyruvate metabolism on adipocyte triglyceride accumulation. *Metab. Eng.* **11**, 382–390 (2009).
205. J. Kałużna-Czaplińska, P. Gałtarek, M. S. Chartrand, M. Dadar, G. Björklund, Is there a relationship between intestinal microbiota, dietary compounds, and

- obesity? *Trends Food Sci. Technol.* **70**, 105–113 (2017).
206. J. Hu, S. Lin, B. Zheng, P. C. K. Cheung, Short-chain fatty acids in control of energy metabolism. *Crit. Rev. Food Sci. Nutr.* **58**, 1243–1249 (2018).
207. V. C. Antharam, *et al.*, Intestinal Dysbiosis and Depletion of Butyrogenic Bacteria in Clostridium difficile Infection and Nosocomial Diarrhea. *J. Clin. Microbiol.* **51**, 2884–2892 (2013).
208. Y. Choi, *et al.*, Gut microbe-derived extracellular vesicles induce insulin resistance, thereby impairing glucose metabolism in skeletal muscle. *Sci. Rep.* **5**, 15878 (2015).
209. I. Moreno-Indias, *et al.*, Insulin resistance is associated with specific gut microbiota in appendix samples from morbidly obese patients. *Am. J. Transl. Res.* **8**, 5672–5684 (2016).
210. Y. Zhang, *et al.*, Insoluble dietary fiber derived from brown seaweed Laminaria japonica ameliorate obesity-related features via modulating gut microbiota dysbiosis in high-fat diet-fed mice. *Food Funct.* **12**, 587–601 (2021).
211. F. F. Anhê, *et al.*, A polyphenol-rich cranberry extract protects from diet-induced obesity, insulin resistance and intestinal inflammation in association with increased Akkermansia spp. population in the gut microbiota of mice. *Gut* **64**, 872–883 (2015).
212. M.-Y. Jeong, H.-M. Jang, D.-H. Kim, High-fat diet causes psychiatric disorders in mice by increasing Proteobacteria population. *Neurosci. Lett.* **698**, 51–57 (2019).
213. H. Cao, *et al.*, Stachyose Improves the Effects of Berberine on Glucose

- Metabolism by Regulating Intestinal Microbiota and Short-Chain Fatty Acids in Spontaneous Type 2 Diabetic KKAY Mice. *Front. Pharmacol.* **11** (2020).
214. S. Stojanov, A. Berlec, B. Štrukelj, The Influence of Probiotics on the Firmicutes/Bacteroidetes Ratio in the Treatment of Obesity and Inflammatory Bowel disease. *Microorganisms* **8**, 1715 (2020).
215. R. E. Ley, *et al.*, Obesity alters gut microbial ecology. *Proc. Natl. Acad. Sci.* **102**, 11070–11075 (2005).
216. G. den Besten, *et al.*, Short-Chain Fatty Acids Protect Against High-Fat Diet–Induced Obesity via a PPAR γ -Dependent Switch From Lipogenesis to Fat Oxidation. *Diabetes* **64**, 2398–2408 (2015).
217. W. Feng, H. Ao, C. Peng, Gut Microbiota, Short-Chain Fatty Acids, and Herbal Medicines. *Front. Pharmacol.* **9** (2018).
218. M. Derrien, C. Belzer, W. M. de Vos, Akkermansia muciniphila and its role in regulating host functions. *Microb. Pathog.* **106**, 171–181 (2017).
219. K. Oliphant, E. Allen-Vercoe, Macronutrient metabolism by the human gut microbiome: major fermentation by-products and their impact on host health. *Microbiome* **7**, 91 (2019).
220. M. Vacca, *et al.*, The Controversial Role of Human Gut Lachnospiraceae. *Microorganisms* **8**, 573 (2020).
221. D. Ribet, P. Cossart, How bacterial pathogens colonize their hosts and invade deeper tissues. *Microbes Infect.* **17**, 173–183 (2015).
222. V. Fuochi, *et al.*, Metabolic Characterization of Supernatants Produced by Lactobacillus spp. With in vitro Anti-Legionella Activity. *Front. Microbiol.* **10**

(2019).

223. I. J. Lodhi, *et al.*, Inhibiting Adipose Tissue Lipogenesis Reprograms Thermogenesis and PPAR γ Activation to Decrease Diet-Induced Obesity. *Cell Metab.* **16**, 189–201 (2012).
224. E. A. Kennedy, K. Y. King, M. T. Baldrige, Mouse Microbiota Models: Comparing Germ-Free Mice and Antibiotics Treatment as Tools for Modifying Gut Bacteria. *Front. Physiol.* **9** (2018).
225. D. Roy, “Fecal Microbiota and Probiotic Yogurt Intake” in *Yogurt in Health and Disease Prevention*, (Elsevier, 2017), pp. 237–258.
226. I. M. L. Vasques-Monteiro, *et al.*, A rise in Proteobacteria is an indicator of gut-liver axis-mediated nonalcoholic fatty liver disease in high-fructose-fed adult mice. *Nutr. Res.* **91**, 26–35 (2021).
227. M. Million, J.-C. Lagier, D. Yahav, M. Paul, Gut bacterial microbiota and obesity. *Clin. Microbiol. Infect.* **19**, 305–313 (2013).
228. J. Jia, *et al.*, Mitigation of Obesity-Related Systemic Low-Grade Inflammation and Gut Microbial Dysbiosis in Mice with Nanosilver Supplement. *ACS Appl. Bio Mater.* **4**, 2570–2582 (2021).
229. J. Auwerx, T.-A. Cock, C. Knouff, PPAR- γ : A Thrifty Transcription Factor. *Nucl. Recept. Signal.* **1**, nrs.01006 (2003).
230. A. Bonen, *et al.*, Regulation of fatty acid transport by fatty acid translocase/CD36. *Proc. Nutr. Soc.* **63**, 245–249 (2004).
231. B. Sulijaya, N. Takahashi, K. Yamazaki, Lactobacillus-Derived Bioactive Metabolites for the Regulation of Periodontal Health: Evidences to Clinical

Setting. *Molecules* **25**, 2088 (2020).

232. N.-R. Shin, T. W. Whon, J.-W. Bae, Proteobacteria: microbial signature of dysbiosis in gut microbiota. *Trends Biotechnol.* **33**, 496–503 (2015).

